Habitat mapping of the Brazilian Pantanal using synthetic aperture radar imagery and object based image analysis

by

Teresa Lynne Evans
B. Sc., University of Victoria, 2009

A Thesis Submitted in Partial Fulfillment
of the Requirements for the Degree of

MASTER OF SCIENCE

in the Department of Geography

Supervisory Committee

Habitat Mapping of the Brazilian Pantanal using Synthetic Aperture Radar Imagery and Object Based Image Analysis

by

Teresa Lynne Evans
B. Sc., University of Victoria, 2009

Supervisory Committee

Dr. Maycira Costa, (Department of Geography)
Supervisor

Dr. Dennis Jelinski, (Department of Geography)
Departmental Member

Abstract

Supervisory Committee

Dr. Maycira Costa, (Department of Geography)
Supervisor

Dr. Dennis Jelinski, (Department of Geography)
Departmental Member

The Brazilian Pantanal, a continuous tropical wetland located in the center of South America, has been recognized as one of the largest and most important wetland ecosystems globally. The Pantanal exhibits a high biodiversity of flora and fauna species, and many threatened habitats. The spatial distribution of these habitats influence the distribution, abundance and interactions of animal species, and the change or destruction of habitat may cause alteration of key biological processes. The Pantanal may be divided into several distinct subregions based on geology and hydrology: flooding in these subregions is distinctly seasonal, but the timing, amplitude and duration of inundation vary considerably as a result of both the delayed release of floodwaters and regional rainfall patterns. Given the ecological importance of the Pantanal wetland ecosystem, the primary goal of this research was to utilize a dual season set of L-band (ALOS/PALSAR) and C-band (RADARSAT-2 and ENVISAT/ASAR) imagery, a comprehensive set of ground reference data, and a hierarchical object-oriented approach. This primary goal was achieved through two main research tasks. The first task was to define the diverse habitats of the Lower Nhecolândia subregion of the Pantanal at both a fine spatial resolution (12.5 m), and a relatively medium spatial resolution (50 m), thus evaluating the accuracy of the differing spatial resolutions for land cover classification of

the highly spatially heterogeneous subregion. The second task was to define on a regional scale, using the 50 m spatial resolution imagery, the wetland habitats of each of the hydrological subregions of the Pantanal, thereby producing a final product covering the entire Pantanal ecosystem. The final classification maps of the Lower Nhecolândia subregion resulted in overall accuracies of 83% and 72% for the 12.5 m and 50 m spatial resolutions, respectively, and defined seven land cover classes. In general, the highest degree of confusion for both fine and medium resolution classifications related to issues of 1) scale of habitats, for instance, *capões, cordilheiras, and lakes,* in relation to spatial resolution of the imagery, and 2) issues relating to variable flooding patterns in the subregion, and 3) arbitrary class membership rules. The 50 m spatial resolution classification of the entire Pantanal wetland resulted in an overall accuracy of 80%, and defined ten land cover classes. Given the analysis of the comparison of fine and relatively medium spatial resolution classifications of the Lower Nhecolândia subregion, I conclude that significant improvements in accuracy can be achieved with the finer spatial resolution dataset, particularly in subregions with high spatial heterogeneity in land cover. The produced habitat spatial distribution maps will provide vital information for determining refuge zones for terrestrial species, connectivity of aquatic habitats during the dry season, and crucial baseline data to aid in monitoring changes in the region, as well as to help define conservation strategies for habitat in this critically important wetland.

Table of Contents

List of Tables

List of Figures

Acknowledgments

I would like to take this opportunity to thank all those who have supported me throughout my graduate studies, in particular, my amazing family and friends for their unwavering support and understanding. I would also like to thank all of my colleagues who have helped me in this process, particularly everyone, past and present, in the SPECTRAL lab at UVic. I would also like to acknowledge the Japanese Aerospace Exploration Agency (JAXA) through the K&C project, Canadian Space Agency (CSA) through the SOAR initiative, and the European Space Agency (ESA), for all of the imagery data; the National Geographic Society (NGS) and the Natural Sciences and Engineering Research Council of Canada (NSERC) for financial support; and EMBRAPA PANTANAL for additional data. Finally, a huge thank you to my supervisor, Maycira Costa for continually pushing me towards success, you have been a true mentor and friend throughout this entire process.

Chapter 1. Introduction

1.1 Overview

Wetlands are one of the most important and fragile ecosystems on Earth, and are generally described as transitional ecosystems between land and water (Mitsch & Gosselink, 2007). Wetland ecosystems provide many essential ecological services, including flood control, climate regulation, carbon storage, aquifer recharge, and biodiversity management. They are natural water filters that improve water quality, and provide habitat for a vast number of flora and fauna species (Keddy et al., 2009). These ecosystems have some of the highest biodiversity of any of the global ecosystems, and serve as permanent habitat for countless species of plants, invertebrates, fish, birds and other higher-order wildlife, as well as temporary habitat and breeding grounds for many migratory species, particularly birds (Junk et al., 2006; Mitsch & Gosselink, 2007; Keddy et al., 2009). Biogeochemically, wetlands recycle many nutrients, and may also act as sinks for organic carbon in the form of peat (Batzer & Sharitz, 2006; Mitsch & Gosselink, 2007). In spite of this importance, global wetland loss has been considerable over the last two centuries, largely due to human land use change and a lack of understanding of the vital role of wetlands in the global environment (Keddy et al., 2009). As such, there is a crucial need for the identification and protection of key wetland habitats; however, the global coverage of wetlands is not well known, with estimates ranging from 7 to 10 million km^2, or 4 to 8% of global land coverage, of which approximately half are located in tropic and subtropic regions (Lehner & Doll, 2004; Mitsch & Gosselink 2007).

The spatial distribution of wetlands is key information for supporting applications in resource management, habitat reconstruction, species at risk recovery, and biogeochemical budgets (Tews et al., 2004; Mitchell, 2005). This information is the most relevant instrument for promoting legal protection and conservation (Mitsch and Gosselink, 2007). Therefore, developing efficient techniques for mapping and deriving biophysical properties of wetland ecosystems is of critical importance for managing and understanding these ecosystems (Rebelo et al., 2009). Information is required at multiple spatial scales, from global to local (Rebelo et al., 2009) and temporally (Hamilton, 1999, Silva et. al, 2010), to allow for guidance to policy-makers. Classic methods for mapping wetland vegetation habitats have been largely based on ground surveys of soil and vegetation inventories gathered through extensive and time consuming field work requiring ancillary data analysis and visual estimations of ground cover. As a consequence, such methods are only practical on small scales, and do not provide spatially continuous information over large regions (Hewes, 1951; Lee and Lunetta, 1996; Mitsch and Gosselink, 2007). In many cases, remote sensing technology offers the most reliable method for determining ecologically valuable information regarding the characteristics of wetland habitats across a diverse range of scales (Kerr & Ostrovsky, 2003; Davidson & Finlayson, 2007; Rebelo et al., 2009).

One of the largest and most important tropical wetland ecosystems is the Pantanal wetland, located in the center of South America, between Brazil, Bolivia, and Paraguay. Estimates suggest that the inundated area of the Pantanal covers approximately 160,000 km^2 during maximum flooding, and with the entire Pantanal watershed occupying an area of approximately 362,000 km^2 (Junk et al., 2006). The upper Paraguay River and its

tributaries feed the Pantanal wetlands, promoting a strong annual unimodal flood that varies in duration, amplitude and extent both yearly and spatially (Hamilton et al., 1996). Such characteristic flood dynamics require morphological, anatomical, physiological, and/or ethological adaptations from the local biota. This interdependence between flood dynamics and biota is well defined by the Flood Pulse Concept (Junk et al., 1989), which defines rivers and their connected floodplains as a single dynamic system with hydrological, biogeochemical, and ecological interactions. This concept also defines the interactions between the periodically flooded Aquatic Terrestrial Transition Zone (ATTZ) and permanent water bodies or permanently dry terrestrial habitats (Junk et al., 1989). As these seasonal water level variations are the driving force of ecological processes in floodplain systems, identifying the various permanent and semi-permanent terrestrial and aquatic habitats in a seasonal flood-pulse ecosystem is critical for understanding the biogeochemical, hydrological and ecological processes of the ecosystem (Junk et al., 1989; Hamilton et al., 1996). The dynamics of inundation in the Pantanal also promote a high diversity of vegetation (Alho, 2008), expressed by a unique landscape characterized by different compositions of savanna vegetation, abundant species of aquatic vegetation, and different types of floodplain forests (Abdon et al., 1998; Pott & Pott, 2000; Alho, 2008). In addition to the floral diversity, a large number of hydrochemically varied lakes, waterways, and other fluvial geomorphological patterns are observed, generating a complex mosaic of wetland habitats (Por, 1995; Costa & Telmer, 2006). More comprehensive descriptions specific to the respective study sites within the Pantanal are found in Chapters 2 and 3.

The vast habitat diversity in the Pantanal is poorly understood, and currently threatened by human development occurring both in the floodplain and on the surrounding plateau. These developments threaten to alter the Pantanal ecosystem in a potentially irreversible manner, mostly through the modification of the natural hydrological cycles of the rivers, and the destruction of natural habitat (da Silva & Girard, 2004; Assine, 2005; Junk et al., 2006; Alho, 2008). Despite the ecological importance of the Pantanal, and potential consequences resulting from habitat alteration/loss, there is a lack of understanding about the spatio-temporal variability of the habitats within this wetland ecosystem. As such, there is an urgent need for methods that allow the quantification and monitoring of the occurring changes and impacts in the Pantanal wetlands, so that sustainable management practices and effective conservation units can be established. Yet, given the size and relative inaccessibility of the Pantanal system, conventional methods of data gathering are difficult and expensive. Thus, remote sensing technology offers a cost-effective alternative for mapping the spatial variability of the habitats within this highly heterogeneous wetland ecosystem.

In light of the critical importance of this ecosystem, and the lack of current knowledge regarding the habitats within it, the main purpose of the present thesis was to determine the spatial variability of the numerous habitats of the Pantanal wetland using a combination of C and L-band multi-temporal SAR imagery, and an object based image analysis approach. This goal was accomplished via the following objectives:

1. Examine and evaluate the SAR backscattering characteristics of the various land cover habitats of the Pantanal wetlands.

2. Develop a method for classification of the various aquatic, terrestrial and transitional habitats of the Pantanal using available SAR imagery (both 12.5 m and 50 m spatial resolution), an Object Based Image Analysis approach and a hierarchical rule-set methodology.
3. Evaluate the accuracy of the output classification maps.
4. Compare the output classification maps produced at the two different spatial resolutions with regard to accuracy, scale, and the spatial heterogeneity of the landscape.

1.2 Thesis Structure

Chapter 1 is an overview of the importance of wetland ecosystems globally, as well as an introduction to the Pantanal wetlands specifically. In addition, a comprehensive literature review outlining various remote sensing and classification techniques is presented.

In Chapter 2, the use of fine spatial resolution multi-temporal L-band ALOS/PALSAR (12.5m), C-band RADARSAT-2 (25m), and ENVISAT/ASAR (12.5m) imagery to map ecosystems and create a lake distribution map of the Lower Nhecolândia subregion in the Brazilian Pantanal is described.

Chapter 3 examines the classification of the entire Pantanal wetland by first dividing the region into ten distinct subregions based on geology and hydrology, and conducting separate classifications on each subregion. Flooding in these subregions is distinctly seasonal, but the timing, amplitude and duration of inundation vary considerably as a result of both the delayed release of floodwaters and regional rainfall patterns. For this part of the study, 50 m spatial resolution, dual-season L-band

ALOS/PALSAR, and C-band RADARSAT-2 imagery was utilized to map the diverse habitats of the subregions of the Pantanal, again, using an OBIA approach.

Chapter 4 discusses the evaluation of the land cover classification products derived from the SAR 12.5 m and 50 m spatial resolution imagery for the Lower Nhecolândia subregion of the Pantanal, and compares the two products with regards to issues of spatial resolution and land cover spatial heterogeneity. Finally, Chapter 4 concludes with a discussion of the usefulness and the limitations of the present research, as well as recommendations for future work.

1.3 Literature Review

This literature review begins with an overview of historical methods of wetlands classification, followed by an outline of current remote sensing data and classification methods. Next, a comprehensive review of Synthetic Aperture Radar (SAR) interactions in tropical wetlands, including an overview of SAR backscattering mechanisms, as well as previous research in the field, is presented. Further issues related to large scale classifications of land cover using remotely sensed imagery are then considered. Finally an in depth review of Object Based Image Analysis (OBIA) techniques is presented.

1.3.1 Wetlands Classification

The earliest studies of wetlands using remote sensing were based on analog aerial photography, and mostly related to identification and border definition of wetland areas (Howland, 1980, Polis et al., 1974). The U.S. Fish and Wildlife Service National Wetlands Inventory used archived colour-infrared air photos extensively for identifying and delineating wetlands in the United States (Wilen et al., 1999). Although currently surpassed in capabilities by digital multispectral or hyperspectral systems, analog aerial

photos are still considered a relatively reliable medium for obtaining high resolution coverage for localized, small-scale mapping purposes, and are still in use in present times (Carpenter et al., 2011), often for historical wetlands mapping looking at change detection for which no satellite data exists (Cserhalmi et al., 2011). Although aerial photographs have proved useful for providing a broader understanding of hydrology and vegetation patterns, aerial photography is expensive to obtain over large areas, and so is also only practical for smaller scale mapping efforts. Furthermore, mapping via aerial photos relies on the subjectivity of the interpreter, and so can be problematic in terms of repeatability (Ramsey & Laine, 1997). The size and relative inaccessibility of many wetland ecosystems renders these traditional methods difficult and expensive. As such, satellite remote sensing presents a cost effective, efficient and practical approach that can be used to map wetland landscape distribution, especially over large geographic areas, with advantages that include multi-spectral and multi-temporal data collection (Rundquist et al., 2001; Ozesmi & Bauer, 2002).

While optical sensors, such as the Landsat Thematic Mapper, are extremely useful for many wetland monitoring purposes, they are limited in that they cannot penetrate cloud cover or dense vegetation canopies (Ulaby et al., 1981; Hess et al., 1995; Dobson et al., 1996; Siqueira et al., 2002). For example, the Global Environment Facility (GEF), an organization that developed the implementation of a detailed watershed management program for the Pantanal and the Upper Paraguay River Basin, used a selection of Landsat imagery compiled over approximately five years to complete a single, cloud-free mosaic of the entire Pantanal: optical imagery has been used in the region mostly for small-scale studies (Abdon et al 1998; Novack et al., 2010). As an alternative, synthetic aperture radar

(SAR) remote sensing instruments overcome the limitations of optical imagery for land cover and inundation mapping, as the longer microwave wavelengths (approximately 1-100 cm) allow penetration of atmospheric water vapour or cloud cover (Kasischke et al., 1997; Henderson & Lewis, 2008).

1.3.2 SAR interactions in tropical wetlands

The use of SAR imagery has long been recognized as an important tool for studying tropical wetlands, largely because of the noticeable difference between the signal recorded from dry and flooded vegetation, the ability to penetrate cloud cover often present in tropical ecosystems, and the ability to penetrate the vegetation canopy. SAR systems operate in different bands of the electromagnetic spectrum, with wavelengths being commonly coded by a single letter: X (3cm); C (5.6cm); S (10cm); L (23cm); and P (75cm) (Oliver & Quegan, 2004). Typically, longer wavelengths tend to allow deeper canopy penetration and are less sensitive to smaller biophysical variations (Henderson & Lewis, 2008). The SAR signal offers information about the target based primarily on canopy biophysical characteristics and dielectric properties, rather than biochemical and morpho-anatomical features as observed by optical systems (Henderson & Lewis, 2008). SAR systems are also “side-looking”, meaning that they view the surface of the earth from an oblique point of view, and the incidence angle can affect the overall response. The incidence angle is the relationship between the incoming radar beam and the surface. It can change from very steep (20° off-nadir) to very shallow (60°off-nadir) (Ulaby et al., 1981). Generally, steeper angles will allow more canopy penetration, while shallow angles exhibit more surface components (Costa et al., 2002). In addition, SAR systems have the ability to send and receive the signal at a variety of linear polarizations and

incidence angles. The signal can either be like-polarized (sent horizontal/received horizontal - HH, or sent vertical/received vertical - VV) or cross-polarized (sent horizontal/received vertical - HV, or sent vertical/received horizontal - VH). These different polarizations can highlight specific attributes from some types of targets (Henderson & Lewis, 1998).

The main scattering mechanisms typical in L and C bands are illustrated in Figure 1.1. With L-band SAR data, smooth surfaces such as flat water or bare soil, or even relatively short vegetation (< 23cm wavelength of L-band) such as pasture, behave like a mirror and specularly reflect most energy away from the sensor. When surface roughness is increased, as happens with the addition of taller vegetation, backscattered radiation also increases (Ulaby et al., 1981). When the forest floor is non-flooded, there is volumetric scattering happening within the forest canopy and at the ground level, depending on the height of the understory. Double-bounce reflection is caused by the interaction of the incident energy with the tree trunk (or any structure perpendicular to the surface) followed by a change in direction towards a specular surface (typically bare soil, very short vegetation, or water), where energy is reflected back towards the sensor; this process also happens in the opposite direction (Ulaby et al., 1981). Once the area is flooded, even shallowly, there is a strong double-bounce reflection between the tree trunks and the water surface, adding to the volumetric scattering within the canopy, and greatly enhancing the return signal to the sensor (Beall & Lewis, 1998; Rosenqvist et al., 2007).

The main scattering processes are the same for C-band as for L-band, however the interactions between the incident radiation and specific cover types vary due to the shorter wavelength of C-band (5.6 cm). For example: the shorter wavelengths of C-band do not

allow for the penetration of dense forest canopy, therefore the majority of backscattering for this cover type results from volumetric scattering within the canopy; short vegetation, such as pasture, that may not be visible at the longer wavelengths due to specular reflection, will provide a moderate backscattering return, also resulting from volumetric scattering (Figure 1.1); C-band double-bounce has been reported for vertical herbaceous vegetation such as *Typha sp.* (Costa and Telmer, 2006; Pope et al., 1997).

A combination of L and C-band SAR imagery has been employed for many wetland studies (Wang, 1994; Hess et al., 1995, 2003; Pope et al., 1997; Costa et al., 2002; Costa & Telmer 2006, Evans et al., 2010). C-band (HH) has been found to have the highest accuracies for delineating sawgrass and cattail marshes, and for classifying other herbaceous wetlands (Pope et al., 1997; Kasischke, 1997). Furthermore, an increase in signal due to double-bounce has been reported for aquatic macrophytes in standing water at shorter C-band wavelength (Brown et al, 1996; Pope et al., 1997). In general, longer wavelengths (L-band) are preferred for detection of inundation for forested wetlands, and shorter wavelengths (C-band) are suggested for herbaceous wetlands. However, current research suggests that a combination of both bands and polarizations is beneficial for a comprehensive understanding of complex wetland dynamics (Schullius & Evans, 1997; Costa, 2004; Costa and Telmer, 2006; Henderson & Lewis, 2008). A more detailed literature review outlining the use of SAR imagery for wetland classification studies is found in Chapter 2.

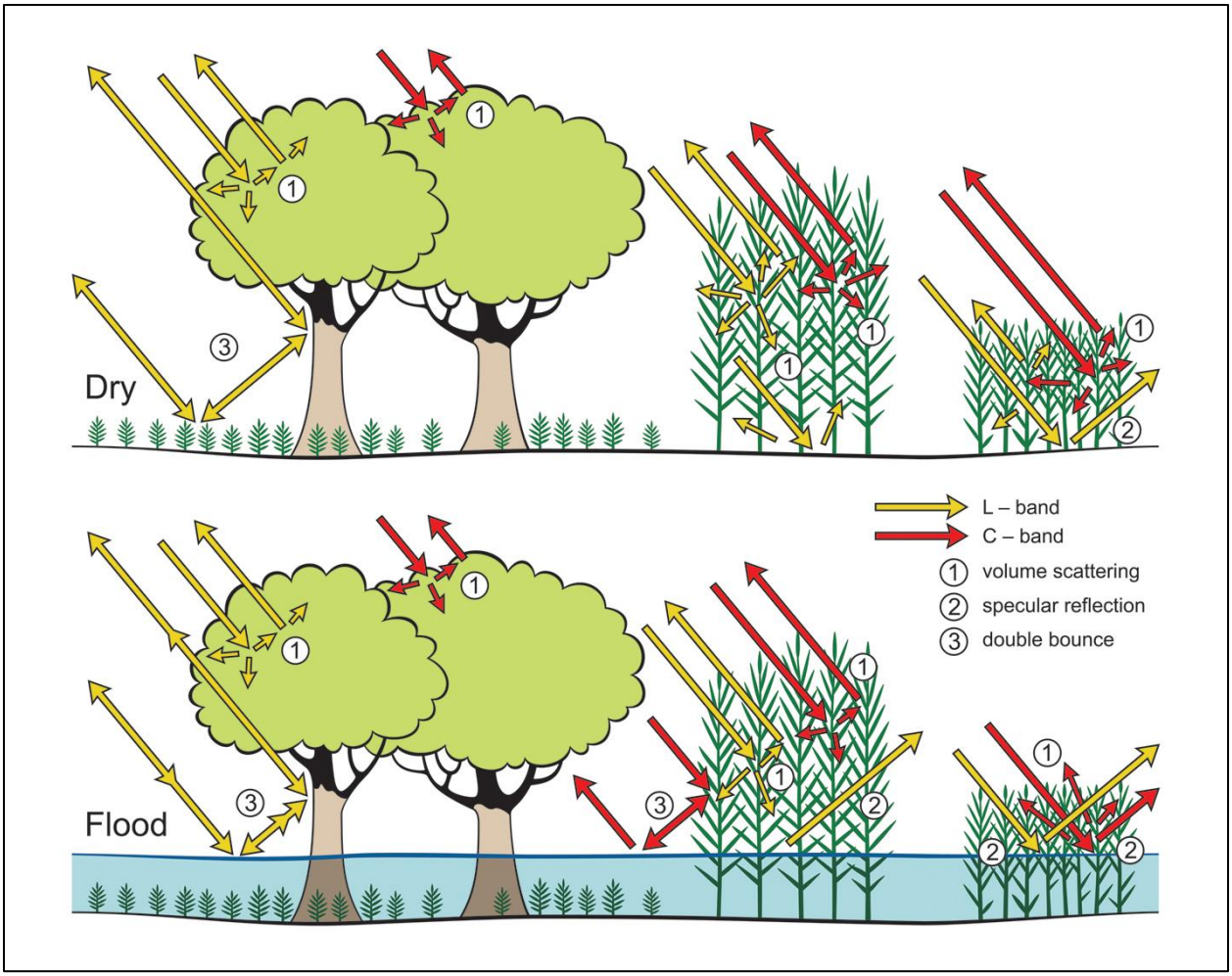

Figure 1.1: C and L-band SAR interactions in tropical wetlands

1.3.3 Further Considerations for Large-Scale Classifications Using Remotely Sensed Imagery

Remote sensing methods of land cover classification require careful consideration of both the temporal, and the spatial scale of the ecological phenomena being studied. Temporally, ecological phenomena may show seasonal, annual, or even decadal cycles of change. Acquiring appropriate temporal imagery to depict these various changes must be considered. This can present a challenge when mapping large areas consisting of several contiguous satellite imagery frames with temporal discontinuity between image dates, as inconsistent moisture conditions and/or phenological differences of just a few weeks can exhibit considerable radiometric differences (Lowry et al., 2007, Lucas et al., 2010). Some studies have suggested that the use of multi-temporal imagery was essential for achieving acceptable classification accuracy results for temporally variable regions (Lowry et al., 2007), and specifically, in temporally dynamic wetland ecosystems (Evans et al., 2010; Silva et al., 2010).

Spatially, scale consists of two components: the spatial resolution of the remotely sensed imagery; and the extent of the study area (Benson & Mackenzie, 1995) – the size of the minimum area which can be depicted depends on the scale and resolution of the imagery (Anderson et al., 1976). Most landscape features are sensitive to changes in spatial resolution; thus, the choice of satellite sensor must be appropriate to the characteristics of the study area, and depends on the scale of the minimum landscape feature or phenomena to be mapped. Ecosystems that are highly heterogeneous in nature must be measured at a finer spatial resolution, or the subsequent classification could overlook significant features of the landscape (Benson & Mackenzie, 1995). The use of multi-temporal and multi-scale images can result in increased accuracy (Lowry et al.,

2007); however, correcting imagery radiometry and geometry accuracies between images from different dates/sensors are of key importance to avoid erroneous land cover classification results.

Two additional sources of error or uncertainty that are possible when producing land cover maps from remote sensing imagery include: 1) thematic error – misclassification of objects or features; and, 2) uncertainty pertaining to class nomenclature (Newton et al., 2009). A carefully determined classification scheme is integral for reducing these uncertainties. Thematic error can be reduced by developing a classification scheme that is appropriate to the specific objectives of the project, as well as the ability of the remotely sensed imagery to discriminate possible land cover classes (Congalton, 1991). A hierarchical classification scheme is recommended for reducing such thematic errors, particularly for complex/heterogeneous landscapes (Anderson et al., 1976; Congalton, 1991; Blaschke & Hay, 2001; Lowry et al., 2007; Rebelo, 2010; Silva et al., 2010; Walker et al., 2010.), and has shown advantages over non-hierarchical classifications, as rules can be refined throughout the process. Moreover, there is a high demand for the standardization of land cover classes and nomenclature to reduce ambiguities across studies of a similar nature (Anderson et al., 1976; Lowry et al., 2007). An explanation of how land cover classes were derived should be clear. For example, when comparing similar land cover classifications, it would be useful to know if classes were determined based on vegetation species (deciduous forest, coniferous forest), vegetation/land structure (herbaceous, woody, bare soil), geomorphological characteristics (riparian, upland, floodplain), or a combination of these. Estimation of such errors and acknowledgement of possible uncertainty needs to be reported.

Therefore, an accuracy assessment is a crucial step in analysing any classification map created from remotely sensed data. A standard error matrix (omission error– user's accuracy/commission error-producer's accuracy) should be adopted as standard reporting convention (Congalton, 1991).

1.3.4 Object Based Image Analysis (OBIA)

The OBIA approach to land cover classification offers several advantages over pixel-based classification methods. OBIA supports examination of features (such as mean and standard deviation of object radiometry, and object size and shape) and spatial and hierarchical relationships of objects rather than single pixels. It allows for easy fusion of data from multiple sources, at varying spatial and spectral resolutions, significantly increasing the amount of information that can be extracted for a given area. Objects are created by a segmentation process, and provide a more intuitive representation of ground features in comparison to traditional pixel-based classifications (Comber, 2010). The initial multi-resolution segmentation is a region-merging algorithm that begins with a single pixel and a pairwise comparison of its neighbours with the goal of minimizing the resulting summed heterogeneity (Benz et al., 2001). Segmentation parameters are data, scale, and research goal specific, thus the user must incorporate a "trial and error" method for determining the ideal inputs for their purpose, based on their knowledge and expertise (Blaschke & Hay, 2001).

Usually, segmentation is followed by a hierarchical rule-based approach to classify resultant image objects. Hierarchical classification rules are developed according to user-defined parameters, which are supported by user expertise in the field, and can be refined iteratively based on results throughout the process. This method allows for the addition of

new rules or datasets without compromising predefined rules, while traditional methods such as maximum likelihood or minimum distance may alter the rules of all classes concurrently based on new information. For instance, in a hierarchical classification, land cover classes, such as forest, or water, once classified can be removed from subsequent processing, and new rules can be created to refine classifications of remaining land cover without compromising the overall classification result (Lucas, 2007).

Often, OBIA has been used for SAR imagery classification because of the nature of the original radiometric signal – the signal of each target must be approximated by averaging backscattering across a neighbourhood of pixels to decrease the effects of speckle (Laur 1997). As such, OBIA and SAR imagery have been successfully integrated for wetland inundation research (Hess et al., 2003; Costa, 2004; Hamilton et al., 2007; Pappenberger et al., 2007; Silva et al., 2010). These investigators accurately achieved their goals by applying different rules for the hierarchical classification approach. Silva et al. (2010) employed a hierarchical, object-oriented method for combining temporal data from SAR and optical sensors to map the seasonal variation in aquatic vegetation cover on the Amazon floodplain. The investigators suggested that object-oriented, hierarchical classification methods were effective in dealing with the large variability associated with SAR backscattering values, and that the use of multi-temporal imagery contributed significantly to the discrimination of multiple land cover types. Similar results for different wetlands in the world were obtained by Hamilton et al. (2007), Durieux et al. (2007), and Lucas et al. (2008) using comparable methods. Hess et al. (2003) and Costa (2004), using a simple OBIA hierarchical approach, defined wetlands regions in the

central and lower Amazon Basin, respectively, using JERS-1 and RADARSAT-1 imagery.

Chapter 2. Landcover Classification of the Lower Nhecolândia Subregion of the Brazilian Pantanal Wetlands Using ALOS/PALSAR, RADARSAT-2 and ENVISAT/ASAR Imagery

Abstract — The Lower Nhecolândia subregion of the Brazilian Pantanal is part of a large continuous tropical wetland that exhibits a high biodiversity of flora and fauna species, and many threatened habitats. The spatial distribution of these habitats influence the abundance and interactions of animal species, and the change or destruction of habitat can cause the disturbance of key biological processes. This study uses multi-temporal L-band ALOS/PALSAR, C-band RADARSAT-2, and ENVISAT/ASAR data to map ecosystems and create a lake distribution map of the Lower Nhecolândia subregion in the Brazilian Pantanal. First, backscattering analysis was conducted on individual training objects to gain a better understanding of the backscattering characteristics of each class. Then, a Level 1 object-based image analysis (OBIA) classification based on hierarchical principles first classified the region into "Lakes" and "Not Lakes". This was followed by a Level 2 classification defining six vegetation habitats (Forest Woodland, Open Wood Savanna, Open Grass Savanna, Agriculture, Swampy Grassland and *Vazantes*) which was achieved at an overall accuracy of 83%. A Level 3 classification defined the "Lakes" class into a) Fresh (*baías*) and Brackish (*salinas*) lakes (accuracy results of 98%); and a further classification level dividing the fresh lakes, b) Fresh Lakes with floating and emergent vegetation (*baías*), and Fresh Lakes with the presence of *Typha (salobras)*, and including the Brackish lakes (*salinas*) (overall accuracy results of 81%). The results of this study provide the first fine spatial resolution

classification showing the spatial distribution of terrestrial and aquatic habitats for the entire subregion of Lower Nhecolândia using dual season, dual polarization C and L-band SAR imagery. The produced maps will provide valuable habitat information to help define conservation strategies and aid further research in the area.

2.1 Introduction

Anthropogenic activities currently influence most of the terrestrial biosphere and are growing in intensity and scope. The consequent habitat loss and degradation weaken ecosystem functions at local, regional and global scales (Kerr & Ostrovsky, 2003). Thus, spatial distribution of land use/land cover data is essential for the analysis of ecosystem processes, both in terms of forming baseline data, and for subsequent monitoring over time (Anderson et al., 1976; Wang et al., 2009). Specifically, land cover data is required to assess environmental impacts, manage wildlife resources, monitor land cover change, and to consider future impacts (Anderson et al., 1976). Yet, given the size and inaccessibility of many global ecosystems, conventional methods of data acquisition can be complex. In many cases, remote sensing technology offers the only reliable process for determining ecologically valuable information regarding the characteristics of habitats, and monitoring land cover changes resulting from anthropogenic or natural processes across large scales (Laba et al., 2002; Kerr & Ostrovsky, 2003; Lowry et al., 2007).

Wetland regions are regarded as one of these difficult areas to monitor through conventional methods due to their relative inaccessibility and seasonally dynamic nature. Prior to the advent of remote sensing technology, wetland mapping was largely based on ground surveys of soil and vegetation inventories gathered through extensive and time

consuming field work requiring ancillary data analysis and visual estimations of ground cover, and consequently, were only practical on small scales (Hewes, 1951; Lee & Lunetta, 1996; Mitsch & Gosselink, 2007). Aerial photographs have proved useful for providing a broader understanding of hydrology and vegetation patterns; however aerial photography is expensive to obtain, and so is also only practical for smaller scale mapping efforts. Furthermore, mapping via aerial photos relies on the subjectivity of the interpreter, and so can be problematic in terms of repeatability (Ramsey & Laine, 1997). The size and relative inaccessibility of wetland ecosystems renders these traditional methods difficult and expensive. As such, satellite remote sensing presents a cost effective, efficient and practical approach that can be used to map wetland landscape distribution over a large area with advantages that include multi-spectral and multi-temporal data collection (Rundquist et al., 2001; Ozesmi & Bauer, 2002).

Optical satellite imagery has shown promising results for many wetland monitoring purposes. One of the first uses of satellite imagery for wetlands mapping involved the use of Landsat MSS to classify the wetlands of Nebraska Sand Hills (Seevers et al., 1976). More recently, for example, optical imagery have been used to classify general vegetation land cover and broad vegetation assemblages, including tropical freshwater swamp in Australia (Harvey & Hill, 2001), coastal salt marsh mapping in California (Li et al., 2005), and classification of marsh and swamp cover in the Harike wetlands ecosystem in Punjab, India (Chopra et al., 2001). However, optical systems are limited in that they cannot penetrate cloud cover or dense vegetation canopies (Hess et al., 1995; Siqueira, 2003; Costa, 2004; Silva et al., 2008). The cloud cover issue can be especially problematic in humid tropical and subtropical regions. For example, the Global Environment Facility

(GEF) used a selection of Landsat imagery compiled over approximately five years to complete a single, cloud-free mosaic of the entire Brazilian Pantanal wetlands (GEF, 2004). As an alternative, synthetic aperture radar (SAR) satellites operate in the microwave region of the electromagnetic spectrum (approximately 1-100 cm in wavelength), typically allowing penetration of both forest canopy and cloud cover, thus overcoming the limitations of optical imagery for land cover and inundation mapping (Dobson et al., 1996; Silva et al., 2008). SAR systems are therefore recommended for tropical/semitropical wetlands, where cloud cover is an issue, and L-band SAR particularly for wetland regions with significant dense canopy cover (Kasischke et al., 1997; Henderson & Lewis, 2008).

The availability of SAR imagery from the Advanced Land Observing Satellite (ALOS) Phased Array L-band Synthetic Aperture Radar (PALSAR), the RADARSAT-2, and ENVISAT/ASAR, and other SAR systems offers a unique opportunity for mapping and monitoring the spatial and temporal dynamics of large tropical wetland ecosystems. For instance, Lucas et al. (2007) evaluated the potential of L-band SAR for quantifying and monitoring mangrove populations in the tropics. In Gabon, Africa, Simard et al. (2002) combined ERS-1 and JERS-1 imagery to map tropical coastal vegetation. Also in Africa, Rebelo (2010) employed a combination of multitemporal L-band ALOS/PALSAR imagery with Landsat TM and ASTER imagery to successfully map two wetland sites: Lake Chilwa, Malawi, and Lake Urema, Mozambique. In the Amazon region of Brazil, Hess et al. (2003) used dual-season L-band SAR imagery from JERS-1 to map seasonal inundation and vegetation for the central Amazon basin, and determined that the use of images acquired at high and low inundation stages allowed the delineation of vegetation

types that could not be distinguished on a single date. Also in the Amazon floodplain, Costa (2004) used a combination of multi-temporal C-band (RADARSAT) and L-band (JERS-1) imagery to classify vegetation communities. More recently, Silva et al. (2010) successfully applied a more complex object-oriented and hierarchical classification method combining temporal imagery from SAR (RADARSAT-1) and optical (MODIS) to map the seasonal variation in aquatic vegetation cover on the Amazon floodplain. In the Pantanal wetlands of Brazil, Costa & Telmer (2006) utilized a combination of C-band (RADARSAT-1) and L-band (JERS-1) imagery to classify the geochemically varied lakes in the Nhecolândia region of the Pantanal, based on the specific types of aquatic vegetation associated with each geochemical condition. Evans et al., (2010) utilized an object based image analysis (OBIA) approach combining temporal SAR (ALOS/PALSAR ScanSAR) and RADARSAT-2 imagery to map the land cover and inundation patterns for the entire Pantanal. The SAR derived classification maps of the Pantanal are either restricted to a single habitat, such as lakes (Costa and Telmer, 2006), or are limited by a coarse spatial resolution imagery (Evans et al., 2010). Therefore, the primary goal of this research is to define on a regional scale the distribution of the variety of habitats in the Lower Nhecolândia sub-region of the Pantanal, using a dual-season set of fine spatial resolution C-band and L-band SAR imagery, employing a hierarchical object-based image analysis approach.

2.2 Study Area

The Pantanal wetlands of South America are one of the largest and most important tropical wetland ecosystems globally, covering an area of approximately 160 000km^2 during maximum inundation (Junk et al., 2006). The Pantanal is primarily located in west

central Brazil, with roughly 10% reaching into Paraguay and Bolivia. The Paraguay River, its tributaries, and the rainfall patterns of the region, support an annual flood regime that varies both temporally and spatially, and helps to characterize the geomorphology and the abundance of biodiversity in the Pantanal ecosystem (Hamilton et al., 1996; Junk et al., 2006). The Pantanal wetland is comprised of a number of floodplain subregions with particular characteristics in terms of ecology, hydrology and geomorphology. Flooding in these subregions is distinctly seasonal, but the timing varies between subregions due to the slow passage and delayed release of floodwaters (Hamilton et al., 1996; 2002).

The Lower Nhecolândia subregion of the Pantanal, the focused area of study for this paper, is located in the south-central Pantanal – northwest latitude, longitude and southeast latitude, longitude: 18°40'S, 57°02'W and 19°35'S, 55°32'W, respectively. This subregion, as defined in Hamilton et al. (1996), is bordered by the Negro River to the south and the Taquari River to the north and occupies an area of approximately 8220 km^2 (Figure 2.1). This subregion exhibits a high diversity of flora and fauna species, and is greater in terms of wildlife species richness and abundance than the rest of the Pantanal due to its high environmental heterogeneity. Because of this high diversity of wildlife, the Lower Nhecolândia subregion is the focus of several threatened species home range studies, including: the marsh deer (*Blastocerus dichotomus*) (Tomas et al., 2000), jaguar (*Panthera onca*) (Cavalcanti & Gese, 2009), and the giant anteater (*Myrmecophaga tridactyla*) (Medri & Mourão, 2005), as well as studies focused on abundance of fish communities in the aquatic habitats (Suarez et al., 2004), deforestation as a result of cattle ranching (Seidl et al., 2000), and wildlife habitat selection studies (Desbiez et al., 2009). Specifically, Desbiez et al. (2009) identifies several key landscapes at a local scale

selected by native mammalian species, including: floodplain landscape (Pampas deer, capybara); *cerrado* (savanna) (crab-eating fox); forest (peccaries, howler monkeys, coati, southern anteater, ocelot, and jaguar); scrub grassland (giant anteater); and forest-edge (grey brocket deer, and southern anteater). Some of these landscape categories, such as forest, are of key importance as night time shelter for species that prefer open grasslands during the day, and also as vital refuges for all terrestrial species during times of extreme flooding, as they occur at slightly higher elevations (Desbiez et al., 2009). Furthermore, aquatic habitats play an important role for many bird species during drought periods (Donatelli, 2001), and temporary waterways formed during flood periods provide vital migration corridors for many fish species (Fernandes et al., 2010). The aquatic macrophytes found in these waterways, as well as within the numerous fresh-water lakes, are an important food source for white-lipped peccaries during periods when fruits are scarce, and saline lakes are key habitats for large concentrations of wading birds (Donatelli, 2001).

An important component of habitat diversity in Lower Nhecolândia is its monomodal flooding cycle, with high waters occurring from February to April, and low waters from August to November (Hamilton et al., 1996). Lower Nhecolândia has a relatively closed drainage system with little connection to major fluvial systems, and an abundance of small lakes/ponds (Pott & Pott, 2011a). The region has a highly heterogeneous and dynamic landscape, with forest, savanna, wild grasslands, introduced pastures, seasonal waterways, herbaceous vegetation, aquatic macrophytes and numerous lakes locally called *baías, salobras,* and *salinas,* all occurring in close proximity to each other (Figure 2.1). However, the internal phytogeography of this entire region is still

inadequately documented (Pott et al., 2011). At a broad scale, the habitats in the Lower Nhecolândia region are characterized by 1) woody vegetation (*cerrado/cerradão*); 2) herbaceous vegetation (*campos*); and, 3) frequently and/or permanently aquatic or swampy terrain, although there is not always a definitive boundary between these three landscapes. Characterization of the smaller scale habitats as described by several authors are outlined in Table 2.1 (Por, 1995; Pott & Pott, 2000, 2011a, 2011b; Campos Filho, 2002; Nunes da Cunha et al., 2007; Nunes da Cunha & Junk, 2011; Pott et al., 2011), with field photos of the corresponding classes in Figure 2.2.

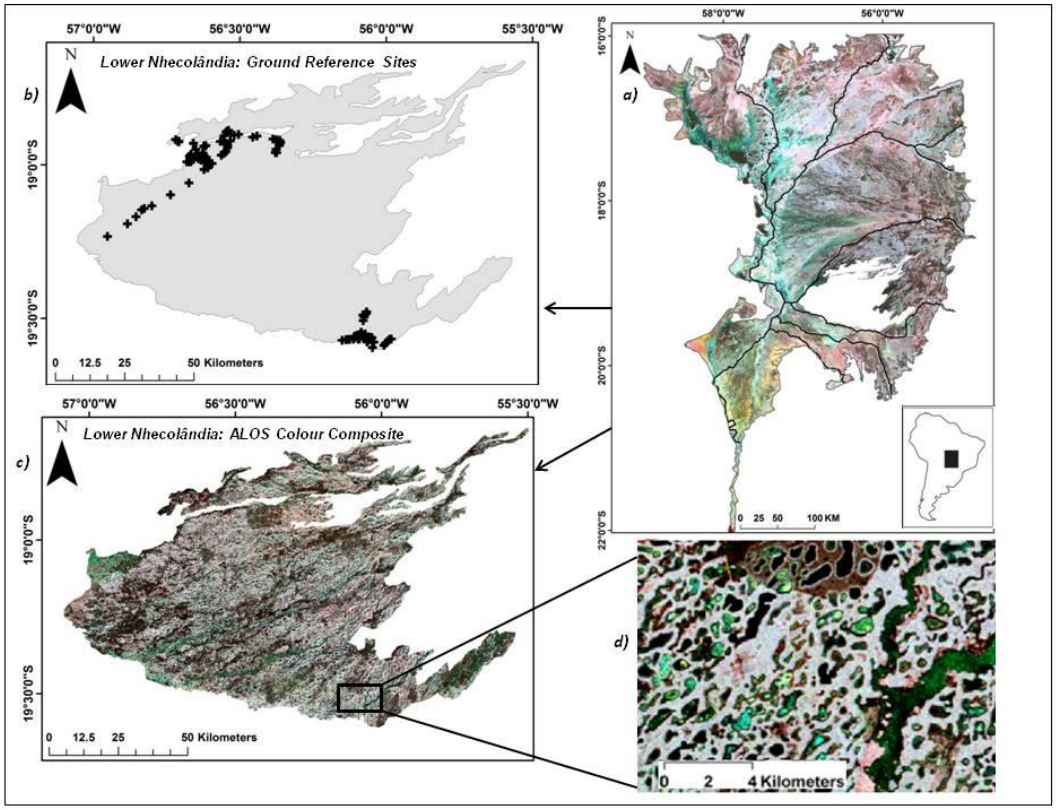

Figure 2.1: Study Area a) The Pantanal wetland ALOS PALSAR colour composite (R-wet season HH; G-dry season HH; B-dry season HV); major waterways shown in black; b) Lower Nhecolândia subregion vector (Hamilton et al., 1996) showing location of ground reference data sites acquired in 2008; c) ALOS PALSAR colour composite of Lower Nhecolândia; d) Zoom inset of (c) imagery showing the high heterogeneity of landscape features.

Table 2.1 Class descriptions: Characterization of habitats of the Lower Nhecolândia subregion (Por, 1995; Pott and Pott, 2000, 2011a, 2011b; Campos Filho, 2002; Nunes da Cunha et al., 2007; 2011; Pott et al., 2011).

Broad Class	Sub Class		Description
Forest Woodland (*Cerradão*)			Dry woody vegetation presenting xeromorphic features; (*cerradão* is characterized by a denser forested canopy than *cerrado*) (**Figure 2.2a**).
	Cordilleira		Elongated elevation in the floodplain with a width of ~100m, a length of up to several kilometres and an elevation of 1-3m above the floodplain; covered with *cerrado/cerradão* vegetation (paleo-levees).
	Capão		Round or oval "island" with a diameter of several tens to a few hundred meters, reaching ~1.5m above the floodplain; covered with *cerrado/cerradão* vegetation.
Open Wood Savanna (open *cerrado*)			Mixed vegetation with shrubs, and scattered trees up to 10m tall on a grassy/herbaceous stratum; may be periodically flooded by excess rainwater and/or by rivers, river channels, or seasonal floodways (**Figure 2.2b**).
Grasslands *(campos)*			Plains area periodically flooded by excess rainwater and/or by rivers, river channels, or seasonal floodways.
	Open Grass Savanna (*campo sujo*)		Predominantly grassy/herbaceous terrain with sparse, scattered trees and/or shrubs, shrub grassland (**Figure 2.2c**).
	Swampy Grasslands (*campo limpo*)		Grassland/herbaceous terrain without woody vegetation, covered by grasses, sedges and herbaceous plants during dry phase, and by aquatic macrophytes during flood (**Figure 2.2d**)
		Campinas	Circular-shaped *campo* 100-300m in diameter surrounded by *cordilheiras*; advanced successional stages of former lakes filled in by sediments that are typically flooded for up to six months by rainwater, ground water and/or flood runoff
		Campo de baixada	Grassy herbaceous cover on low lying areas adjacent to lakes.
Agriculture			Introduced/cultivated pasture and crops, anthropogenic in nature; introduced exotic pastures dominated by *Brachiaria sp*. (**Figure 2.2e**).
Vazantes			Temporary seasonal drainage channels of upstream rainwater runoff from *campos* inhabiting shallow canals where herbaceous/shrubby vegetation grows, but also including amphibious and emergent aquatic species and floating macrophytes during flood (**Figure 2.2f**).
Lakes			Tens of thousands of geochemically diverse lakes
	Baias		Fresh water, floating and emergent aquatic vegetation - pH <9 and TDS <1000 mg/L (**Figure 2.2g**)
	Salobras		Fresh water, characterized by large stands of Typhaceae – typically higher pH and TDS than majority of Baias (**Figure 2.2h**)
	Salinas		Brackish water, no emergent aquatic vegetation - pH >9 and TDS 1000-10000 mg/L (**Figure 2.2i**)

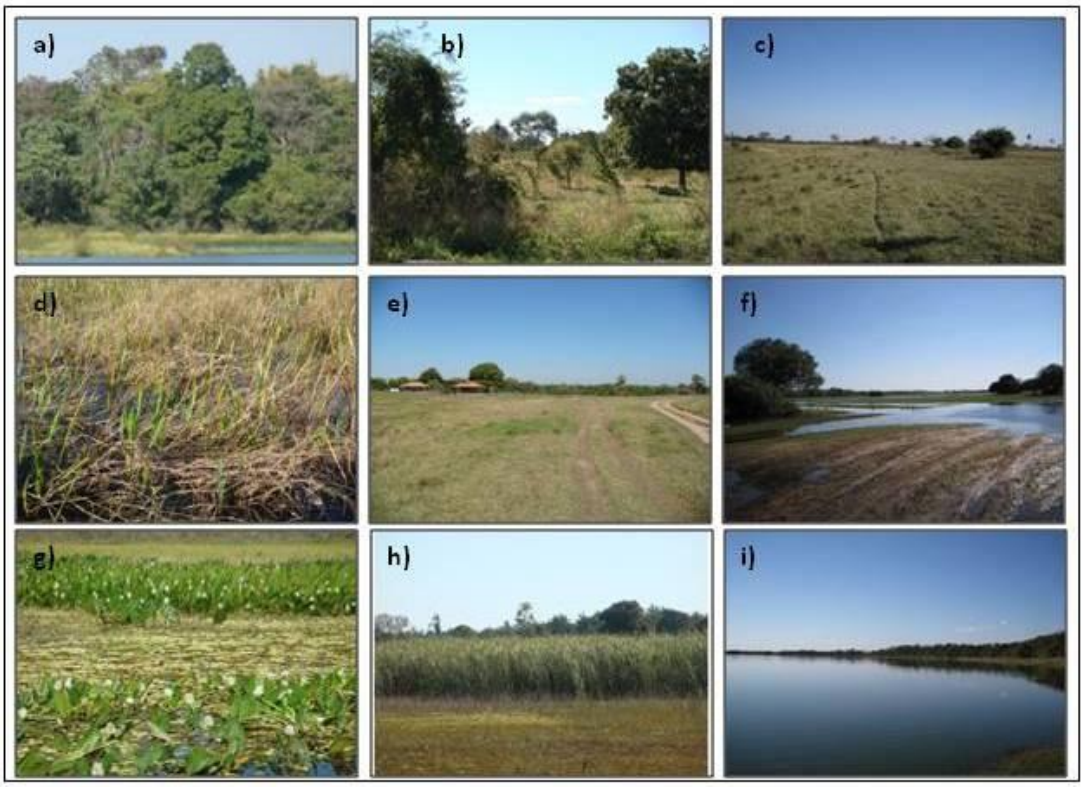

Figure 2.2: Ground reference photos showing land cover units observed in Lower Nhecolândia: a) Forest Woodland - FOR**, b) Open Wood Savanna -** OWS**, c) Open Grass Savanna -** OGS**, d) Swampy Grassland -** GRA**, e) Agriculture -** AGR**, f) Vazantes -** VAZ**, g) Fresh Water Lake – floating and emergent aquatic vegetation (Baía) –** L-AV**, h) Fresh Water Lake – Typha sp. (Salobra) –** L-TYP**, i) Brackish Lake (Salina) –** L-BR**.**

The Lower Nhecolândia region is globally unique, consisting of tens of thousands of geochemically diverse lakes, generally divided into three categories: two classes of fresh water lakes (locally known as *baías* and *salobras*), and brackish lakes (locally known as *salinas*) (Almeida et al., 2003; Galvão et al., 2003; Costa & Telmer, 2006). *Baías* and *salobras* vary in size seasonally, typically expanding and connecting through water channels in the high water season, and shrinking considerably in the dry season. *Baías* are colonized by a variety of floating/emergent aquatic vegetation. *Salobras* can also be colonized by floating and emergent aquatic vegetation, but are distinguished from *baías* by large stands of *Typhaceae*. *Baías* and *salobras* are both fresh water lakes, typically presenting a pH <9 and TDS <1000 mg/L; however, *salobras* generally have a higher pH and TDS concentration than the majority of *baías* (Eaton, 2001; Almeida et al., 2003; Costa & Telmer, 2006). The emergent aquatic vegetation of these lakes essentially falls into two categories: blade-leaved and broad-leaved plants. The first group is comprised of erectophile plants with blade-like leaves that are densely rooted and grass like. They range in height from 30-300 cm tall and are populated by *Cyperaceae* (including *Eleocharis sp*., *Scirpus sp*. and *Cyperus sp*.), and *Typhaceae* (Costa & Telmer, 2006); again, occurrence of *Typha sp.* is restricted to *salobras*. The second group of broad-leaved plants are floating emergent species that can occur in dense or relatively sparse stands, range in height from 2-30 cm tall, and are dominated by *Pontederiaceae* (*Pontedera sp*., *Eicchornia sp*.), *Araceae* (*Pistia stratiotes*), *Salviniaceae* (*Salvinia auriculata*), and *Nymphaeaceae (Nymphaea sp*.) (Por, 1995; Pott & Pott, 2000; Costa & Telmer, 2006). This class of broad-leaved vegetation can be either rooted floating plants or free-floating plants, and are an important primary producer of the Pantanal (Por, 1995).

Salinas tend to be permanent, rounded depressions ~500-1000 m in diameter, 0.5-3.0 m lower in elevation than *baías* and *salobras*, and are cut off from the flood by sandy barriers (*cordilheiras*) which have an elevation 2-3 m higher than the *salinas* (Barbiero et al., 2002; Almeida et al., 2003). Consequently, the majority of *salinas* do not have surface water connections to other water bodies (Eaton, 2001). *Salinas* are devoid of any emergent aquatic vegetation and typically present a pH >9 and TDS 1000-10000 mg/L (Eaton, 2001; Almeida et al., 2003; Costa & Telmer, 2006).

2.3 Methods

2.3.1 Field Data

Field data were acquired for 209 ground sites and 75 lakes in July of 2008. Preliminary analysis of 2007 ALOS PALSAR imagery, Landsat ETM, and field data acquired in 2001, provided the approximate location of regions to be surveyed in the 2008 campaign. In addition, 55 lakes visited in the 2001 campaign were also used as ground reference data for this classification. Some of the ground reference data for the lake sites from the 2001 campaign were comprised of vegetation description only, and were lacking water geochemistry information. Spatial distribution of different land cover and vegetation characteristics (approximate height and dominant species) for a radius of approximately 100 m were determined, photographed, and recorded in visual observation diagrams for the sampling sites. Photographs included differing vegetation species/cover, and north, east, south and west views at each sampling site. For the lakes, vegetation characteristics (species and distribution) were determined from direct observation, then recorded in visual observation diagrams and photographed for each location. Additionally, the same lakes were sampled to characterize the diverse lake types according to the water geochemistry. The relationship between lake water geochemistry and associated

vegetation was defined by Costa & Telmer (2006), and the authors provided a method to use radar imagery to classify the types of lakes in the Pantanal. The method is based on the premise that certain assemblages of vegetation, and therefore the resultant radar backscattering signal, characterize specific types of lake, allowing the classification of lake geochemistry based on the backscattering signal.

The lakes geochemistry was determined by measuring water quality parameters *in situ* (pH) with a handheld multiparameter Y.S.I (model 556), and alkalinity was measured using a HACH digital titrator. In addition, triplicate water samples were collected from each of the lakes for subsequent laboratory analysis of major ions. The water samples were collected at a depth of approximately 20cm and were filtered on site through Millipore 0.45 μm HVLP polyvinyl membranes, preserved and transported back to the laboratory. A Dionex DX-600 ion chromatograph was used to analyze major dissolved cations and anions, and a VG PQII ICO-MS for determining trace elements. The precision and accuracy of these methods were determined by replicate analysis to be better than +/- 7%. With HCO_3^{-1} determined *in situ* via titration, together with the anion and cation constituents, the total dissolved solids (TDS) concentrations were calculated.

From a total of 130 lakes (2001 and 2008 field campaigns) 7 were not usable for this classification as they fell outside of the Lower Nhecolândia border; from the remaining, 60 were used as training samples, and 61 were held back for validation and subsequent accuracy assessment of the classification.

Lakes were coded based on vegetation characteristics observed in the field: 1) floating and/or emergent vegetation only; 2) floating and/or emergent vegetation with the presence of *Typha sp.*; and, 3) absence of above water vegetation. Statistical analysis was

performed to ascertain relationships between observed lake vegetation and water geochemistry parameters (pH and TDS) in order to determine whether or not lake vegetation characteristics are an indicator of water geochemistry. In order to ascertain whether the pH and TDS mean values for the different lake types were significantly different, a Dunnett's T3 post hoc difference of means test was performed because sample sizes were not equal and were relatively small (<50) (Dunnett, 1980; Stoline, 1981).

2.3.2 Satellite Data

L-band images from ALOS/PALSAR were acquired for January/February 2008 (12.5m, HH polarization) coinciding with high water, and for August/September 2008 (12.5m, HH and HV polarization) coinciding with low water and the field campaign. ALOS/PALSAR images were acquired as part of the JAXA ALOS Kyoto and Carbon Initiative – Pantanal. C-band images from RADARSAT-2, obtained as part of the Canadian Space Agency's Science and Operational Applications Research (SOAR) program, were acquired for August 2008 (25m, HH and HV polarization) coinciding with low water and field campaign. Additional C-band data for high water was acquired in February/March 2010 from ENVISAT/ASAR (12.5m, HH and HV polarization), as a part of an agreement with the European Space Agency (ESA). General characteristics of the data are provided in Table 2.2. Images were acquired at a pre-processed level, and thus already radiometrically calibrated for incidence angle and radiometric distortions for RADARSAT-2, ALOS/PALSAR, and ENVISAT/ASAR (Luscombe, 2009; Shimada et al., 2009; Rosich & Meadows, 2004, respectively).

Table 2.2 SAR imagery dataset

SAR Imagery Dataset Characteristics									
Sensor	*Processing Level*	*Band*	*Polarization*	*Spatial Resolution (m)*	*Swath Width (km)*	*Incidence Angle (°)*	*dates (dd/mm/yyyy)*	*scene ID (frame-path)*	*Season*
ALOS PALSAR fine beam mode	1.5	L-band (23.6cm)	HH	12.5	40	34.3	27/01/2008	74-6790	Wet
								74-6800	
								74-6810	
							01/02/2008	77-6790	
								77-6800	
							13/02/2008	75-6790	
								75-6800	
								75-6810	
							01/03/2008	76-6790	
								76-6800	
								76-6810	
			HH/HV				29/07/2008	74-6790	Dry
								74-6800	
								74-6810	
							15/08/2008	75-6790	
								75-6800	
								75-6810	
							01/09/2008	76-6790	
								76-6800	
								76-6810	
							18/09/2008	77-6790	
								77-6800	
ENVISAT ASAR ASA_APP_1P	1P	C-band (5.5cm)	HH/HV	12.5	30	36	11/02/2010	439-3987	Wet
								439-4005	
							27/02/2010	167-3987	
								167-4005	
							15/03/2010	396-3987	
								396-4005	
RADARSAT-2 S4 beam mode	1-SGF	C-band (5.5cm)	HH/HV	25	25	36.5	04/08/2008	91715	Dry
								91728	
								91741	
							11/08/2008	91304	
								91317	
								91330	
RADARSAT-2 S5 beam mode						39.2	22/11/2008	90901	
								90913	
								90927	

2.3.3 Image Processing Steps

Step 1: Radiometric Calibration

ALOS/PALSAR level 1.5 image files were processed using MapReady V 2.3.6 calibration tools made available by the Alaskan SAR facility, using provided geometric and radiometric data. RADARSAT-2 level 1-SGF images were processed and orthorectified using PCI Orthoengine, a SAR specific satellite orbiting model. ENVISAT/ASAR level 1P images were processed using calibration tools included in the Next ESA SAR toolbox, provided by ESA.

Step 2: Geometry and Mosaicking

Primary data geocoding was executed using provider software packages (mentioned above). Images were georeferenced and projected to UTM coordinates (zone 21, row K) using the WGS84 reference ellipsoid. Each set of images were mosaicked to form cohesive coverage of the study area. Cross-sensor geometric inconsistencies were corrected using the RADARSAT-2 mosaic as a master and using a second order polynomial approach (RMS error < 1 pixel). The Lower Nhecolândia subregion vector based on Hamilton et al. (1996) was then utilized to delineate the study area from the mosaics.

Step 3: Speckle Filtering

Images were filtered to reduce the effect of speckle by utilizing a Kuan filter with a 3 x 3 kernel (Evans et al., 2010). The resultant imagery showed preservation of the mean values, while decreasing the standard deviation of homogenous targets, and visually preserving the feature edges (Oliver & Quegan, 2004).

Step 4: Backscattering Analysis and OBIA Classification

The classification was performed using an OBIA approach, executed using the eCognition software package (V.8.0). The OBIA approach to land cover classification offers several advantages over pixel-based classification methods. OBIA supports examination of features (such as mean and standard deviation of object radiometry, and object size and shape) and spatial and hierarchical relationships of objects rather than single pixels. It allows for easy fusion of data from multiple sources, at varying spatial and spectral resolutions, significantly increasing the amount of information that can be extracted for a given area. Specifically for SAR imagery classifications, an OBIA approach is advantageous because of the nature of the original radiometric signal; for example, the signal of each target must be approximated by averaging backscattering across a neighbourhood of pixels to decrease the effects of speckle (Laur, 1997).

Initially, image objects are created by a segmentation process, and provide a more intuitive representation of ground features in comparison to traditional pixel-based classifications (Comber et al., 2010). The initial multi-resolution segmentation is a region-merging algorithm that begins with a single pixel and a pairwise comparison of its neighbours with the goal of minimizing the resulting summed heterogeneity (Benz et al., 2001). Segmentation parameters are data, scale, and research goal specific, thus the user must incorporate a "trial and error" method for determining the ideal inputs for their purpose, based on their knowledge and expertise (Blaschke & Hay, 2001). The multi-resolution segmentation algorithm in eCognition is controlled by three user-defined parameters: *scale, shape* and *compactness*. The *scale* parameter determines the maximum allowable heterogeneity of the image objects, and varies the size of the resulting image objects; for example, larger scale values produce larger objects. The *shape* parameter

determines the degree of influence of radiometry versus object shape in the delineation of image objects. Input values range between 0-1; smaller values result in objects optimized for radiometric homogeneity, higher values optimize for shape homogeneity (Esch et al., 2008). *Compactness* also varies between 0 and 1, and determines the degree of smoothing for object borders. Different sets of parameters were tested, and optimal values selected separately for the classification of land cover and lakes in the Lower Nhecolândia region.

Usually, segmentation is followed by a hierarchical rule-based approach to classify resultant image objects. Hierarchical classification rules are developed according to user-defined parameters, which are supported by field data and expert knowledge, and can be refined iteratively based on results throughout the process. This method allows for the addition of new rules or datasets without compromising predefined rules, while traditional methods such as maximum likelihood or minimum distance may alter the rules of all classes concurrently based on new information (Lucas et al., 2007).

The general adopted approach was as follows:

Step 4.1 Data Exploration and Backscattering Analysis

A primary multiresolution segmentation was performed using an optimal set of parameters for creating image objects sized appropriately to represent landscape features such as small lakes as individual entities: scale = 50; shape = 0.005 (heavily emphasizing radiometry over shape); compactness = 0.5 (equal emphasis on smoothness and compactness); and, more heavily weighting the dry season imagery to better separate the lakes from seasonal flooding areas.

Training image objects were defined on the segmented layer, and were selected based on approximately 50% of the ground reference data (the remaining 50% was held

back for subsequent validation of the finished product). In many cases, individual ground reference points were utilized for more than one training object where photographs were available showing variable vegetation cover in different directions, or where available information expressed more than one vegetation cover (ie. "forest-grassland border"). Individual pixel intensity values were extracted from training objects representative of land cover classes observed in the field for subsequent backscattering analysis. In addition, training object mean intensity values were exported, and standard deviation of the means were calculated for each class, to aid in creating class thresholds. All intensity values were then converted to normalized backscattering coefficients (σ^0) expressed in dB (the standard units for reporting SAR backscattering) in order to facilitate comparison with relevant literature. The conversion process for ALOS/PALSAR (from DN values) is as follows:

$$\sigma^0 = 10*\log_{10} (DN^2) + CF \qquad \text{(Equation 2.1)}$$

where CF is the calibration coefficient for PALSAR standard products, and equals –83 dB (Rosenqvist et al., 2007).

For RADARSAT-2 images (from intensity values), conversion was performed as follows:

$$C = (DN^2 + B) / A \qquad \text{(Equation 2.2)}$$

where C is the calibrated value; B is the offset; and A is the range-dependant gain, both supplied in the LUT file (MDA, 2008). The calibrated values were then expressed in dB via the following calculation:

$$\sigma^0 = 10*\log(C) \qquad \text{(Equation 2.3)}$$

For ENVISAT/ASAR images (from intensity values), σ^0 was derived from the absolute calibration constant (K) via the following calculation (Rosich & Meadows, 2004):

$$\sigma^0 = (DN^2/K)*\sin \alpha \qquad \text{(Equation 2. 4)}$$

where: K = absolute calibration constant

DN^2 = pixel intensity value

σ = sigma nought

α = incidence angle

A backscattering separability analysis was performed by: 1) examining the distribution of pixel backscattering coefficients for each class via box-and-whisker plots (Figure 2.3) in order to gain a broad understanding of the radiometric characteristics of each thematic class, as well as the pixel value variability found within each class, and to compare the backscattering characteristics of the present classes with previous relevant studies (Dobson et al., 1996; Hess et al., 2003; Costa, 2004; Costa & Telmer, 2006; Evans et al., 2010) and, 2) performing a Dunnett's T3 post hoc difference of means test for defining the statistical separability among classes. The Dunnett's T3 analysis further aided in defining which satellite imagery mosaics were the most useful for separating different cover types based on object mean σ^0 values.

Step 4.2 Classification

Figure 2.4 shows the general hierarchical classification scheme for all levels. The general classification scheme was divided into three levels: Level 1 separated the lakes from the rest of the terrain ("Lakes", "Not Lakes"); Level 2 classified all land cover ("Not Lakes"); and, Level 3 classified the "Lakes" based on the vegetation and geochemistry

relationship. In addition to the knowledge gained from the backscattering analysis of the radiometric signatures of the classes (Figure 2.3), the class thresholds for each set of imagery were obtained via calculating the mean +/- 1 standard deviation of the means of all the training objects for each class. The graphs in Figure 2.5 show a visual representation of the range of mean values within which the class samples lie, +/- 1 standard deviation of the means. These ranges were used as a preliminary guide for building mean thresholds for each of the classes.

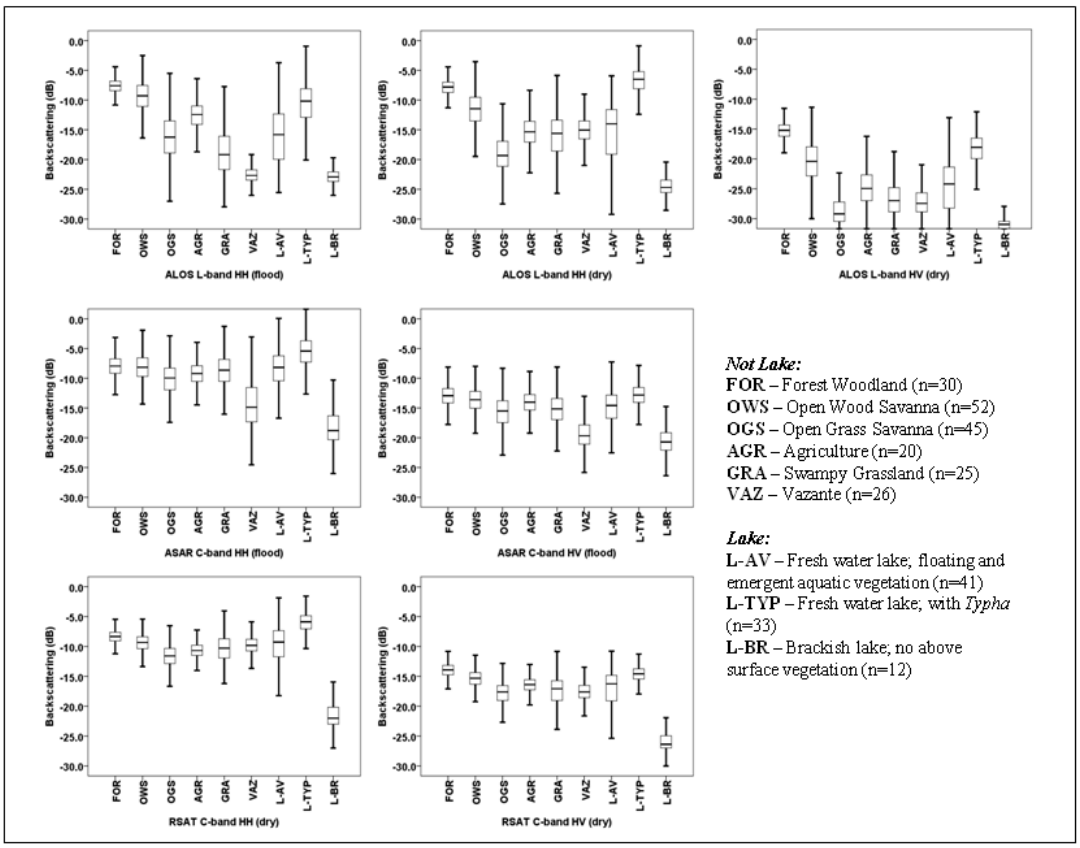

Figure 2.3: Box-and-whiskers diagram of backscattering coefficients for thematic classes derived from pixels values extracted from training objects. Black bar within box indicates median; boxes represent 25th to 75th percentile and whiskers extend to minimum and maximum values (excluding outliers). Number of pixels per image object >300 in all cases.

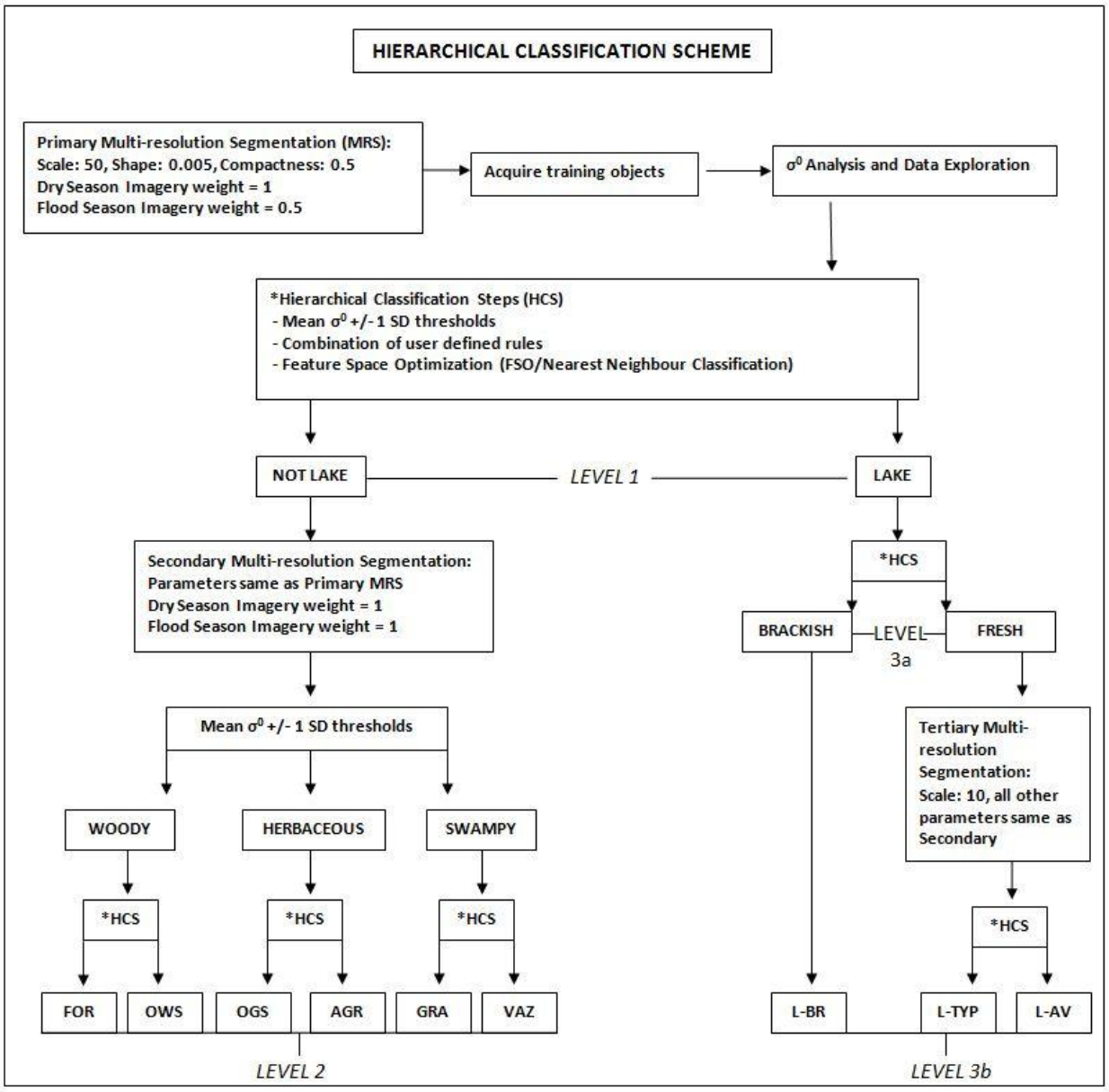

Figure 2.4: Hierarchical classification scheme

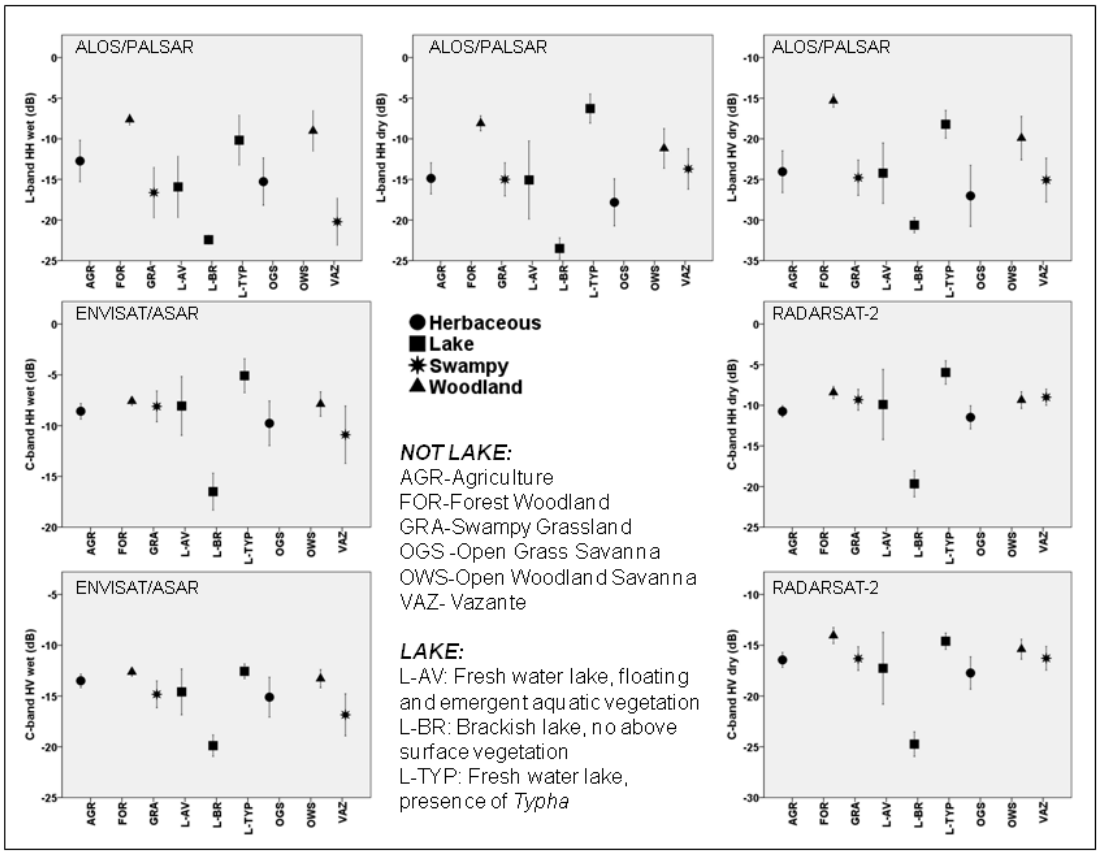

Figure 2.5: Mean threshold analysis based on average of sample object means +/- 1 SD of the means

The general rule-set at each level of classification was as follows: 1) Thresholds were built for each class based on mean backscattering separability and expert knowledge; thresholds were based on more than one image (how many images and which images were decided based on the images deemed best for isolating the class from all other classes, considering band, polarization, and seasonal mean backscattering differences), and used the "AND" operator: for example threshold for class *x* = mean +/- 1 SD in image *a,* AND mean +/- 1 SD in image *b,* AND mean +/- 1 SD in image *c*. This method aided in dealing with the overlap between class object backscattering in any one particular image. 2) Utilization of a supervised nearest neighbour algorithm employing a combination of several features as primary inputs (mean, standard deviation, brightness, maximum difference, proximity, shape and compactness) using the feature space optimization (FSO) routine in eCognition Developer V. 8. The FSO routine compares the training objects for selected classes with respect to the user selected features, and finds the combination of features that produces the largest average minimum distance between the objects of the given classes. FSO input features, imagery, and objects were specific to each task and changed with each iteration. 3) If confusion between two classes was still evident, subsequent iterations of the FSO routine refining the input parameters was performed.

Step 4.2.1 Level 1: Separation of "Lakes" from "Not Lakes"

Image objects generated in the primary multi-resolution segmentation (step 4.1) were deemed appropriate for this level of classification, so no further segmentation was performed at this stage. To separate lakes from the rest of the terrain, basic thresholds were built for each of the classes. This primary classification was aided by the analysis of

the σ^0 variability of pixels extracted from training objects (step 4.1). Given the mean spectral similarity between lake surface covered with aquatic vegetation and areas of seasonal flooding (*vazantes*) also characterized by the presence of aquatic vegetation, as well as the mean spectral similarity between *Typha sp.* present on lakes and Forest Woodland (Figs. 3 and 5), mean backscattering thresholds alone were not sufficient to separate the lakes classes from spectrally similar terrain. For this level, object standard deviation, compactness, size, and proximity parameters were employed in the FSO routine to further discriminate "Lakes" from "Not Lakes". These parameters were particularly useful as in most cases, lakes objects were fairly compact, small and isolated compared to spectrally similar classes such as forest woodland or *vazantes*. For example, a freshwater lake exhibiting aquatic vegetation presents a small, compact image object, typically surrounded by a terrestrial class (forest woodland, open grass savanna, etc.). However, an image object representing the *vazantes* class may appear spectrally similar to the fresh water lake in terms of mean backscattering values, but the object shape is less compact due to the sinuous nature of the *vazantes*, and is found adjacent to other *vazantes* objects. Thus, the "Lake" class is separable from the "Not Lake" class via parameters other than object mean backscattering. For the Level 2 classification, objects classified as "Lakes" were disregarded until subsequent separation into three lake types at Level 3.

Step 4.2.2 Level 2: Land Cover Classification ("Not Lakes")

At this stage, a second multi-resolution segmentation was performed with the same parameters as the primary segmentation, except flood and dry season imagery were given equal weight in the segmentation process in order to exploit the differences in σ^0 signature due to the seasonal variability of the different habitats. Only regions previously classified

as “Not Lakes” in Level 1 were considered at this level. Again, an object oriented supervised classification was performed based on the field data and backscattering analysis of the different classes, as well as visual interpretation of high spatial resolution optical imagery and expert knowledge. Land cover units were classified using a combination of σ^0 thresholds based on training object σ^0 mean values +/- 1 SD (Figure 2.5). Resultant classes and remaining unclassified objects were further classified and refined using the FSO routine and several combinations of features and images as primary inputs (mean, standard deviation, brightness, maximum difference, shape, compactness).This classification resulted in six land cover classifications for Level 2: Forest Woodland (FOR – Figure 2.2a); Open Wood Savanna (OWS – Figure 2.2b); Open Grass Savanna (OGS – Figure 2.2c); Agriculture (AGR – Figure 2.2d); Swampy Grassland (GRA – Figure 2.2e); and *Vazantes* (VAZ – Figure 2.2f).

Step 4.2.3 Level 3: Lakes Classification

The Level 3 classification considered only the “Lakes” mask from Level 1; all other objects were classified at Level 2 and were removed from further consideration. Two further options for Level 3 were defined:

Level 3 (a) Based on the backscattering analysis and the image objects created in the Level 1 classification, the lakes class was further divided into “fresh water lakes” (lakes with a combination of floating and emergent vegetation – *baías,* Figure 2.2g, and lakes with *Typha sp. - salobras,* Figure 2.2h) and “brackish lakes” (lakes with no vegetation – *salinas,* Figure 2.2i). At this stage simple object mean σ^0 thresholds were sufficient to separate fresh water from brackish, and so no FSO routine was performed.

Level 3 (b) A third multi-resolution segmentation was performed only on the "fresh water lakes" defined in the Level 3a classification, using the same parameters as the previous segmentation, however this time, the scale parameter was lowered to 10 to allow for much finer image objects, and a more detailed classification using σ^0 thresholds. In addition, the FSO routine was employed, using standard deviation, maximum brightness and compactness as primary inputs. The same training lakes used in the Level 3(a) classification were utilized for Level 3(b), but the more refined image objects allowed for greater distinction between floating and emergent vegetation, and stands of *Typha sp.*, that may have been combined in a single image object at Level 3(a), thus allowing the classification of *baía* (no *Typha sp.*) and *salobra* (with *Typha sp.*) lakes.

Step 5: Validation of the Classification Results (Levels 2 and 3)

For Level 2, classification results were compared to field data held back for validation purposes. A total of 147 validating image objects were tested against field data for classification accuracy. This validation data was supplemented by a set of 150 randomly generated points across the study area (Stehman, 1996; Silva et al., 2010), which were classified through visual interpretation of ALOS Advanced Visible and Near-Infrared (AVNIR-2) sensor (processing level 1B2, 10 m spatial resolution, four images acquired January 20, 2007 and three images acquired February 02, 2007) obtained from JAXA, Landsat ETM (30 m spatial resolution, acquired April 2002), as well as Landsat ETM (30 m spatial resolution, acquired December 2007) and IKONOS (4 m spatial resolution, acquired in July 2006 and 2007) imagery available in GoogleEarth Pro. Level 3 classification results were compared only to validating objects for which ground reference data was available.

The following accuracy measurements were calculated for both Level 2 and Level 3 classifications: overall (%) accuracy (percentage of validation points corresponding to correctly classified areas for the whole image); commission errors (the ratio of correctly classified objects to the total number of classified objects in each class); and, omission errors (the ratio of correctly classified image objects to the total number of validation objects in each class) (Congalton 1991).

2.4 Results

2.4.1 Backscattering Analysis - Not Lakes

The statistical distribution of backscattering coefficients for the various cover types are shown in Figure 2.3. Each box extends from the 25^{th} to 75^{th} percentile, thus showing the middle half (50%) of the data, with the whiskers extending to the minimum and maximum values (outliers excluded). The number of pixels per training object were always higher than 300.

The backscattering analysis indicated a high degree of similarity between the Woody classes (Forest Woodland – FOR and Open Woodland Savanna – OWS), particularly at C-band: HH and HV polarizations, for both classes, wet and dry season. L-band dry season σ^0 showed better separation for these two classes, with median Forest Woodland approximately 3.0 dB higher than median Open Woodland Savanna at HH polarization, and 4.0 dB higher for the HV polarization, although L-band wet season σ^0 showed a small difference between the two classes. The range of σ^0 values was low for the Forest Woodland class for all imagery, but higher for the Open Wood Savanna class, particularly at L-band. Overall, with the exception of the *Typha sp.* class, these two woodland classes showed the highest overall distribution of σ^0 values for both L-band

and C-band, at both seasons, although the dry season imagery showed slightly lower σ^0 than the wet season imagery for both classes.

The Herbaceous classes (Agriculture - AGR and Open Grass Savanna - OGS) showed a great degree of overlap for all imagery, although median values for Open Grass Savanna were generally 3.0 dB and 1.0 dB lower than Agriculture for all L-band and C-band imagery, respectively. For both L-band and C-band, median σ^0 values were approximately 2.0-3.0 dB lower in the dry season as compared to the wet season (comparing like-polarizations).

No clear separation for σ^0 values was apparent for the Swampy areas (*Vazantes* - VAZ and Swampy Grassland - GRA) during the dry season. The difference between median σ^0 values for Swampy Grassland and *Vazantes* was <1.0 dB for all dry season imagery. However, there was a considerable difference between the two classes for the wet season, with Swampy Grassland exhibiting 3.0-4.0 dB higher median values than *Vazantes* for both L and C-bands. The Vazantes class showed a greater range of σ^0 values compared to Swampy Grasslands, particularly at L-band.

The Dunnett's T3 difference of means analysis (Table 2.3) on the σ^0 values of the different classes showed further confirmation of the difficulty involved in separating these classes based on object mean σ^0 values alone. The test also confirmed the need of a multi-image approach for the classification. Generally, this test showed that 1) L-band imagery was the most useful for separating the woody classes (FOR and OWS) from all other classes, 2) C-band wet season imagery was most useful for separating the herbaceous classes (AGR and OGS) from the swampy classes (GRA and VAZ), and 3)

C-band dry season imagery was most useful for separating GRA and VAZ, and for separating AGR and OGS.

Table 2.3 Dunnett's T3 difference of mean analysis: boxes shaded gray denote pairs of mean values that do not come from significantly different populations at a 95% confidence level (AGR-Agriculture; L-AV-Fresh water lake with floating and emergent aquatic vegetation; FOR-Forest Woodland; OGS-Open Grass Savanna; GRA-Swampy Grassland; L-BR-Brackish lake; OWS-Open Wood Savanna; L-TYP-Fresh water lake with the presence of Typha sp.; VAZ-Vazante).

ALOS wet-HH	AGR	L-AV	FOR	OGS	GRA	L-BR	OWS	L-TYP	VAZ
AGR		.047	.000	.275	.089	.000	.000	.241	.000
L-AV	.047		.000	1.000	1.000	.000	.000	.016	.405
FOR	.000	.000		.000	.000	.000	.002	.817	.000
OGS	.275	1.000	.000		1.000	.000	.000	.029	.066
GRA	.089	1.000	.000	1.000		.031	.000	.012	.987
L-BR	.000	.000	.000	.000	.031		.000	.000	.258
OWS	.000	.000	.002	.000	.000	.000		1.000	.000
L-TYP	.241	.016	.817	.029	.012	.000	1.000		.002
VAZ	.000	.405	.000	.066	.987	.258	.000	.002	

ALOS dry-HH	AGR	L-AV	FOR	OGS	GRA	L-BR	OWS	L-TYP	VAZ
AGR		.879	.000	.111	.204	.000	.000	.000	.018
L-AV	.879		.000	.002	.004	.000	.001	.000	.891
FOR	.000	.000		.000	.000	.000	.000	.007	.000
OGS	.111	.002	.000		1.000	.000	.000	.000	.000
GRA	.204	.004	.000	1.000		.051	.000	.000	.000
L-BR	.000	.000	.000	.000	.051		.000	.000	.000
OWS	.000	.001	.000	.000	.000	.000		.000	.434
L-TYP	.000	.000	.007	.000	.000	.000	.000		.000
VAZ	.018	.891	.000	.000	.000	.000	.434	.000	

ALOS dry-HV	AGR	L-AV	FOR	OGS	GRA	L-BR	OWS	L-TYP	VAZ
AGR		1.000	.000	1.000	.243	.001	.000	.000	1.000
L-AV	1.000		.000	1.000	.030	.000	.000	.000	1.000
FOR	.000	.000		.000	.000	.000	.000	.000	.000
OGS	1.000	1.000	.000		.981	.072	.000	.000	1.000
GRA	.243	.030	.000	.981		.727	.000	.000	.093
L-BR	.001	.000	.000	.072	.727		.000	.000	.000
OWS	.000	.000	.000	.000	.000	.000		.029	.000
L-TYP	.000	.000	.000	.000	.000	.000	.029		.000
VAZ	1.000	1.000	.000	1.000	.093	.000	.000	.000	

ASAR wet-HH	AGR	L-AV	FOR	OGS	GRA	L-BR	OWS	L-TYP	VAZ
AGR		.248	.001	1.000	.027	.000	.039	.000	.005
L-AV	.248		1.000	.107	.000	.000	1.000	.000	.000
FOR	.001	1.000		.000	.000	.000	1.000	.000	.000
OGS	1.000	.107	.000		.161	.000	.012	.000	.056
GRA	.027	.000	.000	.161		.000	.000	.000	1.000
L-BR	.000	.000	.000	.000	.000		.000	.000	.000
OWS	.039	1.000	1.000	.012	.000	.000		.000	.000
L-TYP	.000	.000	.000	.000	.000	.000	.000		.000
VAZ	.005	.000	.000	.056	1.000	.000	.000	.000	

ASAR wet-HV	AGR	L-AV	FOR	OGS	GRA	L-BR	OWS	L-TYP	VAZ
AGR		.815	.002	.941	.000	.000	.999	.001	.000
L-AV	.815		.000	1.000	.011	.000	.107	.000	.000
FOR	.002	.000		.000	.000	.000	.001	1.000	.000
OGS	.941	1.000	.000		.002	.000	.188	.000	.000
GRA	.000	.011	.000	.002		.000	.000	.000	1.000
L-BR	.000	.000	.000	.000	.000		.000	.000	.000
OWS	.999	.107	.001	.188	.000	.000		.003	.000
L-TYP	.001	.000	1.000	.000	.000	.000	.003		.000
VAZ	.000	.000	.000	.000	1.000	.000	.000	.000	

RSAT dry-HH	AGR	L-AV	FOR	OGS	GRA	L-BR	OWS	L-TYP	VAZ
AGR		.012	.000	.187	1.000	.000	.000	.000	.000
L-AV	.012		1.000	.001	.007	.000	.969	.000	1.000
FOR	.000	1.000		.000	.000	.000	.000	.000	1.000
OGS	.187	.001	.000		1.000	.000	.000	.000	.000
GRA	1.000	.007	.000	1.000		.000	.002	.000	.000
L-BR	.000	.000	.000	.000	.000		.000	.000	.000
OWS	.000	.969	.000	.000	.002	.000		.000	.033
L-TYP	.000	.000	.000	.000	.000	.000	.000		.000
VAZ	.000	1.000	1.000	.000	.000	.000	.033	.000	

RSAT dry-HV	AGR	L-AV	FOR	OGS	GRA	L-BR	OWS	L-TYP	VAZ
AGR		1.000	.000	.021	.126	.000	.000	.000	.158
L-AV	1.000		.000	.338	.310	.000	.191	.000	.899
FOR	.000	.000		.000	.000	.000	.000	.089	.000
OGS	.021	.338	.000		1.000	.000	.000	.000	.000
GRA	.126	.310	.000	1.000		.000	.000	.000	.000
L-BR	.000	.000	.000	.000	.000		.000	.000	.000
OWS	.000	.191	.000	.000	.000	.000		.004	1.000
L-TYP	.000	.000	.089	.000	.000	.000	.004		.007
VAZ	.158	.899	.000	.000	.000	.000	1.000	.007	

2.4.2 Lake Geochemistry and Backscattering Analysis - Lakes

Figure 2.6 shows the ranges of both TDS and pH for the different classes of lake. The scatterplot generally shows separation in terms of pH; from the sampled lakes, all lakes with vegetation (fresh - *baías* and *salobras*) had a pH approximately ranging from 5.0 to 9.0, and those with no vegetation (brackish - *salinas*) > 9.0. However, grouping via TDS was not as well-defined; in general, fresh water lakes contained total TDS ≤ 500 mg/L, and brackish 500 mg/L to 2500 mg/L, but a few outliers were present.

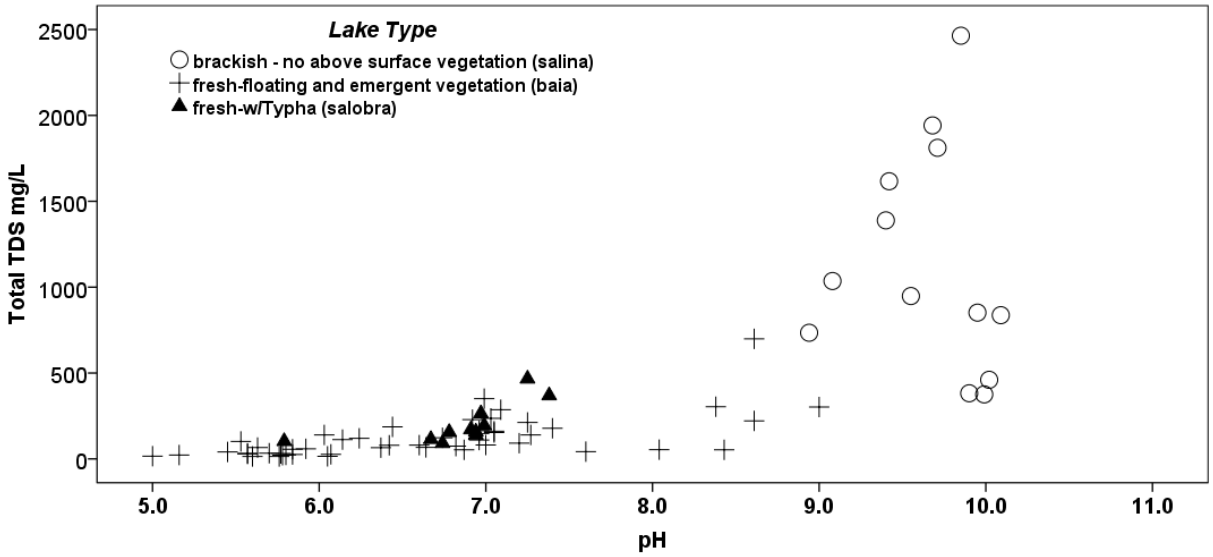

Figure 2.6: Ranges of TDS and pH for different classes of lake/vegetation assemblages

Dunnett's T3 analysis determined that both fresh water lakes with floating and emergent vegetation only, as well as fresh water lakes with the presence of *Typha sp.* showed significant difference in mean values from brackish lakes at a 95% confidence level using TDS and pH water geochemistry parameters (p-values of 0.001 and 0.000, respectively). However, the separation was not considered significant between fresh water (*baías*), and fresh water with *Typha sp.* (*salobras*) (p-values of 0.144 and 0.519 for TDS and pH, respectively). While no straightforward separation was found to distinguish these two fresh water lakes by their geochemistry, the association between lake vegetation and geochemistry suggests that there is an optimal range of approximately, pH 6.8–8.0, and TDS 100-500 mg/L preferred by *Typha sp.* in Lower Nhecolândia (Figure 2.6) generally corresponding with values reported for *Typha sp*. globally (Eaton, 2001; Muasya et al., 2004; Ah et al., 2007; Mufarrege et al., 2011).

Backscattering analysis was performed using the training objects from the three lake categories to determine which combination of band/polarization/season was best able to separate the three lake types (Figure 2.3). The results showed that fresh water vegetation (floating and emergent) lakes (*Baias*) exhibited high σ^0 variability, regardless of band or season. Median σ^0 values for this vegetation class were approximately -14.0 dB at L-band, HH for both flood and dry season, and -23.0 dB for L-band HV, and the variability was slightly lower in the dry season than the wet season. For C-band, variability was slightly lower than at L-band, particularly in the dry season; however, median σ^0 was higher in the wet season at both polarizations (-7.5 dB for HH and -14.0 dB for HV compared to -9.0 dB HH and -16.5dB HV for dry), and both wet and dry season showed higher median σ^0 values at C-band than at L-band.

Brackish lakes (*Salinas*) exhibited the lowest σ^0 values and the lowest variability overall for all imagery. Median σ^0 values were approximately -23.0 dB at L-band HH, flood and dry seasons, and -30.0 dB and at HV polarization, dry season. *Salinas* showed a greater range of values at C-band than at L-band, and median σ^0 values were slightly higher (-18.0 dB and -20.0 dB for wet, and -22.0 dB for HH and -25.0 for dry, HH and HV, respectively).

Fresh water lakes with the presence of *Typha sp.* (*Salobras*) exhibited the highest overall σ^0 values for all imagery, with median values of approximately -6.0 dB and -9.0 dB for L-band HH dry and wet seasons, and -17.0 dB for L-band HV dry season. C-band median σ^0 values for the wet season were -5.0 and -12.5 dB for HH and HV, and for dry season were -5.5 dB and -14.5 dB for HH and HV, respectively. *Typha* σ^0 values also showed a high degree of variability in the wet season compared to the dry season.

The Dunnett's T3 analysis on the mean σ^0 values for the three lake types (Table 2.3) revealed significantly different populations, and therefore the lake types should be separable via a combination of the mean σ^0 thresholds for each of the sets of imagery. One expectation was the lower separability between L-AV and L-TYP for the ALOS HH wet season image.

2.4.3 Classification

2.4.3.1 Level 2 - Land Cover (Not Lakes)

The Level 2 classification map (Figure 2.7) shows the distribution of land cover units distinguishable at 12.5 m spatial resolution: Forest Woodland (~1790 km^2, 22% total land cover); Open Wood Savanna (~1270 km^2, 15% total land cover); Open Grass Savanna (~2230 km^2, 27% total land cover); Agriculture (~300 km^2, 4% total land

cover); Swampy Grassland (~940 km^2, 12% total land cover); *Vazante* (~520 km^2, 6% total land cover); and Lakes (~1170 km^2, 14% total land cover).

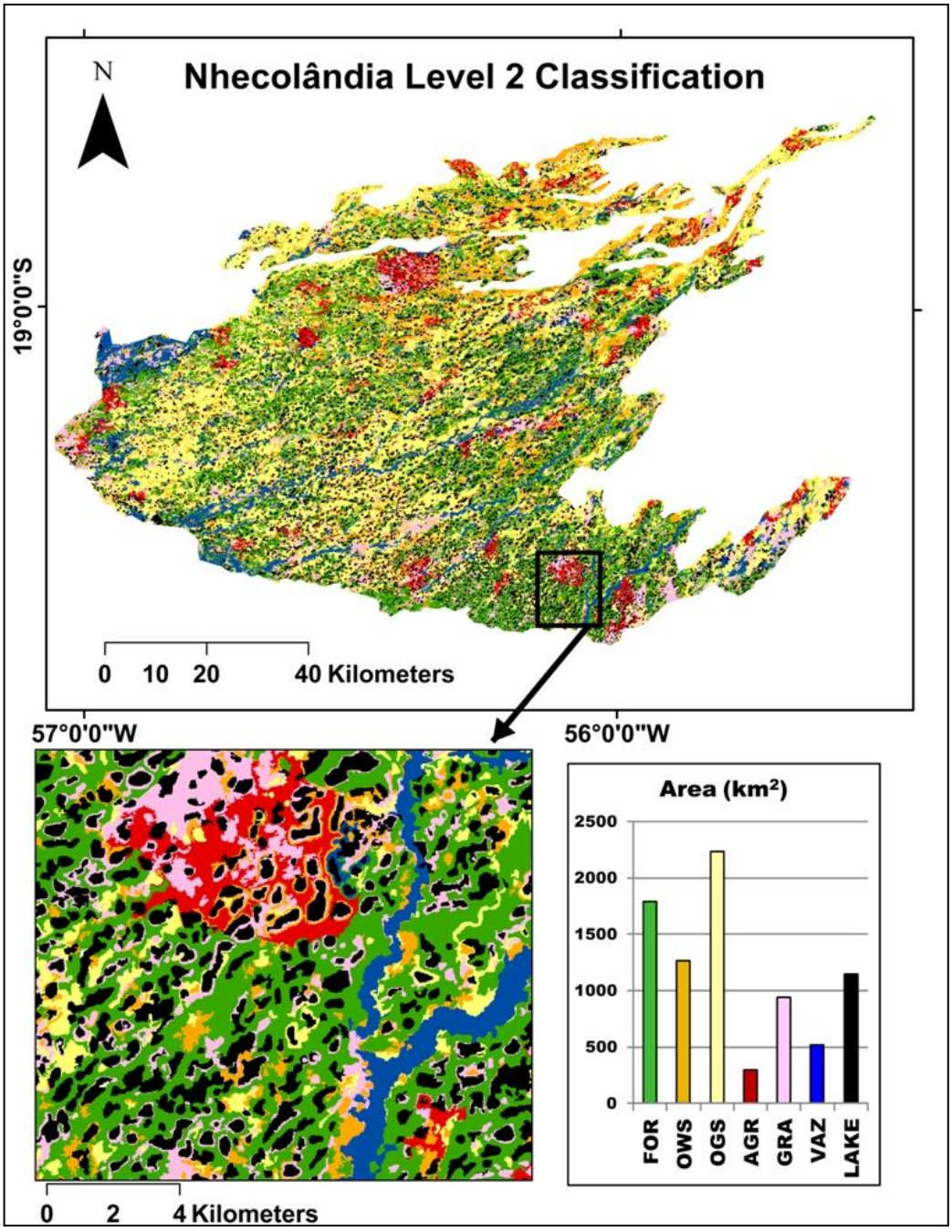

Figure 2.7: Level 2 classification: FOR (Forest Woodland); OWS (Open Wood Savanna); OGS (Open Grass Savanna); AGR (Agriculture); GRA (Swampy Grassland); VAZ (Vazante); LAKE (all Lakes).

The overall accuracy of Level 2 was 83%, with Forest Woodland correctly classified in 85% of cases, Open Wood Savanna in 79%, Open Grass Savanna in 81%, Agriculture in 81%, Swampy Grassland in 68%, *Vazante* in 74% and Lakes in 90% of cases (Table 2.4). The largest confusion was found in the Swampy Grassland class (omission error 32%, commission error 30%), where ~6% of validation data was misclassified as *Vazante*, and ~26% misclassified as Open Grass Savanna (omission errors). 14% of the *Vazante* class, and a small percentage (<5% each) of Open Grass Savanna, Agriculture and Lakes were erroneously classified as Swampy Grassland (commission error). Similarly, the greatest confusion for the *Vazante* class was found with Swampy Grassland, and to a lesser degree, Open Grass Savanna, Agriculture and Lake (overall omission error of 26% and commission error of 23%). In general, the greatest confusion for all classes was found with adjacent successional classes: for example, Forest Woodland with Open Wood Savanna; Open Wood Savanna with Forest Woodland and Open Grass Savanna; Swampy Grassland with *Vazante* and Open Grass Savanna.

Table 2.4 Accuracy assessment, levels 2 and 3a-b

LEVEL 2		CLASSIFIED AS								
		Forest Woodland	Open Wood Savanna	Open Grass Savanna	Agriculture	Swampy Grassland	Vazante	Lake	Row Total	Error of Omission(%)
REFERENCE DATA	Forest Woodland	39	5	2	0	0	0	0	46	15
	Open Wood Savanna	2	27	3	1	0	1	0	34	21
	Open Grass Savanna	1	2	38	0	1	2	0	44	14
	Agriculture	0	1	2	21	1	1	0	26	19
	Swampy Grassland	0	0	9	0	23	2	0	34	32
	Vazante	0	0	1	1	4	20	1	27	26
	Lake	0	0	4	0	4	0	78	86	9
	Column Total	42	35	59	23	33	26	79	297	
	Error of Commission (%)	7	23	36	9	30	23	1	overall accuracy (% correct)=	83

LEVEL 3a		CLASSIFIED AS			
		Fresh Water Lakes - Baias, Salobras	Brackish Lakes - Salinas	Row Total	Error of Omission(%)
REFERENCE DATA	Fresh Water Lakes - Baias, Salobras	46	1	47	2
	Brackish Lakes - Salinas	0	11	11	0
	Column Total	46	12	58	
	Error of Commission (%)	0	92	overall accuracy (% correct)=	98

LEVEL 3b		CLASSIFIED AS				
		Floating and Emergent Aquatic Vegetation (Baia)	Presence of *Typha sp. (Salobra)*	No Above-Surface Vegetation (Salina)	Row Total	Error of Omission(%)
REFERENCE DATA	Floating and Emergent Aquatic Vegetation (Baia)	27	3	1	31	13
	Presence of *Typha sp.(Salobra)*	7	9	0	16	44
	No Above-Surface Vegetation (Salina)	0	0	11	11	0
	Column Total	34	12	12	58	
	Error of Commission (%)	21	25	8	overall accuracy (% correct)=	81

2.4.3.2 Level 3 - Lakes

The Level 3a classification map shows the broad distribution of fresh (shown together in green and red) and brackish lakes (shown in blue) in the Lower Nhecolândia region of the Pantanal (Figure 2.8). An overall accuracy of 98% was achieved at this level. The only misclassification was a single fresh water lake classified as brackish.

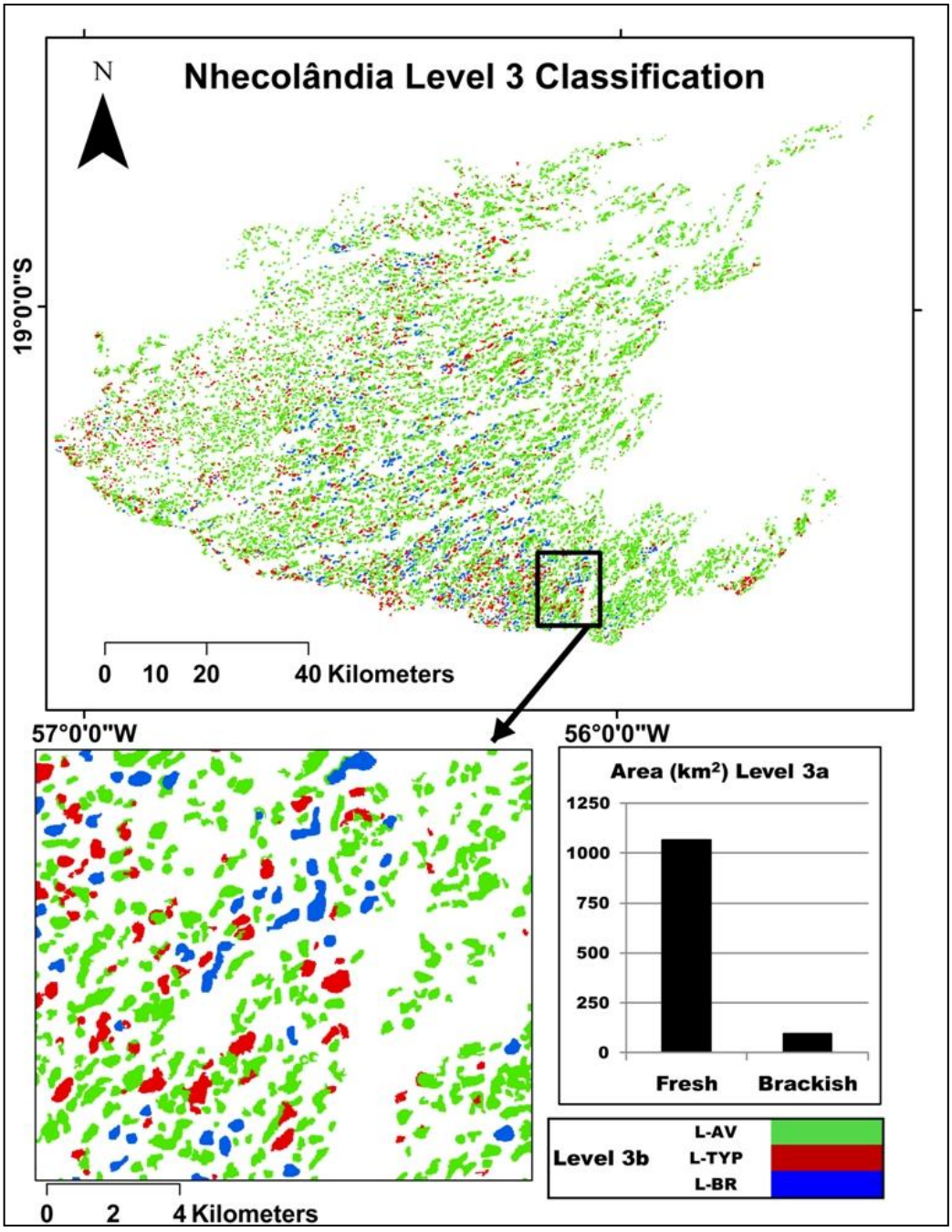

Figure 2.8: Level 3 classification: Level 3a (Fresh Water and Brackish Water); Level 3b: L-AV (Fresh Water Lake, floating and emergent vegetation only, *baías*); L-TYP (Fresh Water Lake, presence of *Typha, salobras*); L-BR (Brackish Lake, no above surface vegetation - *salinas*).

This classification map also shows the finer separation of aquatic vegetation into floating/emergent (*baías*), and *Typha* classes (*salobras*) (Level 3b). For this level, an overall accuracy of 81% was achieved. The largest confusion, and thus the highest error of omission (44%), and error of commission (25%) was for the *Typha* class, where approximately less than half of *salobras* (with *Typha sp*.) observed in the field were misclassified as *baías*. Out of a total area of ~1170 km^2 for lakes in the Lower Nhecolândia region, ~1070 km^2 was classified as fresh water (*baías* and *salobras*) and ~100 km^2 was classified as brackish water (*salinas*).

2.5 Discussion

2.5.1 Backscattering Analysis – Not Lakes

Overall, with the exception of the *Typha sp.* class, the Forest Woodland and Open Wood Savanna classes showed the highest overall median σ^0 values for both L-band (23.6cm) and C-band (5.5cm), both seasons (Figure 2.3), as a result of the likely dominance of volumetric and multiple scattering mechanisms (Henderson & Lewis, 2008; Silva et al., 2010; Dobson et al., 1996), and were comparable to values reported for similar cover types (Hess et al., 1995; Wang et al., 1994; Evans et al., 2010).

For the Forest Woodland class, the multiple scattering mechanisms are likely due to interactions with the various components present in forested regions including: backscatter from the canopy surface directly back to the sensor; volume scattering within the canopy; multiple interactions of the canopy and the ground; and double-bounce scattering (Wang et al., 1994; Dobson et al., 1996; Silva et al., 2008). At the long wavelength of L-band, the leaves of the canopy are quasi-transparent, thus the radiation penetrates through to interact with branches, trunks and the underlying surface. The combination of all of these components results in a higher σ^0 return than other cover

types. However, for this class, the σ^0 values are slightly lower in C-band HH (median value approximately -8 to -7 dB) than in L-band HH (median value approximately -6 dB) as a result of dominance of volume scattering within the canopy at C-band, as suggested in Wang et al. (1994).

Conversely, the σ^0 values observed for Open Wood Savanna suggests the interaction of energy not only with forest but also grasslands. Herbaceous vegetation can be partially transparent at L-band (Dobson et al., 1996), contributing to the lower overall σ^0 values found with the Open Wood Savanna class compared to the Forest Woodland class at L-band. Lower returns from open woodlands (compared to forest) can be attributed to the interaction of L-band energy with smaller stems and branches, and increased ground scatter away from the sensor as a result of the more open canopy (Lucas et al., 2010).

The low variability of the σ^0 values (Figure 2.3) of the Forest Woodland class is due to the homogeneity of the relatively closed forest canopy (Figure 2.2a); conversely, the mixed vegetation nature of the Open Woodland Savanna class (tree, shrub, and grass species) (Figure 2.2b) contributes to the relatively higher degree of variability, which also results in the slightly lower median σ^0 values for this class (Figure 2.3). These woodland classes showed slightly lower median σ^0 values in the dry season imagery compared to the wet season imagery, possibly due to a lower dielectric content of the vegetation due to the dry conditions (Dobson et al., 1996).

Compared to the Woody classes, Agriculture and Open Grass Savanna had relatively lower median σ^0 values at L-band. This is because the longer wavelength of L-band renders some of the smaller vegetation transparent to the incoming radiation and

causes a specular reflection away from the sensor, thereby reducing the overall σ^0 signal, although volumetric scattering is still present within the denser, taller vegetation (Dobson et al., 1996; Hill et al., 1999). At C-band, the primary scattering mechanism with this type of short vegetation and sparse trees is expected to be volumetric scattering (Dobson et al., 1996), resulting in a relatively high σ^0 return – this accounts for the similarity in σ^0 values between the herbaceous classes and the woody classes at C-band.

The similarity in median σ^0 values between the herbaceous classes (Agriculture and Open Grass Savanna) can be attributed to the similarity in vegetation cover – both are primarily grassland with sparse woody vegetation; however the Agriculture class may have a slightly higher degree of woody vegetation, and in some cases, man-made structures, which may contribute to higher overall σ^0 values at L-band due to double-bounce mechanisms. We also speculate that the consistent σ^0 difference may be due to different vegetation species inhabiting the Agriculture class compared to the Open Grass Savanna. Typically the introduced pasture characteristic of the Agriculture class is dominated by *Brachiaria decumbens* and *Brachiaria humidicola* (Alho et al., 2011). These non-indigenous, high biomass species may contribute to a higher overall median σ^0 value than native grasslands. Similarly, Hill et al. (1999) found that thick, lush, herbaceous pastures had a σ^0 value as high as –8.8 dB at L-band. The relatively lower σ^0 values for the dry season, compared to wet season, are likely a result of the lack of precipitation resulting in senescence of the vegetation which may reduce the biomass and dielectric component and, thus, the overall σ^0 signal (Dobson et al., 1996).

Overall, our results were consistent with those reported in Evans et al. (2010) for both L and C-band ALOS ScanSAR data with the exception of the Open Grass Savanna

class, where σ^0 values were approximately 2.0 dB lower than those observed for their Non-Floodable Grasslands class. In the present study, no assumptions were made about the possibility of flooding occurring in the Open Grass Savanna class, therefore it is possible that some flooding may occur, thereby lowering the overall σ^0 value for this class. As both studies were conducted in the same region, we speculate that the difference in values at L-band could also be due to the much coarser spatial resolution used for the Evans et al. study (50-100 m compared to 12.5 m for the present study), thus representing a pixel size that may incorporate other vegetation types.

The swampy classes (Swampy Grassland and *Vazantes*), in particular the *Vazantes* class, displayed the lowest σ^0 values at both L and C-band during the wet season, compared to the dry season. This is a result of 1) a lack of any woody vegetation within these classes, and 2) the presence of water, causing a decrease in overall σ^0 values as a result of specular reflection (Silva et al., 2008). The lack of separation via σ^0 values between the Swampy Grassland and *Vazantes* classes for all dry season imagery is due to the similarity in the characteristics of these cover types during this season: both exhibit a combination of herbaceous grass and some aquatic vegetation, and both have reduced water components (compared to the wet season imagery) due to run-off, evaporation, and lack of rain. In the wet season, the *Vazantes* class exhibits lower σ^0 values than Swampy Grassland due to the greater water component providing increased specular reflection (Dobson et al., 1996). During the wet season, the *Vazantes* act as natural flood spillways transporting the majority of run-off to rivers, whereas the Swampy Grasslands class should exhibit relatively shallow water and a greater cover of herbaceous vegetation, increasing the σ^0 signal. This difference in cover also contributes to the higher σ^0

variability for the Swampy Grassland class in the wet season: during the wet season at maximum flood, *Vazantes* are relatively homogenous large areas of open moving water, while the Swampy Grassland class is characterized by a mix of shallow water and herbaceous vegetation.

For these specific classes, *Vazantes* and Swampy Grassland, the observed L-band σ^0 values were approximately 5.0 dB higher than those reported in Evans et al. (2010), although the observed C-band dry season results were comparable. As mentioned previously, we speculate that the difference in values at L-band is likely a result of the different spatial resolutions of the imagery.

2.5.2 Lake Geochemistry and Backscattering Analysis - Lakes

Overall, the measured pH ranges for fresh water lakes (5.0 - 9.0) and brackish lakes (> 9.0) are within the range of those reported in literature for these lake types in the Pantanal (Eaton, 2001; Almeida et al., 2011). Also, the measured TDS values for freshwater lakes (<500 mg/L) and for brackish lakes (>500 mg/L) are in agreement with those previously reported (Almeida et al., 2011); however, a comparison of the measured TDS concentrations with those reported in Costa & Telmer (2006) shows that some of the brackish lakes exhibited slightly lower TDS concentrations than Costa & Telmer's range of 1000 – 10000 mg/L, and many of the fresh water lakes had greater TDS concentrations than the reported range of <100 mg/L. This may be due to the greater number of sampled lakes in this study (75 lakes sampled for TDS compared to Costa & Telmer's 11) providing a greater variability in water quality parameters – in fact, a large diversity in water quality parameters has been observed for both fresh and brackish lakes in Lower Nhecolândia (Almeida et al., 2003; 2011).

The combination of the geochemical analysis with the different types of above water vegetation, or lack of it, suggested that the fresh water class may be further divided in two groups: lakes colonized by floating and emergent aquatic vegetation only, locally called *baías*, and lakes with the presence of *Typha sp*., alone or in combination with floating and emergent aquatic vegetation, locally called *salobras* (Pott & Pott, 2000; Eaton, 2001; Costa & Telmer, 2006). The results of this study suggest that there is a pH and TDS range preferred by *Typha sp.*, and those lakes exhibiting pH and TDS values above these ranges, while not yet *Salinas* may not be the preferential habitat for *Typha sp*. The TDS concentrations for *Salobras* do fall within the optimal range of 100 to 1000 mg/L reported in Costa and Telmer (2006), albeit at the lower end of the range, and pH around 7.0, consistent with that reported in Eaton (2001), as well as being generally in agreement with other reported values for preferential *Typha sp*. ranges of pH and TDS (Muasya et al., 2004; Ah et al., 2007; Mufarrege et al., 2011). *Salobras* geochemistry shows pH and TDS values that are intermediate compared to *Salinas* and *Baías*. Consequently, they may show an intermediate level of hydrologic isolation, and may be transitional habitats that shift towards *Salinas* in the dry season and towards *Baías* during flood season (Eaton, 2001). Although the mechanisms responsible for the formation of *salinas* is a matter of some debate, it is likely due to combination of a gradual increase in isolation from ground water/surface water recharge, evaporation, and biogeochemical processes happening within the lakes (Barbiero et al., 2002; Almeida et al., 2011).

The scattering mechanisms for *Typha sp.* characteristic of *Salobra* lakes are different from the other aquatic vegetation due to its dense and tall structure. The vertical structure of the vegetation acts as a dihedral corner reflector resulting in a double-bounce

mechanism at C-band, and even occasionally at L-band, greatly increasing the σ^0 signal (Pope et al., 1997; Baghdadi et al., 2001; Silva et al., 2010). This mechanism combined with volumetric scattering within the vegetation structure of the floating and emergent aquatic vegetation present in some of the *Salobras*, is responsible for the high σ^0 values observed at C-band. At L-band, scattering is largely due to volumetric scattering within the *Typha* canopy structure, and, to a lesser degree, volumetric scattering within any of the taller, grass-like vegetation present. Some specular reflection may also be present at L-band, depending on the degree of open water and/or small floating vegetation present in the lake, thereby decreasing the overall σ^0 signal. The relatively higher degrees of variability during the wet season compared to the dry season for this lake type may be due to a higher water level in the lakes corresponding to a decrease in floating and emergent vegetation cover, resulting in more area subject to specular reflection at the wet season. This would not only decrease the overall σ^0 signal, but also the overall variability within the image object. Our findings are consistent with Costa & Telmer (2006) in that the *Salobra* class had the highest observed σ^0 values of the three lake types, and similar σ^0 values at C-band; however, their value of -14.0 dB for dry season L-band HH is considerably lower than our observed -9.5 dB. This is possibly due to the long time gap between L-band imagery acquisition (1993) and observed field observations (2001) in Costa & Telmer's work. *Typha sp*. stands may have colonized these lakes after the imagery acquisition, and therefore would not contribute to overall σ^0 values reported in Costa & Telmer (2006) lakes. As their C-band imagery was acquired concurrent to the field campaign, this issue is not present for C-band analysis. Also, the present observed σ^0 values are slightly lower than those reported in Pope et al. (1997), possibly due to a

steeper incidence angle (~26° for both bands HH polarizations compared to ~34° and 38° in this work for L-band and C-band, respectively) allowing a deeper penetration of the canopy resulting in an increased double-bounce component.

Baias showed a broader range of pH and TDS values generally on the lower end of the scale. These lakes are also mainly colonized with floating broad-leaf vegetation species (approximately < 0.5m in height) and taller grass-like emergent aquatic vegetation species (0.5-1.0m in height). As with the herbaceous vegetation classes, the primary scattering mechanism at C-band is likely comprised of volumetric scattering, and the longer wavelength of L-band renders some of the smaller vegetation transparent to the incoming radiation and causes a specular reflection, thereby reducing the overall σ^0 signal, although again, some volumetric scattering is still expected for the more dense taller grass-like aquatic vegetation. The lower values observed at L-band (-14.0 dB) compared to C-band (approximately -8.0 dB) are due to a mix of volumetric and specular scattering at L-band (Costa et al., 2002; Silva et al, 2008). The observed σ^0 values for both C and L-band (HH) are consistent with those reported in both Costa et al. (2002) for similar aquatic macrophytes in the Amazon, and with Costa & Telmer (2006) for the same vegetation categories in the Pantanal; however, Hess et al. (1995) reported higher values for both C and L-bands HH. We speculate that this is due to differing species of macrophyte and possible a higher degree of the larger grass-type emergent vegetation, as well as a possible higher overall biomass of vegetation occurring in the Amazon compared to the Pantanal *baias*.

Brackish lakes (*salinas*) do not contain any floating or emergent vegetation, and therefore most of the incoming radiation is specularly reflected from the water surface

away from the sensor, resulting in very low σ^0 returns (Dobson et al., 1996). Observed median values of -23.0 db and -30.0 dB for L-band HH and HV polarizations, respectively, are typical for this type of scattering mechanism. However, the C-band σ^0 values for dry season imagery (-18.0 dB HH, and -20.0 dB HV) were higher than expected. This could be a result surface roughness caused by wind at the time of imagery acquisition which could result in higher than expected σ^0 values (Costa & Telmer, 2006). This surface roughness could also account for the higher degree of variability at C-band compared to L-band. These higher σ^0 values and variability at C-band could also be a result of some lake border pixels being incorporated in the generated image objects thereby increasing the overall σ^0 values for these objects as well as the variability. As observed in the field and also reported by others (Novack et al., 2010; Almeida et al., 2011) *salinas* are typically bordered either by sand beaches or short grass, which may be detected at C-band, but not at L-band. Also, *salinas* evaporate and shrink in the dry season (Almeida et al., 2011), possibly resulting in a dry crusted surface around the edges – this increase in surface texture could enhance the overall σ^0 return at C-band. The observed σ^0 values for this study were not consistent with those reported for *salinas* in Costa & Telmer (2006); the authors observed dry season mean σ^0 values of approximately -17.8 dB and -23.5 dB at L and C-band, respectively, which is the opposite of the present findings. However, Costa & Telmer also speculate that there may have been some surface roughness during the time of acquisition of their images thereby increasing σ^0 values as explained above.

2.5.3 Classification and Accuracy Assessment

Overall, the greatest confusion for all Level 2 Classification results was found with adjacent successional classes: for example, Forest Woodland with Open Wood Savanna; Open Wood Savanna with Forest Woodland and Open Grass Savanna; Swampy Grassland with *Vazantes* and Open Grass Savanna, etc. These errors were expected given 1) the similarity of these classes as exhibited in the backscattering analysis, and 2) the highly heterogeneous nature of the landscape. In many cases these habitats are found adjacent to one another, and clear cut borders between the different cover types are not readily apparent, especially given the dynamic nature of the landscape in terms of inundation: *Vazantes* and Swampy Grassland are fundamentally the same type of cover in terms of vegetation structure and inundation characteristics, differentiated only by the defined drainage channel aspect of the *Vazantes* compared to the more amorphous shape of the Swampy Grassland, and the timing and duration of inundation. Similarly, Open Grass Savanna and Agriculture are both, in the context of the study area, essentially different forms of grasslands, and both can exhibit sparsely distributed woodland/shrub vegetation. Forest Woodland and Open Wood Savanna are comprised of differing degrees of woody vegetation with no straightforward border between the two, contributing to the degree of confusion observed between those two classes. As noted in Hoekman et al. (2010) in a landcover classification conducted in Borneo, many classes form continua along a biomass and/or wetness gradient, and when arbitrary ranges are chosen delineating membership to each class, some confusion among adjacent classes is likely.

The only misclassification at Level 3a was a single fresh water lake classified as brackish, likely a result of a minimum of aquatic vegetation at the edges of a large, open

water lake surface being mixed in the same pixels as the surrounding terrain. However, there were also three very small lakes in the testing data that were erroneously classified as "Not Lake" in the primary stage. This was likely due to a combination of factors: the scale parameter chosen for this stage may not have been fine enough to capture lakes of this size; lakes may have been dry at the time of image acquisition (3-6 weeks later than field campaign) thus causing confusion between the lakes and the surrounding terrain.

For the next classification level, Level 3b, the largest confusion, and thus the highest error of omission (44%) and error of commission (25%) was for the *Typha* class, where approximately half of *salobras* were misclassified as *baías*. This confusion is a result of several factors: the stand of *Typha sp.* observed in a lake may have been too small to be captured as a single object; the stand of *Typha sp*. may have been sparse and mixed with other aquatic vegetation, thereby reducing the backscattering signal considerably; *Typha sp.* stands observed in the 2001 field campaign may no longer be present, or may have been reduced in size and/or density.

Comparison of the classification results with other classifications of the Pantanal

The achieved classification results for Levels 2 and 3 will be compared with large scale classification data that encompass at least the Lower Nhecolândia subregion region of the Pantanal. Generally, these are maps produced by GEF (2004), PROBIO (2007), Evans et al. (2010), Costa & Telmer (2006), and Novack et al. (2010). A visual comparison of a combination of the Level 2 and Level 3a classification to the landscape classification map supplied by GEF (2004) based on a mosaic of 5 years of Landsat mosaicked imagery, shows that the current produced map offers a more detailed spatial distribution of habitats in the Lower Nhecolândia region. For instance, the GEF map

classifies the entire region as Savanna (*cerrado),* with minor areas of pasture and water; although this does not necessarily disagree with our assessment, our classification is far more comprehensive, breaking down the *cerrado* class into finer habitats such as Forest Woodland, Open Wood Savanna, Open Grass Savanna, and Swampy Grassland. As such, these two different approaches cannot be compared at the same level; additionally, no accuracy assessment was provided with the GEF classification.

Further visual comparison of the present results with the PROBIO (2007) derived map, which was based on 2002 Landsat imagery acquired from July to October (dry season), shows a considerable amount of agreement between the two. The spatial distribution of both our Forest Woodland, and Agriculture classes correspond well with PROBIO's *Cerradão* and Planted Pasture classes, respectively, and the rest of the region is classified by PROBIO as varying combinations of Forested (*Florestada*), Woody (*Arborizada*) and Grassy (*Gramineo-Lenhosa*) Savannas, thus matching our Forest Woodland, Open Wood Savanna and Open Grass Savanna classes, respectively. PROBIO does not acknowledge *Vazantes* and Swampy Grassland as separate classes from Grassy Savanna, as the authors were not concerned with a flooding dynamic to their classification. Also, the PROBIO map does not include a lake component. The key difference between the generated Level 2/Level3a classification and PROBIO is, again, one of scale: our classification is comprised of much smaller habitats, and therefore offers a more finely detailed output map. As with GEF (2004), the accuracy assessment of the classification map from PROBIO was not included.

Evans et al. (2010) used a combination of C and L-band (50m and 100m spatial resolution, respectively) to map 5 classes for the whole Pantanal wetland using an OBIA

approach with an overall accuracy of 81%. As explained previously, the present classification cannot be reasonably compared with the classification because 1) the Evans et al. work was conducted at a much coarser spatial resolution (100/50m compared to the present 12.5m), and 2) the Lower Nhecolândia subregion of the Pantanal is a highly heterogeneous ecosystem with smaller ecological habitats and a profusion of small lakes compared to the Pantanal as a whole.

A comparison of the present Level 3a results (Fresh Water Lake vs. Brackish Lake) with Novack et al. (2010) Lower Nhecolândia Lakes classification performed using a similar OBIA classification methods, but using ASTER imagery (optical bands, 15m-30m spatial resolution), revealed a much higher overall accuracy of the present classification results (fresh water/brackish water classes - 98%) compared to Novack et al. (80% non-*salina*/*salina* classes). Moreover, Novack et al.'s study was comprised of only a small subset of the Lower Nhecolândia subregion, and did not include a separation of fresh water aquatic vegetation. A more suitable comparison is found with Costa & Telmer (2006)'s lake classification of a larger subset of Lower Nhecolândia using L and C-band HH dry season SAR imagery (JERS-1 and RADARSAT-2, respectively). A visual comparison of the present Level 3a-b classifications with the 2006 Level 1-2 classifications (same classes for both levels) shows general agreement in the spatial distribution of the lakes, however, Costa & Telmer's brackish water is overrepresented compared to the present results. The imagery dataset used for this study included both HH and HV polarization, dual season imagery, which may have resulted in detection of aquatic vegetation not possible with HH polarization only, or the detection of vegetation present only during the wet season. Regardless, the present overall accuracy results are

comparable to the above authors (98% and 81% compared to 91% and 83% for levels 3a/1 and 3b/2 respectively). However, the current study presents a classification of the entire Lower Nhecolândia subregion, and offers an updated spatial distribution map using more recent and comprehensive field data.

Comparison of accuracy assessment results with other similar land cover classification studies

An assessment of our Level 2 accuracy results with several other related studies that consider classes with similar vegetation structure shows comparable results in terms of overall accuracy values (Table 2.5). For instance, using a pixel-based classification method and a combination of Optical and L-band SAR imagery at 12.5m spatial resolution, two African wetlands sites were classified: Lake Chilwa, Malawi, 6 classes, 89% accuracy; and Lake Urema, Mozambique, 5 classes, 84% accuracy (Rebelo, 2010). We speculate that the use of optical data combined with SAR likely resulted in increased accuracy for the African wetland sites. The present classification results were considerably lower than those reported in Amazon wetlands (Costa, 2004) using similar imagery (L and C-band, 12.5 spatial resolution); however, the author only included three wetland classes compared to our total of six classes at Level 2. Conversely, the present classification results were higher than those reported by Walker et al. (2010) for mixed landcover, also in the Amazon; however, Walker included a total of fifteen classes. Overall, given the various reported classification accuracies (Table 2.5), the present study falls well within the acceptable range for classification accuracies of land cover, and specifically, for wetlands.

Table 2.5 Classification results from comparable land cover/wetlands studies

Author	*Sensor(s)*	*Spatial Resolution (m)*	*Classification Method*	*Location*	*Land Cover*	*Number of Classes*	*Overall Accuracy (%)*
Laba et al (2002)	Optical	30	OBIA	New York state	mixed land cover (including wetland)	6	74
Hoekman et al (2010)	L-band SAR	50	pixel based	Borneo	mixed land cover (including wetland)	17	85
Rebelo (2010)	Optical and L-band SAR	12.5	pixel based	Lake Chilwa, Malawi	wetland	6	89
Rebelo (2010)	Optical and L-band SAR	12.5	pixel based	Lake Urema, Malawi	wetland	5	84
Baghdadi et al (2001)	C-band SAR	4	pixel based	Mer Bleue, Canada	wetland	6	77
Durieux et al (2007)	Optical and L-band SAR	100-300	OBIA	West Siberia, Russia	wetland	7	89
Grenier et al (2008)	Optical and C-band SAR	10-20	OBIA	Eastmain Region, Quebec, Canada	wetland	5	81
Li & Chen (2005)	Optical and C-band SAR	12.5-30	Pixel and OBIA	3 sites in Quebec, Canada	wetland	5	71-92
Simard et al (2002)	L and C-band SAR	100-400	pixel based	Gabon, Africa	mixed land cover (including wetland)	10	84
Souza-Filho et al (2011)	airborne L-band SAR	10	pixel based	Bragança coastal plain, Brazil	coastal wetland	4	83
Costa (2004)	L and C-band SAR	12.5	OBIA	Amazon floodplain, Brazil	wetland	3	>95
Hess et al (2003)	L-band SAR	100	pixel based	Amazon basin, Brazil	wetland	8	81
Martinez & le Toan (2007	L-band SAR	12.5	pixel based	Óbidos floodplain, Brazil	wetland	5	81
Walker et al (2010)	Optical and L-band SAR	12.5-30	OBIA	Amazon, Brazil	mixed land cover (including wetland)	15	58
Evans et al (2010)	L and C-band SAR	50-100	OBIA	Pantanal wetlands, Brazil	wetland	5	81
Novack et al (2010)	Optical	15-30	OBIA	Pantanal wetlands, Brazil	lakes	2	80
Costa & Telmer (2006)	L and C-band SAR	12.5	OBIA	Pantanal wetlands, Brazil	lakes	3	83

2.6 Conclusions

The Pantanal wetland provides habitat for a great biodiversity of flora and fauna species, many of them threatened; yet, it is one of the least protected ecosystems with respect to the International Union for Conservation of Nature, with less than 5% of the ecosystem in reserve (Rylands & Brandon, 2005). The Lower Nhecolândia subregion of the Pantanal has some of the highest biodiversity found anywhere in the Pantanal wetland system, and is a globally unique environment due to its tens of thousands of geochemically diverse lakes. Despite its importance, Lower Nhecolândia specifically, is under threat from a number of anthropogenic causes: agrochemicals and other pollutants from farms located outside the subregion, on the surrounding plateau, are contaminating the water supply (da Silva & Girard, 2004). Within this subregion, the removal of endemic vegetation in favour of exotic grasses optimal for cattle grazing, as well as the burning of grasslands to renew pasture and control weeds, have resulted in increased natural habitat loss (Harris et al., 2005; Desbiez et al., 2009). As such, there is a vital need for 1) a detailed account of present habitat spatial distribution; and 2) methods that allow the quantification and monitoring of the occurring changes and impacts in the region so that sustainable management practices and effective conservation units can be established.

The results of this research provide the first fine spatial resolution land cover classification showing the spatial distribution of aquatic, terrestrial and transitional habitats for the entire Lower Nhecolândia subregion of the Pantanal based on a combination of L and C-band, dual polarization, dual season SAR satellite imagery, and using a relatively new object-oriented image analysis approach. The backscattering analysis showed that a single image does not allow for proper separation among the

classes of interest. The combination of dual-season, C and L-band, high spatial resolution imagery was essential for providing a relatively high overall accuracy of 83% for the Level 2 land cover classification, and 98% and 81% for the Levels 3a and 3b lakes classification, respectively. These classification results are well within the overall accuracy ranges reported by similar wetlands studies (Costa & Telmer, 2006; Evans et al., 2010; Rebelo, 2010) especially given the highly heterogeneous nature of the landscape. Additionally, results were consistent with the map produced by PROBIO (2007); however flood dynamic classes and lakes and accuracy assessment were not included in the PROBIO classification. Further, utilizing SAR imagery allowed the advantage of image acquisition year-round regardless of cloud cover, thus allowing classification of dynamic land cover affected by seasonal inundation, while the PROBIO map was compiled using imagery only from July to October, generally during the dry period, due to the lower degree of cloud cover present in this season.

The spatial distribution of these habitats influence the abundance and interactions of animal species, and the change or destruction of this habitat can cause the disturbance of key biological processes. It is therefore imperative to have a detailed classification of the spatial distribution of habitats in this region to better understand species home ranges, migration corridors and consequences of habitat change as a result of natural and anthropogenic disturbances, so that sustainable management practices and effective conservation units can be established.

The produced fine spatial resolution maps will provide vital habitat information for determining refuge zones for terrestrial species, connectivity of aquatic habitats during the dry season and implications for aquatic dependent species, examination of species

distribution as a result of a flood-pulse regime, and risks of environmental changes to the animal population. The generated maps will also provide valuable baseline data to aid in monitoring changes in the region, and to help define conservation strategies for habitat in this wetland.

Chapter 3. Large-Scale Habitat Mapping of the Brazilian Pantanal Wetland: A Synthetic Aperture Radar Approach

Abstract: This study uses 50 m spatial resolution, dual-season L-band ALOS/PALSAR, and C-band RADARSAT-2 data, as well as a comprehensive set of ground reference points, to map the diverse habitats of the hydrologically variant subregions of the Pantanal by using a hierarchical object based image analysis approach. First, mean and standard deviation values of image object training sites were evaluated, and used as the basis for forming preliminary land cover class thresholds for each subregion. Then, a combination of additional refined thresholds, hierarchical rules, and a supervised nearest neighbour algorithm (eCognition feature space optimization) employing several features as primary inputs (mean, standard deviation, seasonal change detection, brightness, maximum difference, shape and compactness) was utilized, resulting in the definition and classification of ten habitat classes: Forest/Woodland, Riparian Forest, Open Wood Savanna, Open Wood Savanna subject to prolonged flooding, Open Grass Savanna, Agriculture, Swampy Grassland, Swampy Mixed Savanna, *Vazantes*, and Water. This classification was achieved with an overall accuracy of 80% for the entire Pantanal. The produced habitat spatial distribution maps will provide vital information for determining refuge zones for terrestrial species, and connectivity of aquatic habitats during the dry season, as well as providing crucial baseline data to aid in monitoring changes in the region, and to help define conservation strategies for habitat in this wetland.

3.1 Introduction

Wetlands throughout the world are recognized as biodiversity hotspots (Mitsch & Gosselink, 2007), particularly large and environmentally heterogeneous wetland systems, which play a key role in biodiversity due to the variety of habitats that provide a multitude of feeding and reproductive niches (Alho, 2008). One such heterogeneous wetland ecosystem, the Pantanal Wetland of South America, is made up of a complex of seasonally inundated floodplains, and is considered a category of temporary wetlands subject to a spatially and temporally variable monomodal flood pulse (Junk et al., 1989). Such seasonally inundated floodplain ecosystems are characterized as being periodically flooded through lateral overflow of the main course of the river(s), as well as through rainfall and run-off channels, resulting in a seasonally dynamic mosaic of aquatic, semi-aquatic, and terrestrial habitats (Junk et al. 1989). The ecotone between aquatic and terrestrial zones shifts location seasonally over the inundation cycle. This variability, combined with local topography, is a key driver of the ecological complexity found in aquatic, semi-aquatic and terrestrial vegetation patterns (Hamilton, 2002a), and thus contributes to a high degree of habitat diversity within the Pantanal expressed by a unique landscape distinguished by different compositions of savanna vegetation, abundant species of aquatic vegetation, and different types of floodplain forests (Abdon et al., 1998; Pott & Pott, 2000; Nunes da Cunha & Junk, 2011). In addition to the floristic diversity, a large number of hydrochemically varied lakes, waterways, and other fluvial geomorphological patterns are observed, generating a complex mosaic of wetland habitats (Por, 1995; Costa & Telmer, 2006; Mariot et al, 2007; Nogueira et al., 2011).

This diversity of habitats support a vast array of flora and fauna: 263 species of fish, 96 species of reptiles, 40 species of amphibians, 170 species of mammals, 463 species of

birds (making it the world's richest single wetland site for birds) (Tubelis & Tomas, 2003), 1903 higher plant species and countless invertebrate species (Junk et al., 2006; Alho, 2011a). Several key species considered threatened outside the Pantanal, including the Marsh Deer (*Blastocerus dichotomus*), Giant River Otter (*Pteronura brasiliensis*), South American Tapir (*Tapirus terrestris*), Giant Anteater (*Myrmecophaga tridactyla*), Jaguar (*Panthera onca*) and Hyacinth Macaw (*Anodorhynchus hyacinthinus*), retain significant populations within this wetland ecosystem (Junk & Nunes da Cunha, 2005; Alho, 2008).

As a result of this rich diversity of habitats and flora and fauna species, the Pantanal wetland was recognized as a "National Heritage" site in the 1988 Constitution of Brazil, and as a Wetland of International Importance in the Ramsar Convention. Referring to its biological distinctiveness, conservation, and priority status, Olson et al. (1998) concluded that the Pantanal is a region that is "globally outstanding, vulnerable and with highest priority for conservation at regional scale." Although still considered a relatively pristine wetland (Junk et al, 2006), the Pantanal is currently under threat as a result of habitat loss and habitat degradation, primarily caused by agricultural pressures occurring both on the surrounding plateau, and increasingly, within the floodplain itself (Seidl et al., 2000; Godoy et al., 2002; Harris et al., 2005; Junk et al., 2006; Alho, 2011b). The expansion of agriculture on the region of the Taquari River Basin located on the plateau east of the Pantanal has significantly increased sedimentation of the Taquari floodplain in the last twenty-five years, resulting in an alteration of the hydrological regime, permanently flooding extensive areas that previously only flooded seasonally (De Souza et al., 2002; Godoy et al., 2002; Harris et al., 2005). Within the floodplain, wildlife habitat loss and/or

degradation linked to cattle ranching has been largely a result of conversion of natural habitats to cattle pasture through deforestation and fire "management" (Alho, 2008a).

The change or destruction of landscape within this spatially complex wetland habitat system can cause the disturbance of key biological processes, such as the abundance and interactions of animal species (Tews et al., 2004; Mitchell, 2005). Furthermore, knowledge regarding the spatial distribution of ecologically significant wildlife habitat is vital in terms of forming baseline data for identifying habitat protection zones, for implementing future change detection studies, and supporting applications in resource management, habitat reconstruction, and species at risk recovery (Tews et al., 2004; Mitchell, 2005). Therefore, developing efficient techniques for mapping wetland vegetation habitats is of critical importance for implementing appropriate conservation strategies.

Classic methods for mapping wetland vegetation habitats have been largely based on ground surveys of soil and vegetation inventories gathered through extensive and time consuming field work requiring ancillary data analysis and visual estimations of ground cover. As a consequence, such methods are only practical on small scales, and do not provide spatially continuous information over large regions (Hewes, 1951; Lee & Lunetta, 1996; Mitsch & Gosselink, 2007). In many cases, remote sensing technology, combined with ground truth data, offers the most economical and reliable process for determining ecologically valuable information regarding the characteristics of habitats, and monitoring environmental changes resulting from anthropogenic or natural processes, across large scales (Kerr & Ostrovsky, 2003). Furthermore, Synthetic Aperture Radar (SAR) imagery has been successfully used for mapping inundation, land-cover, and

biophysical properties in regions of dense vegetation or with frequent cloud cover (Hess et al., 2003, Silva et al., 2010; Rebelo, 2010).

Specifically in the Pantanal, various remote sensing methods have been used to map features of the landscape, but the resulting classification maps have been restricted to: 1) a single habitat, such as lakes in the Nhecolândia subregion (Costa & Telmer, 2006; Novack et al., 2010); 2) a single subregion or a small subset at a local scale (Abdon et al., 1998; Galvão et al., 2003; Novack et al., 2010; Ariera et al., 2011); or 3) a large scale classification of the entire Pantanal at a either a coarse spatial resolution (Evans et al, 2010), or using imagery over a time span of approximately five years (GEF, 2004; PROBIO, 2007).

Evans et al. (2010) used a combination of C and L-band Synthetic Aperture Radar (SAR) imagery (100m spatial resolution) to map 5 classes for the whole Pantanal wetland using an object-based image analysis (OBIA) approach. The authors concluded that improvements over the classification could be achieved by 1) utilizing finer spatial resolution imagery, 2) acquisition of a more spatially robust ground reference data set, and 3) dividing the Pantanal into hydrological subregions and classifying these regions separately to exploit the spatially and temporally dynamic nature of the vegetation habitats.

The objective of this research is to address some of the limitations encountered in the above-mentioned publications by defining on a regional scale the wetland habitats of each of the hydrological subregions of the Pantanal, thus producing a final product covering the entire Pantanal, using a finer spatial resolution SAR imagery set (50m), a

comprehensive set of ground reference data, and employing a hierarchical Object Based Image Analysis (OBIA) approach.

3.2 Study Area

The Pantanal wetlands are located in the center of South America, primarily in Brazil, with roughly 10% reaching into Bolivia, and Paraguay (Figure 3.1). This wetland ecosystem is one of the largest and most important tropical wetlands globally, with estimates suggesting that the inundated area covers approximately 160,000 km^2 during maximum flooding. The Pantanal floodplain is bordered by an upland drainage basin of elevated plateaus and low mountains to the north and east, and heavily eroded ancient volcanic mountains to the west (Por, 1995; Heckman, 1998), with the entire Pantanal watershed occupying an area of approximately 362,000 km^2 (Junk et al., 2006). The climate of the Pantanal is tropical, semi-humid to humid, with seasonally intense rainfall and a marked dry season. Average annual precipitation is approximately 1400 mm, with 70-80% occurring in the rainy season from October to April. Rainfall is more intense in the northern and eastern uplands bordering the floodplain than within the floodplain itself, with average annual precipitation reaching 1600-1800 mm. Within the floodplain, average annual precipitation ranges from 1000-1200 mm, with the southern subregion of Nabileque receiving only 800-900 mm annually (GEF, 2004). Mean annual temperatures range from 22-26° C: in summer temperatures above 38° C are common, while the winter months average about 18° C (Por, 1995).

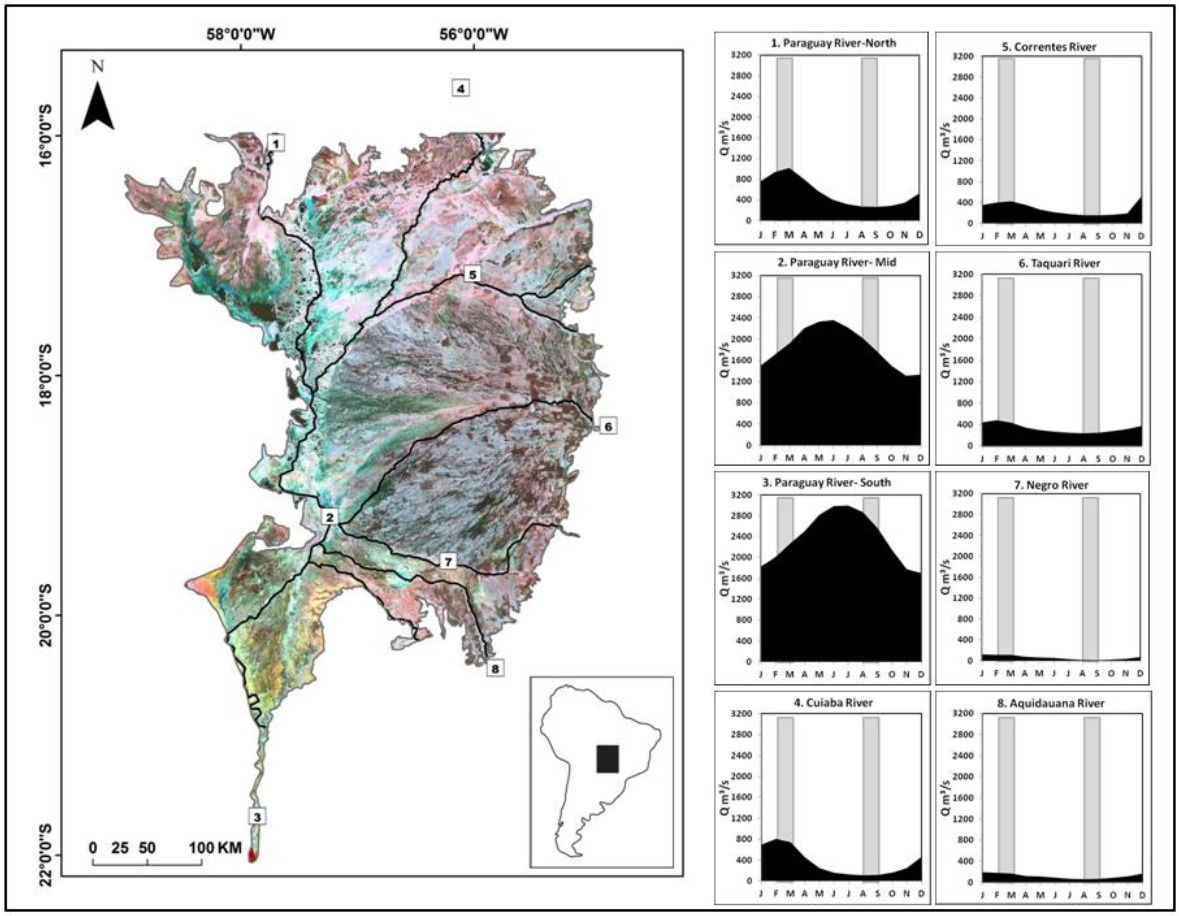

Figure 3.1: Study area/hydrology - Geographic extent of the Pantanal Wetland. Black lines represent the major rivers influencing the wetland, numbers indicate the location of existing hydrological stations, and corresponding graphs show average monthly river discharge recorded by each station. A lag time of 1-2 months is typically observed between peak discharge and maximum inundation/extent of the surrounding floodplain. On the hydrological graphs, gray bars represent dates of imagery acquisition. Generally, ground reference data was collected during low water for each subregion. The Pantanal is represented here by a SAR colour composite (Red – February/March ALOS/PALSAR HH; Green – August/September ALOS/PALSAR HH; Blue - August/September ALOS/PALSAR HV. (Hydrological data acquired from the Brazilian National Water Agency – ANA at http://hidroweb.ana.gov.br/)

The Pantanal floodplain is situated in a large depression of post-Cretaceous origin (Junk et al., 2011), and is a sedimentary basin composed of a mosaic of alluvial fans of Pleistocene origin (Alho, 2008a). The altitude in the floodplain varies from roughly 80 to 150 m asl and the topographical gradients are negligible, with the slope ranging from 0.3 to 0.5 m/km east-west and 0.03 to 0.15 m/km north-south (Mamede & Alho, 2006). According to Alho (2008a), the current topographical and ecological arrangement of the Pantanal is the result of three key factors: 1) geological changes occurring since the Quaternary, likely influencing drainage patterns; 2) intra and interannual fluctuations in the hydrological cycle, and 3) anthropogenic activity (introduced pastures, artificial ponds, deforestation).

The Pantanal is a rich hydrological complex formed by several major tributaries of the Paraguay River. The low topographical variation of the floodplain results in a slow release of water from the upland drainage basin, through the floodplain via these tributaries to the Paraguay River running north-south along the western border (Hamilton, 2002a). The riverbeds of the main tributaries are fairly well-delineated at their upper reaches, but become less defined as they approach the Paraguay River as a result of the low topographical gradient of the floodplain. Consequently, river discharge volume often decreases downstream rather than increasing, as is the norm (Por, 1995). Expansive areas are covered by water during annual flooding that extends from January to July. The drainage network and the rainfall patterns of the Pantanal support an annual monomodal flood regime that varies both temporally and spatially (Figure 3.1), thus delineating several sub-regions with diverse characteristics in terms of ecology, hydrology and geomorphology. Flooding in these subregions is distinctly seasonal, but the timing,

amplitude and duration of inundation vary considerably as a result of both the delayed release of floodwaters and regional rainfall patterns (Table 3.1). Maximum inundation can occur as early as January in the north and east, and as late as July in the south (4-5 months after peak rainfall). A lag time of 1-2 months typically occurs between peak river channel discharge and maximum inundation depth/extent of the surrounding plain (Hamilton et al., 1996; Girard, 2011). Hamilton et al. (1996) delineated ten Pantanal subregions based on geological and hydrological differences: Corixo Grande (CORI), Paraguay (PARA), Cuiaba (CUIA), Piquiri/ São Lourenço (PIQU), Taquari Fan (TAQF), Taquari River (TAQR), Nhecolândia (NHEC), Aquidauana/Negro (AQUI), Miranda (MIRA), and Nabileque (NABI) (Figure 3.2). In general, the duration and intensity of the inundation regime increases from east to west, and from north to south: the lowest amplitude, short duration flooding occurs in the eastern PIQU, TAQF, NHEC and AQUI subregions, while the highest amplitude, long duration flooding occurs adjacent to major river systems, particularly along the Paraguay River in the CORI, PARA and NABI subregions (Hamilton et al., 1996; GEF, 2004). Typically, the seasonal inundation patterns in the northern subregions are fairly regular; however, the MIRA, NHEC and AQUI subregions in the south show some short-term variability, and often lack a discrete seasonal flood peak, and the NABI region in the south can be highly variable in flood extent among years (Hamilton et al., 1996) (Table 3.1). This highly variable and dynamic flooding regime, and the connections and disconnections established between different elements of the landscape via the seasonal flood-pulse, are the most important ecological phenomena in the Pantanal, and the key drivers behind the high habitat diversity of the wetland (Junk et al., 1989; Junk et al., 2006; Mamede & Alho, 2006).

Table 3.1 Flooding characteristics of the various subregions of the Pantanal (from Hamilton et al., 1996; GEF, 2004; ANA, 2008); refer also to Figure 3.1 for river discharge - the number following river name refers to the hydrological stations shown in Figure 3.1

Subregion	Feb. Flood extent	Aug. Flood extent	Flood Characteristics	Main River(s) influencing subregion	Peak Discharge
Corixo Grande (CORI)	Rising water	Receding water	*Medium height/medium duration for most of floodplain, increasing towards southern border. Partial flooding to the north and center, generalized flooding to the south.*	N. Paraguay (1)	Feb-Mar
Paraguay (PARA)	Rising water	Receding water	*High amplitude, long duration, generalized flooding; peak flood occurs from Apr-Jun, however much is permanently flooded.*	Mid Paraguay (2)	May-Jun
Cuiaba (CUIA)	Rising water	Receding water	*Medium height, medium duration partial flooding.*	N. Paraguay (1)	Feb-Mar
				Cuiaba (4)	Jan-Feb
Piquiri/ São Lourenço (PIQU)	High water	Low water	*Mainly low, short duration localized flooding.*	Cuiaba (4)	Jan-Feb
				Correntes (5)	March
Taquari Fan (TAQF)	High water	Receding water	*Low, short duration localized flooding in the east, gradually increasing to medium height/medium duration partial flooding towards the Paraguay River along the western border, long duration (and some permanent) flooding along main lobes of the Taquari Megafan itself.*	Correntes (5)	March
				Taquari (6)	Jan-Feb
Taquari River (TAQR)	Rising water	Receding water	*Medium height/medium duration general flooding along tributary, spreading to partial flooding away from the river itself.*	Mid Paraguay (2)	May-Jun
				Taquari (6)	Jan-Feb
Nhecolândia (NHEC)	High water	Receding water	*Medium height/medium duration partial and localized flooding.* **no distinct peak*	Taquari (6)	Jan-Feb
				Negro (7)	Jan-Feb
Aquidauana/Negro (AQUI)	High water	Receding water	*Short localized flooding in the east, increasing to medium height/long duration generalized flooding in the west.* **no distinct peak*	Negro (7)	Jan-Feb
				Aquidauana (9)	Jan-Feb
Miranda (MIRA)	Rising water	Receding water	*Mainly medium height/long duration generalized flooding, some partial flooding in the east.* **no distinct peak*	Aquidauana (9)	Jan-Feb
				Miranda (8)	Jan-Feb
Nabileque (NABI)	Low water	Receding water	*Medium-high/variable duration (some permanent) generalized flooding.*	S. Paraguay (3)	Jul-Aug

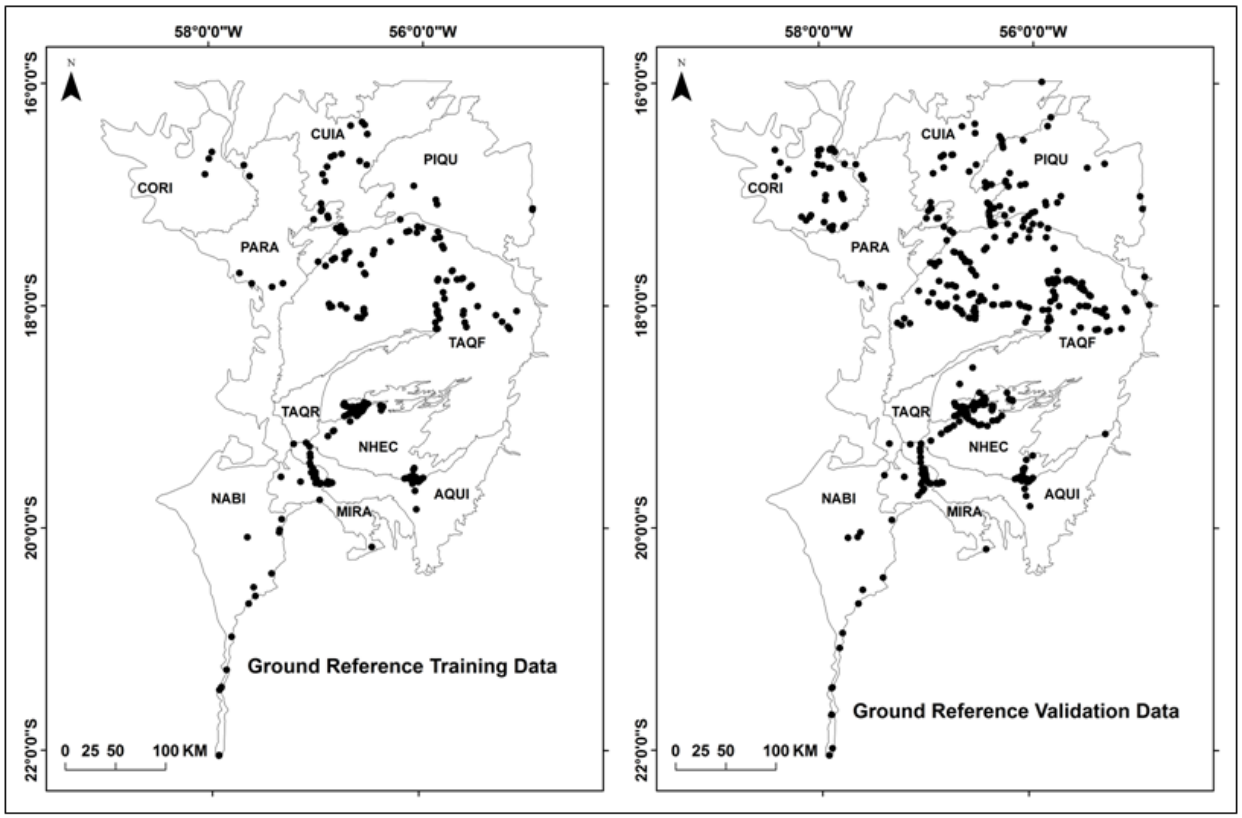

Figure 3.2 Spatial distribution of ground reference data locations split into training and validation sites. Black lines represent borders between hydrological subregions as defined in Hamilton et al. (1996): Aquidauana/Negro (AQUI), Corixo Grande (CORI), Cuiaba (CUIA), Miranda (MIRA), Nabileque (NABI), Nhecolândia (NHEC), Paraguay (PARA), Piquiri/ São Lourenço (PIQU), Taquari Fan (TAQF), Taquari River (TAQR).

As a geologically young landscape, endemism is rare in the Pantanal; rather, the flora of the wetland is heavily influenced by the main neighbouring phytogeographic domains. The Pantanal is primarily a savanna (*cerrado*) landscape, borrowing from the *Cerrado* biome to the east; however the Paraguay floodplains are also influenced by the Amazon forest biome, and a strong Chaco biome influence can be seen in the Nabileque and Miranda subregions (Pott et al, 2011). At a broad scale, the habitats in the Pantanal wetland are characterized by 1) forest; 2) savanna; and, 3) frequently and/or permanently aquatic or swampy terrain, although there is not always a definitive boundary between these three landscapes, and some classes of forest and savanna also periodically flood. The

phytogeographic units of the Pantanal can be defined in terms of geomorphology (inundation regime/elevation) (Nunes da Cunha et al., 2007), vegetation structure (Pott et al., 2011), or a combination of both (Nunes da Cunha & Junk, 2011). There are five main geomorphologic subunits that categorize the landscape of the Pantanal as described in Nunes da Cunha et al. (2007): 1) elevations that reach 1-2 m above mean flood level, and thus are rarely or never subject to inundation; 2) periodically flooded flat plains; 3) shallow natural drainage channels; 4) depressions that remain swampy, even in dry months; and 5) permanent lakes and river channels. Classification units in terms of vegetation structure can generally be divided into: 1) woody vegetation; 2) scrub vegetation; 3) herbaceous/grass; 4) aquatic vegetation; 5) a combination of these structures; 6) areas of no vegetation (open water). For the purposes of this research, a combination of geomorphology and vegetation structure characteristics were examined, and habitats were grouped according to features which could be distinguished via the imagery dataset: characterization of these habitats as described by several authors are seen in Table (3.2), and Figure (3.3). Class nomenclature was chosen based on collaboration with several Brazilian researchers studying in the Pantanal in order to incorporate local terminology where possible. (Por, 1995; Pott & Pott, 2000, 2011a, 2011b; Campos Filho, 2002; Nunes da Cunha et al., 2007; Pott et al., 2011).

Table 3.2 Class descriptions

Class Name	Class Code/Subclass	Description
Forest/ Woodland	**FOR**	Dense canopy woody vegetation – terrestrial, some may be shortly inundated during extreme flood events; includes
	Forest	Deciduous and semi-deciduous forest
	Cerradão	Dry woody savanna vegetation presenting xeromorphic features
	Cordilheira	Paleo-feature - elongated elevation in the floodplain with a width of ~100m, a length of up to several kilometres and an elevation of 1-3m above the floodplain; covered with cerrado/cerradão vegetation
	Capão	Paleo-feature - round or oval "island" with a diameter of several tens to a few hundred meters, reaching ~1.5m above the floodplain; covered with *cerrado/cerradão* vegetation
Riparian Forest	**RIP**	Dense canopy fluvial forest, typically found adjacent to rivers although can be located several kilometers away– may be subject to seasonal flooding, includes many pioneer species.
Open Wood Savanna	**OWS**	Open canopy, mixed vegetation with shrubs, and scattered trees up to 10m tall on a grassy/herbaceous stratum; may be periodically flooded by excess rainwater and/or by rivers, river channels, or seasonal floodways; Also influenced by Chaco vegetation in MIRA and NABI subregions - also includes:
	Campo de murunduns	Termite savanna - and some open grass savanna with small *capãos*; neither of which could be distinguished as individual entities at the spatial resolution of the imagery
Open Wood Savanna-Flood (subject to intense and/or prolonged flooding	**OWS_F**	Often characterized by monodominant stands of woody vegetation (*Carandazal, Cambarazal, Abobral, Pimental, Canjiquieral, Pombieral, Paratudal*), and many pioneer species; Also influenced by Chaco vegetation in MIRA and NABI subregions. Also includes:
	Landis	Continuous drainage channels covered with wood savanna vegetation
Open Grass Savanna	**OGS**	*Cerrado, campo sujo* - predominantly grassy/herbaceous terrain with sparse, scattered trees and/or shrubs, shrub grassland; may be subject to periodic flooding
Swampy Grassland	**SGR**	*Campo limpo* - grassland/herbaceous terrain without woody vegetation, covered by grasses, sedges and herbaceous plants during dry phase, and by aquatic macrophytes during flood. Also includes:
	Campinas	Circular-shaped *campo* 100-300m in diameter surrounded by *cordilheiras*; advanced successional stages of former lakes filled in by sediments that are typically flooded for up to six months by rainwater, ground water and/or flood runoff
	Campo de baixada	Grassy herbaceous cover on low lying areas adjacent to lakes
	Brejo	Permanently flooded or waterlogged herbaceous cover
Swampy Mixed Savanna	**SMS**	Dense mix of herbaceous, scrub, bramble, and some woody vegetation – subject to prolonged flood or permanently waterlogged. Includes many pioneer species, and is strongly influenced by the Amazon forest biome
Agriculture	**AGR**	Introduced/cultivated pasture and crops, anthropogenic in nature; introduced exotic pastures dominated by *Brachiaria sp.*
Vazantes	**VAZ**	Temporary seasonal drainage channels of upstream rainwater runoff from *campos* inhabiting shallow canals where herbaceous/shrubby vegetation grows, but also including amphibious and emergent aquatic species and floating macrophytes during flood
Water	**WAT**	permanent water bodies; lakes, rivers

Figure 3.3 Field photographs of classes - a) Forest/Woodland (FOR); b) Riparian Forest (RIP); c) Open Wood Savanna (OWS); d) *Open Wood Savanna subject to prolonged flooding (OWS_F); e) Open Grass Savanna (OGS); f) *Swampy Grassland (SGR); g) Swampy Mixed Savanna (SMS); h) Agriculture (AGR); i) *Vazantes* (VAZ); j) Water (WAT). *Note: although the OWS_F and SGR classes are subject to prolonged flooding, at the time of photograph acquisition for these examples, conditions were dry; however, vegetation species/structure is representative of the respective classes.

3.3Methods

3.3.1 Field data

The ground reference database is comprised of 599 points, including latitude/longitude coordinates, dominant vegetation description, and in many cases, photographs. Of the total ground reference points, 223 were acquired in July of 2008 when the hydrology of the main rivers of the Pantanal vary with the north, east, and central regions under the influence of receding to low waters, and the west and south regions (along the Paraguay River) under high to receding water conditions (Table 3.1). The remaining 376 ground reference points are part of the EMBRAPA Pantanal database, and contain detailed descriptions of the landscape and associated coordinates. These 376 points were acquired in 2008 during the local low water period for each subregion. The strategy for defining the location of ground reference points was based on a stratified approach considering preliminary backscattering analysis of previously acquired ALOS/PALSAR and ALOS/AVNIR-2 imagery as well as logistics in the field. Ground reference data was then split into training and validation points. Specific numbers for training and validation image objects for each class, as well as the spatial distribution for training and validation data are found in Table (3.3) and Figure (3.2) respectively.

Table 3.3 Breakdown of ground reference points into training and validation data by class – Forest/Woodland (FOR**); Swampy Grassland (**SGR**); Open Grass Savanna (**OGS**); Open Wood Savanna (**OWS**); Open Wood Savanna subject to prolonged flooding (**OWS_F**); Swampy Mixes Savanna (**SMS**); Riparian Forest (**RIP**); *Vazantes* (**VAZ**); Water (**WAT**).**

CLASS		Number	Percent of total
FOR	**Train**	81	12.2
	Validation	83	21.3
RIP	**Train**	51	7.7
	Validation	31	8.0
OWS	**Train**	99	14.9
	Validation	68	17.5
OWS-F	**Train**	68	10.2
	Validation	41	10.5
OGS	**Train**	52	7.8
	Validation	23	5.9
SGR	**Train**	111	16.7
	Validation	62	15.9
SMS	**Train**	37	5.6
	Validation	9	2.3
AGR	**Train**	64	9.6
	Validation	27	6.9
VAZ	**Train**	46	6.9
	Validation	31	8.0
WAT	**Train**	57	8.6
	Validation	14	3.6
Total	**Train**	**666**	
	Validation	**389**	

3.3.2 Satellite data

L-band orthorectified mosaics from ALOS/PALSAR were acquired for February/March 2008 (50m, HH polarization), and for August/September 2008 (50m, HH and HV polarization) coinciding with the 2008 ground reference data acquisition. ALOS/PALSAR images were acquired as part of the JAXA ALOS Kyoto and Carbon Initiative – Pantanal. C-band images from RADARSAT-2, obtained as part of the Canadian Space Agency's Science and Operational Applications Research (SOAR) program, were acquired for August/September 2008 (ScanSAR Narrow 50m, HH and HV polarization) coinciding with field campaign. Both ALOS/PALSAR and RADARSAT-2 images were acquired at a pre-processed level, and thus already radiometrically calibrated for incidence angle and radiometric distortions (Luscombe, 2009; Shimada & Ohtaki, 2010; for RADARSAT-2 and ALOS/PALSAR respectively).

3.3.3 Image Processing Steps

3.3.3.1 Radiometric/geometric calibration, and mosaicking

ALOS/PALSAR imagery was processed and mosaicked prior to delivery. These mosaics were derived from level 1, FBS (February/March) and FBD (August/September) imagery (12.5 m spatial resolution), with the equivalent number of looks for the output mosaics at 16 and 4 for the azimuth and slant ranges, respectively. The method developed for mosaicking of ALOS FBS and FBD images resulted in an average RMS error of 34 m when compared to Landsat 30 m mosaics created by USGS (Shimada & Ohtaki, 2010). RADARSAT-2 level 1-SGF images were processed and orthorectified using PCI Orthoengine, and a SAR specific satellite orbiting model. Mosaics were georeferenced and projected to UTM coordinates (zone 21, row K) using the WGS84 reference ellipsoid. A comparison of the RADARSAT-2 images from the two adjacent paths revealed a minor

shift of two pixels in the x-axis: because this error was consistent along the entire path a simple pixel shift executed the required correction. Due to the temporal gap between adjacent RADARSAT-2 paths (approximately five weeks) appropriate mosaic cutlines were created along subregion boundaries to avoid temporal variability within individual subregions. Cross-sensor geometric inconsistencies between ALOS/PALSAR and RADARSAT-2 mosaics were corrected using the RADARSAT-2 mosaic as a master and using a second order polynomial approach. The RMS error for this correction was < 0.5 pixels for both the x and the y-axis. The Pantanal wetland vector based on Hamilton et al (1996) was then utilized to delineate the study area from the mosaics.

3.3.3.2 Speckle Filtering

Images were filtered to reduce the effect of speckle by utilizing a Kuan filter with a 3 x 3 kernel (Oliver & Quegan, 2004). The resultant imagery showed preservation of the mean values, while decreasing the standard deviation of homogenous targets, and visually preserving the feature edges.

3.3.4 OBIA Classification Steps

The classification was performed using an OBIA approach, executed using the Definiens eCognition software package (V.8.0). All imagery mosaics, as well hydrological subregion vectors from Hamilton et al., (1996), and a lakes mask for the Nhecolândia subregion produced in Chapter 2 were imported into eCognition for subsequent segmentation and classification. The lakes mask was created from a previous land cover classification of the Nhecolândia subregion only, using fine spatial resolution (12.5 m) ALOS/PALSAR imagery. All land cover under this lakes mask was classified as "Nhecolândia – Water" and removed from further consideration. The mask step was

deemed necessary for the present classification to avoid confusion with adjacent classes given the relatively small size of the lakes within this subregion and the coarser spatial resolution (50m) of the present classification. The hydrological subregion vectors identify borders for the following ten areas based on spatially variable inundation timing and duration of the subregions (Hamilton et al., 1996): Aquidauana/Negro – AQUI; Corixo Grande – CORI; Cuiaba – CUIA; Miranda – MIRA; Nabileque – NABI; Nhecolândia – NHEC; Paraguay – PARA; Piquiri/São Lourenço – PIQU; Taquari Fan – TAQF; Taquari River – TAQR (Figure 3.2). Given the spatial variation in inundation timing and duration between subregions, each subregion was classified separately as suggested in Evans et al. (2010). A flow diagram of the general hierarchical classification approach for all subregions is shown in Figure (3.4).

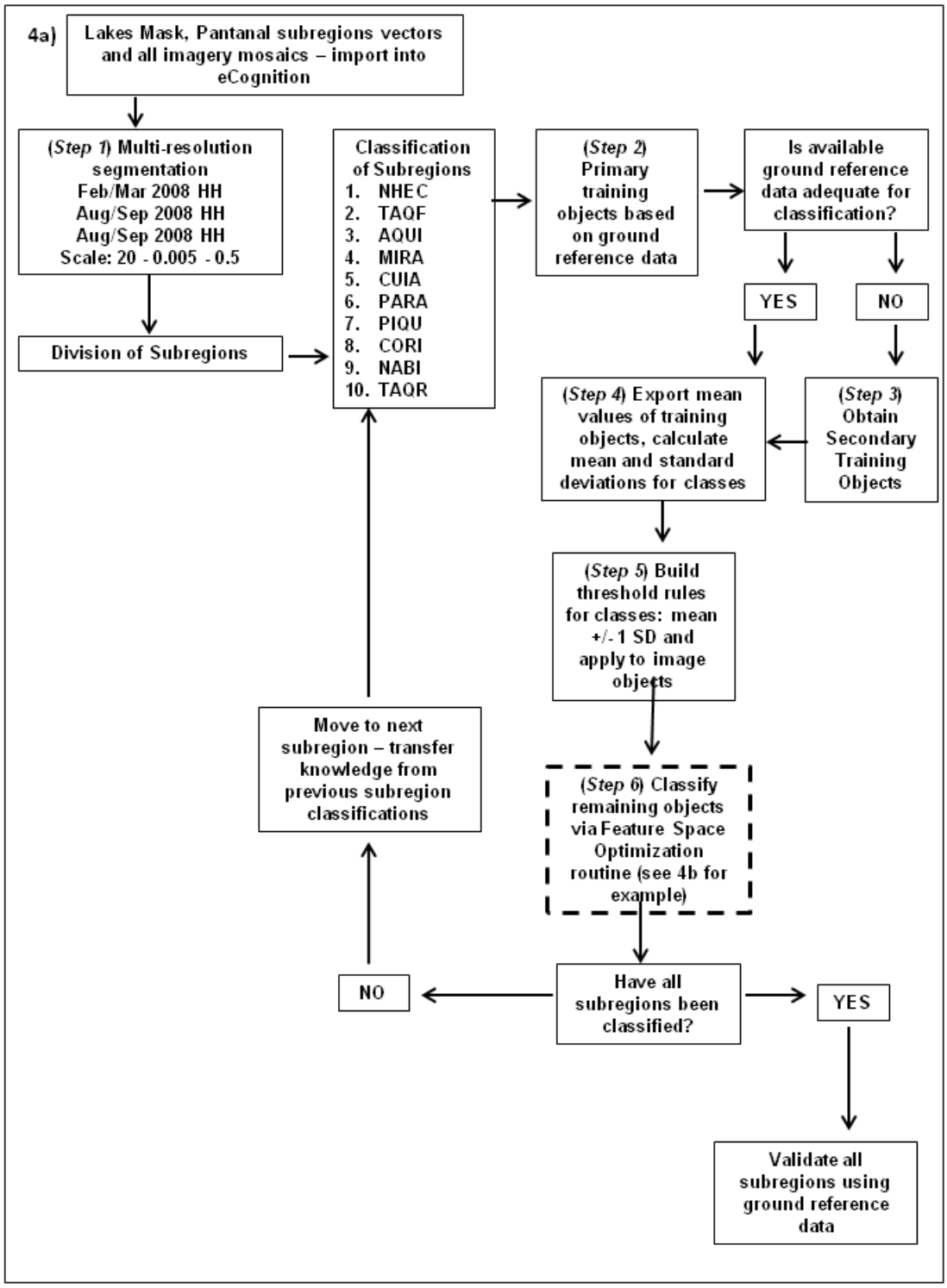

Figure 3.4a Hierarchical classification flow diagram - main classification steps

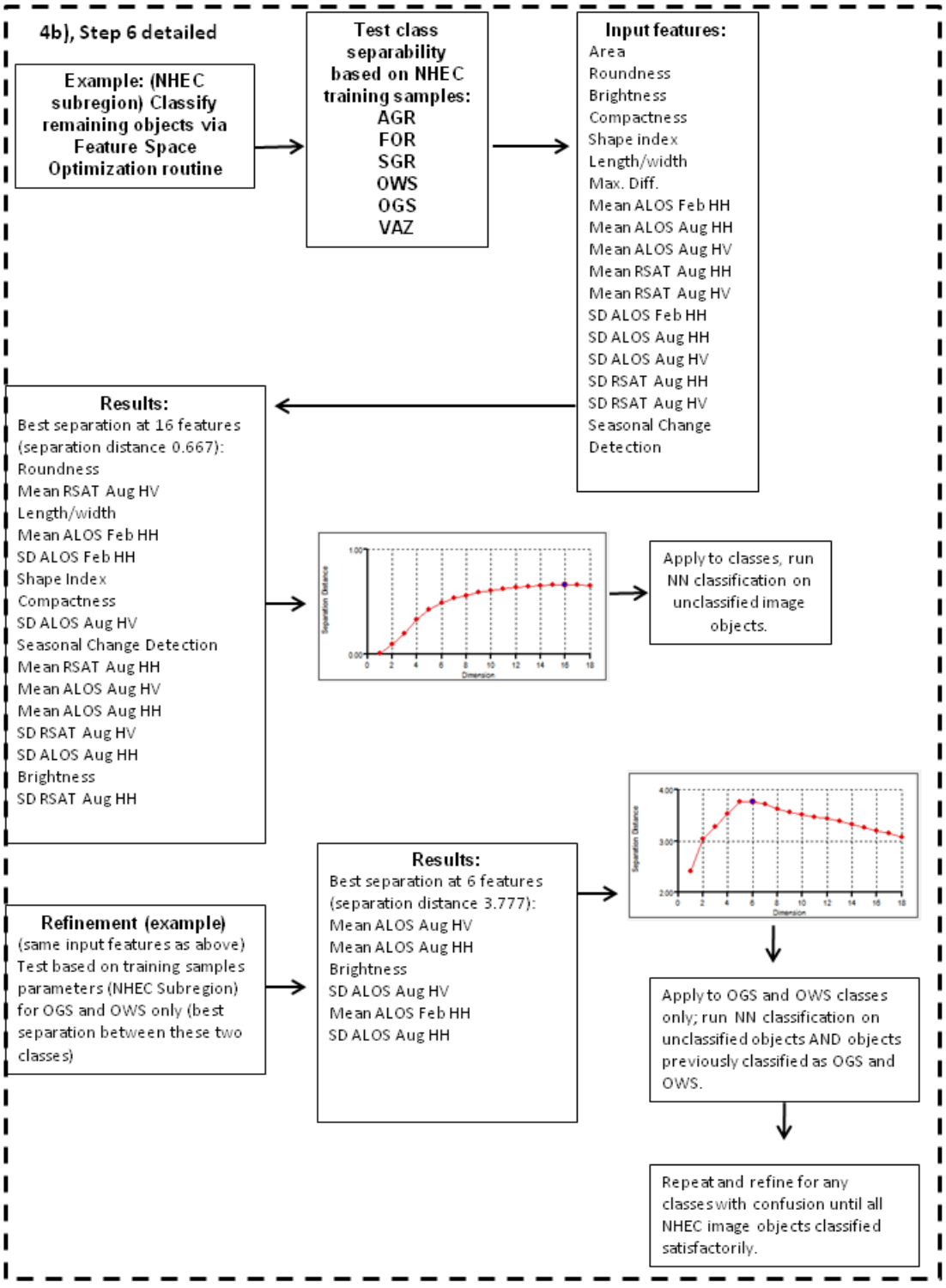

Figure 3.4b Hierarchical classification flow diagram - detailed example of the FSO methodology

3.3.4.1 Creation of Image Objects

Segmentation of the subregion mosaics into image objects was conducted at the pixel level, using the multiresolution segmentation algorithm (Figure 3.4a, Step 1). This algorithm applies an optimization process which locally reduces the average heterogeneity of image objects for a given resolution, and is controlled by three user-defined parameters: *scale*, *shape* and *compactness*. The *scale* parameter determines the maximum allowed heterogeneity, and thus, the size, of resultant image objects - larger scale values produce larger objects and smaller scale values produce smaller objects. The *shape* parameter determines the degree of influence of spectral radiometry versus object shape in the delineation of image objects, and *compactness* determines the degree of smoothing for object borders. Both the shape and compactness parameters are assigned a value between 0-1, thus defining the degree to which each of these criteria influence the image object output. Segmentation parameters are data, scale, and research goal specific, thus the user must incorporate a "trial and error" method for determining the ideal inputs for their purpose, based on their knowledge and expertise regarding the study area and the intended outcome of the classification (Blaschke & Hay, 2001). For the present study, the multiresolution segmentation was performed using an optimal set of parameters for creating image objects sized appropriately to represent relatively small landscape features as individual entities, given the highly heterogeneous nature of the landscape: scale = 20; shape = 0.005 (heavily emphasizing radiometry over shape); compactness = 0.5 (equal emphasis on smoothness and compactness). Segmentation was performed giving equal weight to the wet and dry season L-band, and dry season C-band HH polarization mosaics to best exploit both the temporal differences in flooding patterns, as well as the unique spectral signatures of different land cover classes available with a dual-band approach. All

vector layers were included in the segmentation process ensuring that resultant image objects respected both the subregion and lakes boundaries. Once the segmented layer was created, all objects under the lakes mask were classified as "Nhecolândia – Water" and removed from further consideration.

Usually, segmentation is followed by a hierarchical rule-based approach to classify resultant image objects. Hierarchical classification rules are developed according to user-defined parameters, which are supported by field data, and expert knowledge, and can be refined iteratively based on results throughout the process. This method allows for the addition of new rules or datasets without compromising predefined rules, while traditional methods such as maximum likelihood or minimum distance may alter the rules of all classes concurrently based on new information. For instance, in a hierarchical classification, land cover classes, such as forest, or water, once classified can be removed from subsequent processing, and new rules can be created to refine classifications of remaining land cover without compromising the overall classification result (Lucas et al., 2007).

3.3.4.2 Classification by Subregion

Training objects for land cover classes for all subregions of the Pantanal were chosen based on available ground reference data (Figure 3.4a, Step 2; primary training objects, n=210), and, where ground reference data was lacking, were chosen based on expert knowledge, previous backscattering analysis of the region (Evans et al., 2010; Chapter 2) and additional ancillary data (Figure 3.4a, Step 3; secondary training objects, n=456) .

The general classification strategy by subregion involved starting with the subregion for which the most information (ground reference data, photographs, and expert knowledge) was available, and then moving to the subregion with the second most information, and so forth, through all subsequent subregions. For subregions with inadequate or missing ground reference data, secondary training objects were obtained through 1) expert knowledge of backscattering variability for land cover classes of one subregion transferred to another with similar vegetation and inundation patterns, 2) visual interpretation of ALOS Advanced Visible and Near-Infrared (AVNIR-2) sensor (processing level 1B2, 10 m spatial resolution, four images acquired January 20, 2007 and three images acquired February 02, 2007) obtained from JAXA, Landsat ETM (30 m spatial resolution, acquired April 2002), as well as Landsat ETM (30 m spatial resolution, acquired December 2007) and IKONOS (4 m spatial resolution, acquired in July 2006 and 2007) imagery available in GoogleEarth Pro; although this additional imagery was acquired during years previous to field data and imagery acquisition, examination of monthly hydrological data for 2002, 2006, and 2007 for the Taquari, Cuiaba and Paraguay Rivers shows similar hydrological patterns for these years compared with 2008 when SAR imagery and ground reference data was acquired, and 3) expert knowledge regarding backscattering characteristics of similar land cover classes from relevant literature (Dobson et al., 1996; Hess et al., 2003; Costa, 2004; Evans et al., 2010). For example, the first subregion to be classified was Nhecolândia because the authors had previous knowledge of the backscattering behaviour for different cover types found in this subregion (Chapter 2), as well as a high number of ground reference training sites available for this subregion (n=49). This knowledge was then applied to aid in the

classification of the neighbouring subregion (Taquari Fan), which exhibited relatively similar hydrological characteristics (Table 3.1) and land cover. This transferred knowledge, combined with the ancillary data mentioned above, was used as supplementary information along with the ground reference data available for the Taquari Fan subregion.

For each subregion, mean backscattering values for each training object (primary and secondary) were exported, standard deviation of the collective means for each cover type were calculated, and then these statistics were converted to normalized backscattering coefficients (σ^0) expressed in dB (the standard units for reporting SAR backscattering) in order to facilitate comparison with relevant literature (Figure 3.4a, Step 4). The conversion process for ALOS/PALSAR (from amplitude values) is as follows:

$$\sigma^0 = 10*\log_{10} (DN^2) + CF \qquad \text{(Equation 3.1)}$$

where CF is the calibration coefficient for PALSAR standard products, and equals –83 dB (Rosenqvist et al., 2007).

For RADARSAT-2 images (from intensity values), conversion was performed as follows:

$$C = (DN^2 + B) / A \qquad \text{(Equation 3.2)}$$

where C is the calibrated value; B is the offset; and A is the range-dependant gain, both supplied in the LUT file (MDA, 2008). The calibrated values were then expressed in dB via the following calculation:

$$\sigma^0 = 10*\log(C) \qquad \text{(Equation 3.3)}$$

The classification process for each subregion involved two main steps: 1) the building of preliminary thresholds for each class based on collective training object

backscattering mean values +/- 1 SD of the means for each class in each respective subregion (Figure 3.4a, Step 5; Figure 3.5), and 2) the utilization of the Feature Space Optimization (FSO) tool in eCognition in conjunction with a nearest neighbour classification strategy (Figure 3.4a, Step 6).

For the first step, mean and standard deviation values for each class/subregion/band were displayed graphically (Figure 3.5) in order to gain a broad understanding of the backscattering variability of the classes. The backscattering ranges were used as a preliminary guide for building thresholds for each of the classes (separately for each subregion). These preliminary class thresholds were based on more than one image, which were selected based on the appropriateness to separate a specific class from all other classes for each subregion. The "AND" operator was used to define a class based on several images thresholds; for example, threshold for class *i*, subregion *j* = mean +/- 1 SD in image *a*, AND mean +/- 1 SD in image *b*, AND mean +/- 1 SD in image *c*, and so on. Backscattering overlap between classes prevented the use of one single image to separate among classes. In some cases thresholds for three or four different images were used for characterizing one particular class. The collective thresholds for all classes were programmed into eCognition and run concurrently.

For the second step, the FSO tool was utilized employing several features as primary inputs: area, roundness, compactness, shape index, length/width, maximum difference, mean, and standard deviation (all features included in the eCognition software package), as well as a seasonal change detection algorithm (Silva et al., 2010). This algorithm was created in order to exploit the seasonal differences in land cover for subregions where flood and dry season roughly corresponded to the ALOS

February/March and August/September mosaics, respectively (seasonal change = ALOS Feb/March HH mosaic subtracted from ALOS Aug/Sept HH mosaic). FSO uses the Euclidean distance algorithm to select a feature combination that provides the best class separation among all user-selected classes. Once the optimal set of features is defined, a standard nearest neighbour supervised classification is run on image objects using the optimal feature combination as the input. The FSO tool was first run to define separability among all classes (separately for each subregion), and then on pairs of classes for which confusion was still evident (Figure 3.4b). In addition to the FSO tool, supplementary rules were defined to deal with specific and localized confusion among classes. For example, in the Nhecolândia subregion, some confusion was noted between the Swampy Grassland and *Vazantes* classes; in this case, various shape parameters were utilized to further separate the two classes: as a temporary flood runoff channel, *Vazantes* present a long and sinuous shape (similar to a river), compared to the more amorphous shape of the flooded fields making up the Swampy Grassland class. The FSO parameters, and the various additional rules were refined and the process repeated until all image objects within the subregion were classified. Although both the initial class thresholds and the FSO routine were performed for each subregion, the optimal feature combinations and the specific rules changed, given the variability between flood timing and land cover amongst all of the subregions.

Once classification was complete, areas of elevation (ELEV) known as *Morrarias*, groups of hills a few hundred metres high, located primarily along the western border or isolated within the Pantanal (Nunes da Cunha et al., 2007), were manually classified by indentifying foreshortening and layover, which are common types of relief displacement

observed on radar imagery in areas with hilly terrain. This identification was confirmed with supplemental local topographical maps.

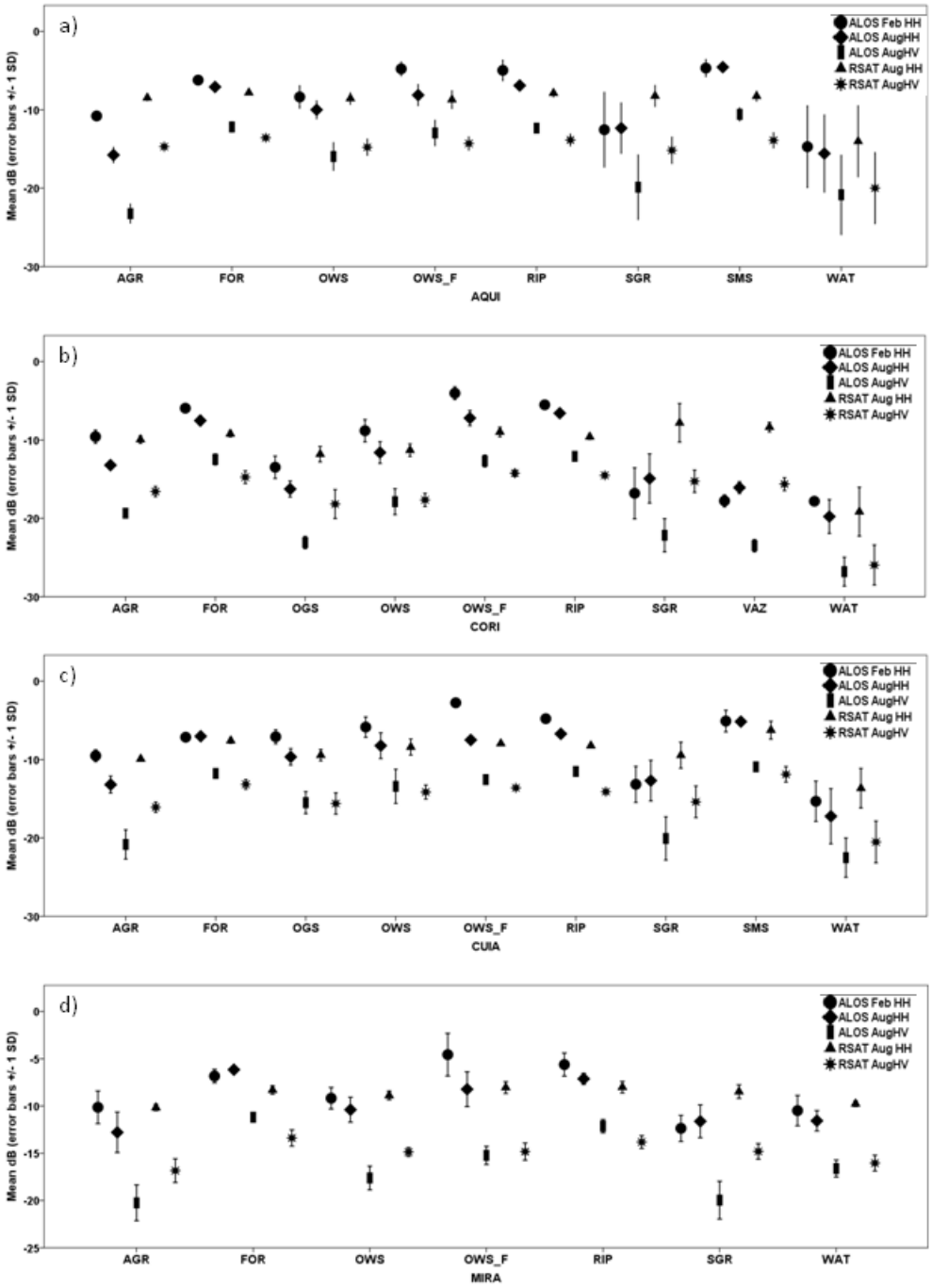
a)
ALOS Feb HH
ALOS AugHH
ALOS AugHV
RSAT Aug HH
RSAT AugHV
Mean dB (error bars +/- 1 SD)
0
-10
-20
-30
AGR
FOR
OWS
OWS_F
RIP
SGR
SMS
WAT
AQUI
b)
ALOS Feb HH
ALOS AugHH
ALOS AugHV
RSAT Aug HH
RSAT AugHV
Mean dB (error bars +/- 1 SD)
0
-10
-20
-30
AGR
FOR
OGS
OWS
OWS_F
RIP
SGR
VAZ
WAT
CORI
c)
ALOS Feb HH
ALOS AugHH
ALOS AugHV
RSAT Aug HH
RSAT AugHV
Mean dB (error bars +/- 1 SD)
0
-10
-20
-30
AGR
FOR
OGS
OWS
OWS_F
RIP
SGR
SMS
WAT
CUIA
d)
ALOS Feb HH
ALOS AugHH
ALOS AugHV
RSAT Aug HH
RSAT AugHV
Mean dB (error bars +/- 1 SD)
0
-5
-10
-15
-20
-25
AGR
FOR
OWS
OWS_F
RIP
SGR
WAT
MIRA

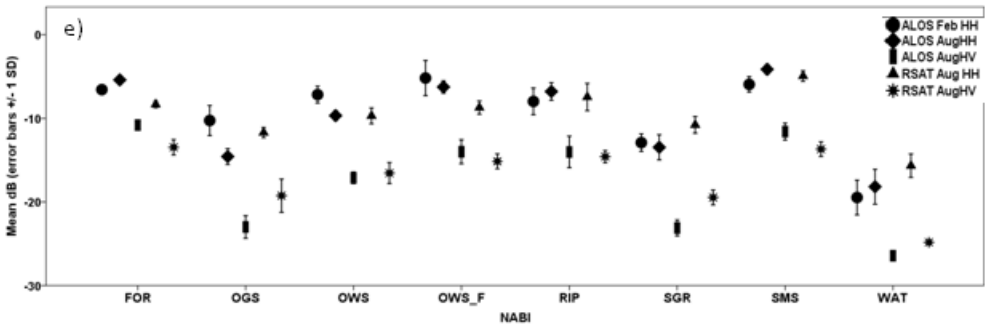
e)
ALOS Feb HH
ALOS AugHH
ALOS AugHV
RSAT Aug HH
RSAT AugHV
Mean dB (error bars +/- 1 SD)
0
-10
-20
-30
FOR
OGS
OWS
OWS_F
RIP
SGR
SMS
WAT
NABI

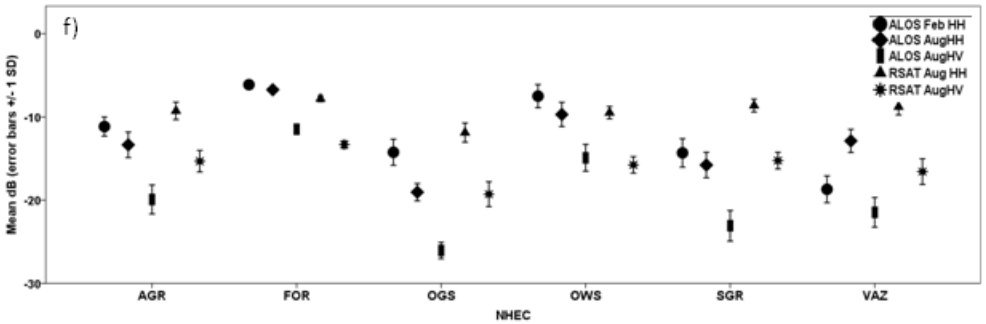
f)
ALOS Feb HH
ALOS AugHH
ALOS AugHV
RSAT Aug HH
RSAT AugHV
Mean dB (error bars +/- 1 SD)
0
-10
-20
-30
AGR
FOR
OGS
OWS
SGR
VAZ
NHEC

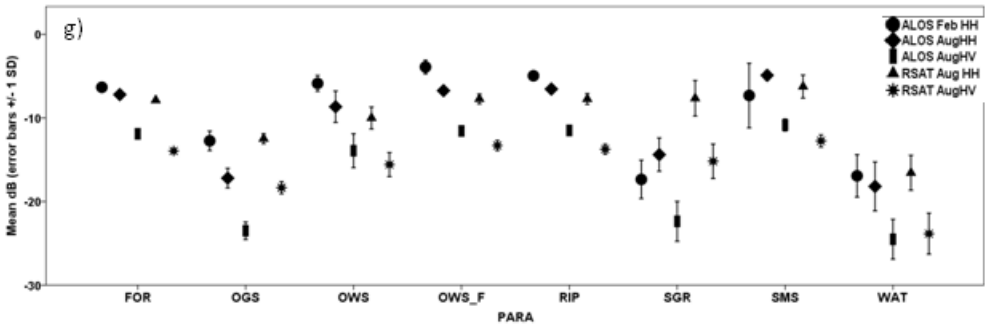
g)
ALOS Feb HH
ALOS AugHH
ALOS AugHV
RSAT Aug HH
RSAT AugHV
Mean dB (error bars +/- 1 SD)
0
-10
-20
-30
FOR
OGS
OWS
OWS_F
RIP
SGR
SMS
WAT
PARA

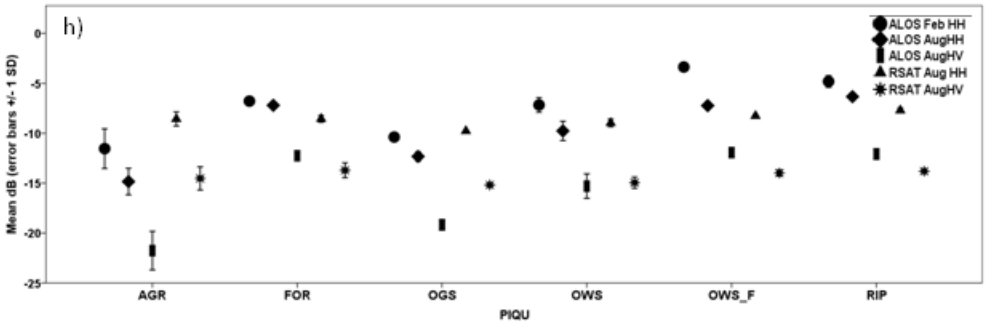
h)
ALOS Feb HH
ALOS AugHH
ALOS AugHV
RSAT Aug HH
RSAT AugHV
Mean dB (error bars +/- 1 SD)
0
-5
-10
-15
-20
-25
AGR
FOR
OGS
OWS
OWS_F
RIP
PIQU

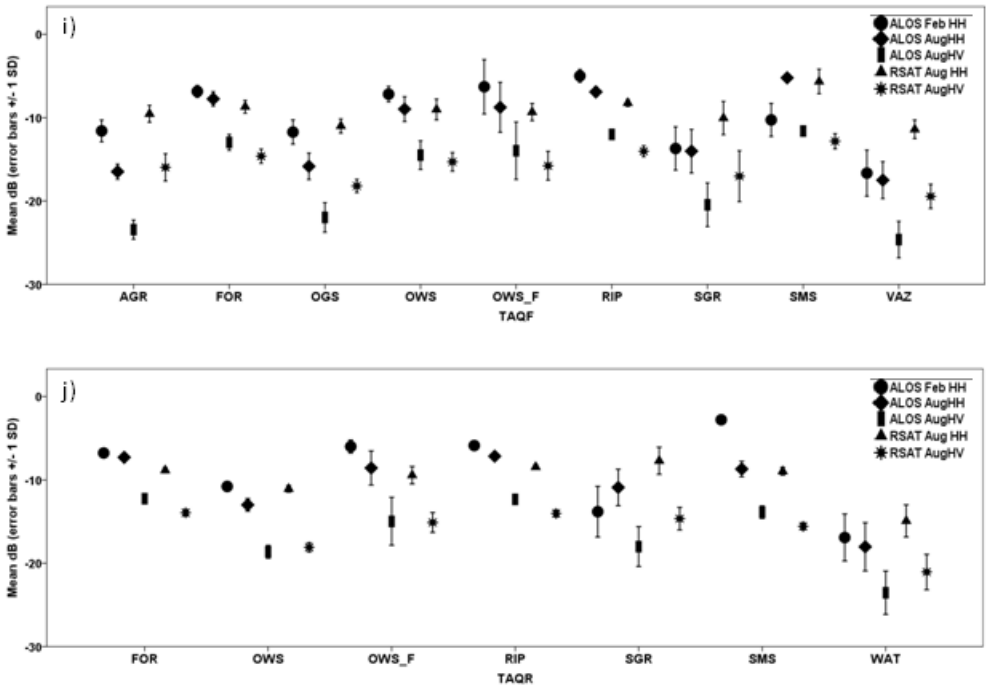

Figure 3.5 Backscattering analysis graphs for class training samples in each subregion/band: a) Aquidauana/Negro (AQUI), b) Corixo Grande (CORI), c) Cuiaba (CUIA), d) Miranda (MIRA), e) Nabileque (NABI), f) Nhecolândia (NHEC), g) Paraguay (PARA), h) Piquiri/ São Lourenço (PIQU), i)Taquari Fan (TAQF), j)Taquari River (TAQR). Classes - Agriculture (AGR); Forest/Woodland (FOR); Swampy Grassland (SGR); Open Grass Savanna (OGS); Open Wood Savanna (OWS); Open Wood Savanna subject to prolonged flooding (OWS_F); Swampy Mixed Savanna (SMS); Riparian Forest (RIP); *Vazantes* (VAZ); Water (WAT).

3.3.4.3 Validation

Once all subregions were classified, results were compared to the ground reference data resulting in a total of 389 validation objects for the entire Pantanal. The following accuracy measurements were calculated for each subregion: overall (%) accuracy (percentage of validation points corresponding to correctly classified areas for the whole image); commission errors (the ratio of correctly classified objects to the total number of classified objects in each class); and, omission errors (the ratio of correctly classified image objects to the total number of validation objects in each class) (Congalton, 1991). Following individual subregion accuracy assessment, results were combined to calculate an overall accuracy assessment for the entire Pantanal.

3.4 Results

3.4.1Backscattering Analysis

Overall, the highest mean backscattering values (approximately -10 to -5 dB for L-band HH polarization, both seasons) were generally found among the woody land cover classes: Forest/Woodland, Riparian Forest, Open Wood Savanna, and Open Wood Savanna subject to prolonged flooding, as well as the Swampy Mixed Savanna class. Of these classes, Forest/Woodland and Riparian Forest are mainly comprised of fairly dense, homogenous canopy, and the total backscattering signal is the result of multiple scattering mechanisms and interactions with the various components present in dense woody vegetation. Backscattering in these classes is partially due to volumetric scattering with the canopy surface, however, the longer wavelength of L-band (23.6cm) combined with a relatively steep incidence angle (34.3°) allows for penetration of the radiation past the canopy surface, resulting in additional sub canopy interaction with leaves, stems and woody branches, increasing the volumetric scattering component. With both of the Open

Wood Savanna classes (Figure 3.3c-d), land cover is a mixture of open canopy woody vegetation, shrubs and brush, and herbaceous grassy cover: with these classes, backscattering is comprised of a mixture of volumetric scattering at the surface and within the canopy, and a lesser component of volumetric scattering due to energy interaction with the herbaceous vegetation. For all of the woody classes, an increase in the backscattering signal (approximately 1 to 3 dB) is observed during flood conditions due to the addition of the double-bounce interaction between vertical vegetation structures and water surfaces. However, with the Open Wood Savanna classes there may also be a slight decrease in the overall backscattering return if the grassy/herbaceous vegetation is very short, or completely submerged, as this would contribute to some loss of the signal as energy is specularly reflected away from the sensor. The Swampy Mixed Savanna class (Figure 3.3g) is comprised of a mixture of some scattered woody vegetation, bramble, and scrub. This class is subject to prolonged, or even permanent, flooding; therefore, it is expected that a strong double-bounce component is present, which contributes to the high overall backscattering values.

The lowest mean backscattering values were generally found with the Swampy Grassland, Water, and *Vazantes* classes (approximately -30 to -15 dB for L-band HH polarization, both seasons). Of these classes, Water was typically the lowest due to a reduced backscattering signal as a result of specular reflection of energy away from the sensor. Both the Swampy Grasslands and *Vazantes* class are characterized by prolonged (and even permanent, in some cases) periods of flooding, thereby contributing a high water component to the backscattering signal, also resulting in a lower backscattering return. For the Swampy Grasslands class (Figure 3.3f), even during a dry phase when

little to no water is present, these habitats can be covered in relatively short vegetation, and therefore are often not visible at L-band. All three of these classes exhibited some variability around the mean values, likely caused by a vegetation component (either aquatic, in the case of *Vazantes* and Water, or partially submerged grasses in the case of Swampy Grasslands) adding a small degree of volumetric scattering to the overall backscattered signal.

Generally, the Open Grass Savanna and Agriculture classes fell into the mid-range of backscattering values (approximately -10 to -15 dB for L-band HH polarization, both seasons). These classes are not subject to the high degree of flooding (and therefore, reduced backscattering signal caused by high specular reflectance) of the water/swampy classes. The Open Grass Savanna (Figure 3.3e) and Agriculture classes (Figure 3.3h) are both inhabited predominantly by grasses (typically taller and/or more robust than the grasses found in the Swampy Grassland class) and other herbaceous vegetation with a much lesser shrub and sparse tree component. Backscattering from these two classes is dominated by volumetric scattering within the vegetation.

Very little difference in backscattering mean values was found among any of the classes for C-band (dry season only). The shorter wavelength at C-band (5.5 cm for C-band, compared to 23.6 cm for L-band) allows for little or no sub canopy penetration of the woody vegetation, therefore, for the wooded classes backscattering is largely due to volume scattering at the canopy surface. However, at the shorter C-band wavelength, herbaceous vegetation (Agriculture, Open Grass Savanna, and even some of the shorter grasses found in the Swampy Grassland class), as well as any floating/emergent aquatic vegetation present for the Water and *Vazantes* classes, show a stronger backscattering

signal compared to L-band as a result of multiple volume scattering interactions within the vegetation assemblages. The only class generally distinguishable from the others at C-band was the Water class, where the majority of the energy was specularly reflected away from the sensor, except in the cases where aquatic vegetation was present (as explained previously).

3.4.2 Classification

Figure 3.6 (a-j) shows the spatial distribution of land cover units distinguishable at 50 m spatial resolution for each of the subregions of the Pantanal wetland. The merged results of this classification show the overall spatial distribution of land cover units for the entire Pantanal wetland (Figure 3.6k). Validation results for the land cover classes over the entire Pantanal are seen in Table 3.4. Overall accuracy results by subregion from highest to lowest were as follows: PARA (95%); NABI (93%); PIQU (87%); MIRA (84%); TAQF (81%); CORI (80%); AQUI (76%); NHEC (75%); CUIA (50%). There was no accuracy assessment for the TAQR subregion as no validation data points were available for this area. The combined classification of ten land cover classes for the whole Pantanal was achieved with an overall accuracy of 80%. In general, the highest degrees of confusion were found among classes with similar vegetation structure and/or flooding regime: Forest/Woodland with Open Wood Savanna; Riparian Forest with Open Wood Savanna subject to prolonged flooding; Swampy Grassland with *Vazantes*; Open Grass Savanna with Agriculture and Open Wood Savanna.

Table 3.4 Validation results

REFERENCE DATA	PANTANAL (50m)	CLASSIFIED AS: Forest Woodland	Riparian Forest	Open Wood Savanna	Open Wood Savanna Flood	Open Grass Savanna	Swampy Grassland	Swampy Mixed Savanna	Agriculture	Vazante	Water	Row Total	Error of Omission (%)
	Forest Woodland	60	4	14	5	0	0	0	0	0	0	83	28
	Riparian Forest	4	23	0	3	0	0	1	0	0	0	31	26
	Open Wood Savanna	1	0	66	0	0	1	0	0	0	0	68	3
	Open Wood Savanna Flood	0	4	5	31	0	0	0	1	0	0	41	24
	Open Grass Savanna	0	0	3	0	17	0	0	3	0	0	23	26
	Swampy Grassland	0	0	1	0	4	51	0	3	2	1	62	18
	Swampy Mixed Savanna	0	1	0	3	0	1	4	0	0	0	9	56
	Agriculture	0	0	0	0	3	2	0	22	0	0	27	19
	Vazante	0	0	0	0	1	6	0	1	23	0	31	26
	Water	0	0	0	0	0	0	0	0	0	14	14	0
	Column Total	65	32	89	42	25	61	5	30	25	15	389	
	Error of Commission (%)	8	28	26	26	32	16	20	27	8	6	accuracy (%	80

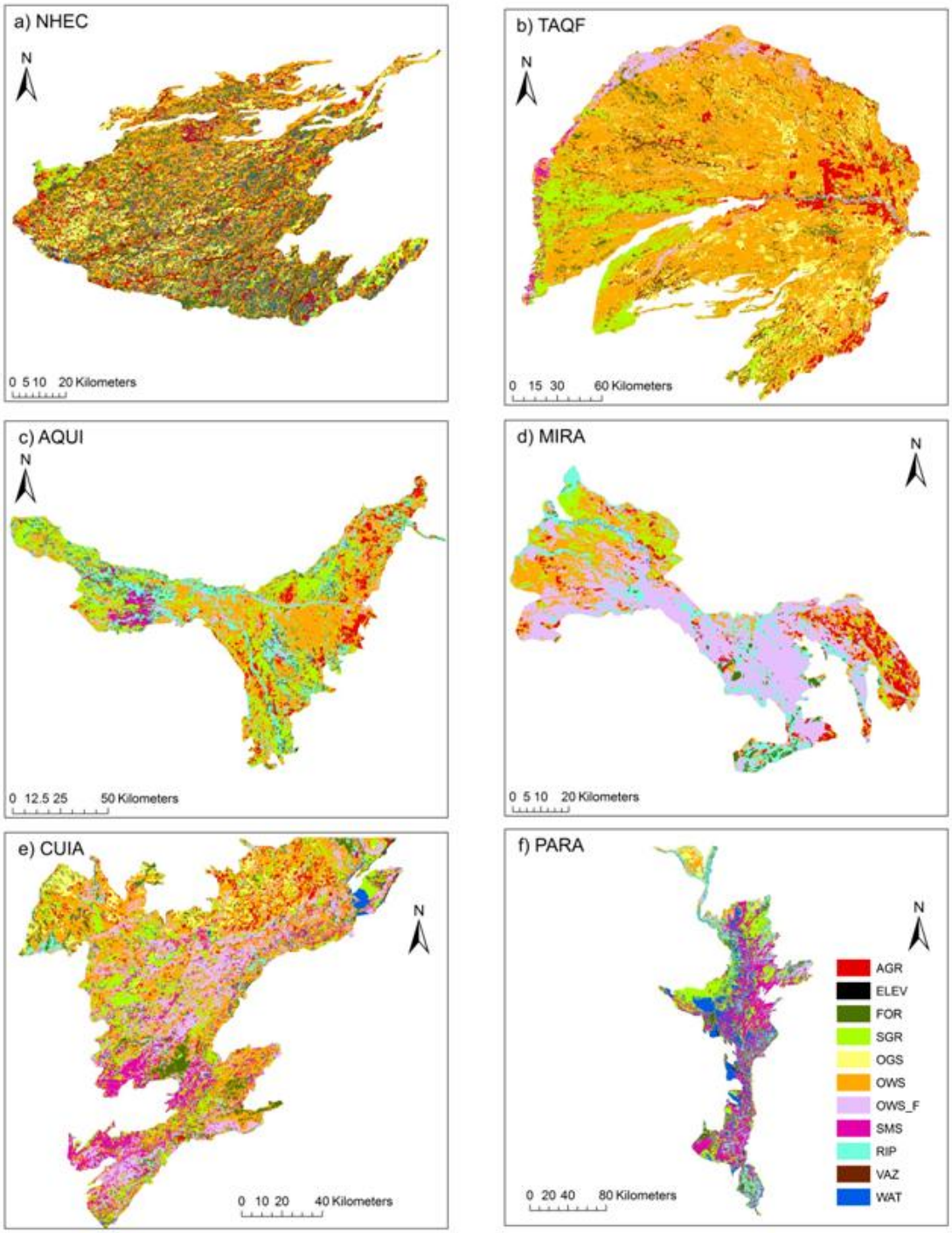
a) NHEC
N
0 5 10 20 Kilometers
b) TAQF
N
0 15 30 60 Kilometers
c) AQUI
N
0 12.5 25 50 Kilometers
d) MIRA
N
0 5 10 20 Kilometers
e) CUIA
N
0 10 20 40 Kilometers
f) PARA
N
0 20 40 80 Kilometers
AGR
ELEV
FOR
SGR
OGS
OWS
OWS_F
SMS
RIP
VAZ
WAT

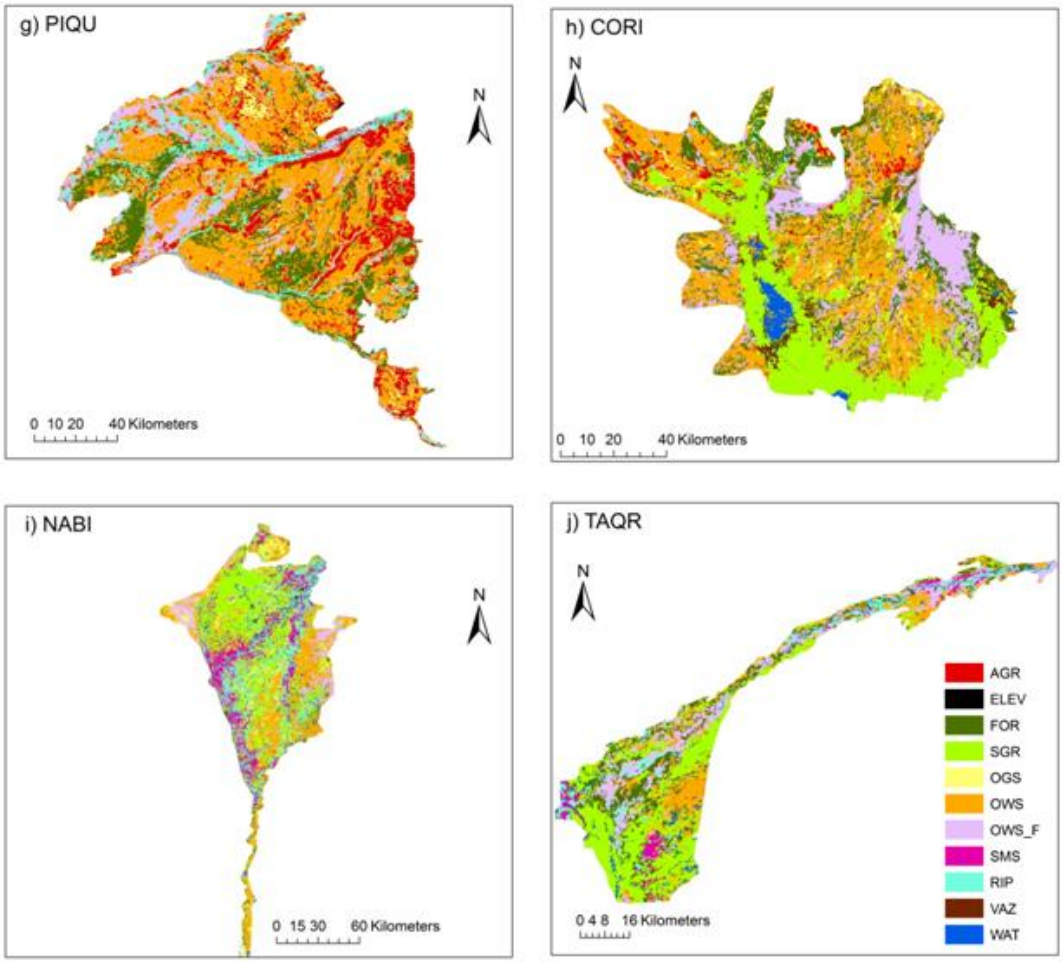

Figure 3.6(a-j): Classification outputs maps by subregion- a) Nhecolândia (NHEC), b) Taquari Fan (TAQF), c) Aquidauana/Negro (AQUI), d) Miranda (MIRA), e) Cuiaba (CUIA), f) Paraguay (PARA), g) Piquiri/ São Lourenço (PIQU), h) Corixo Grande (CORI), i) Nabileque (NABI), j) Taquari River (TAQR). Agriculture (AGR); Elevation (ELEV – *Morrarias,* manually classified); Forest/Woodland (FOR); Swampy Grassland (SGR); Open Grass Savanna (OGS); Open Wood Savanna (OWS); Open Wood Savanna subject to prolonged flooding (OWS_F); Swampy Mixed Savanna (SMS); Riparian Forest (RIP); *Vazantes* (VAZ); Water (WAT). Note: scales are variable for each subregion to aid in visualization.

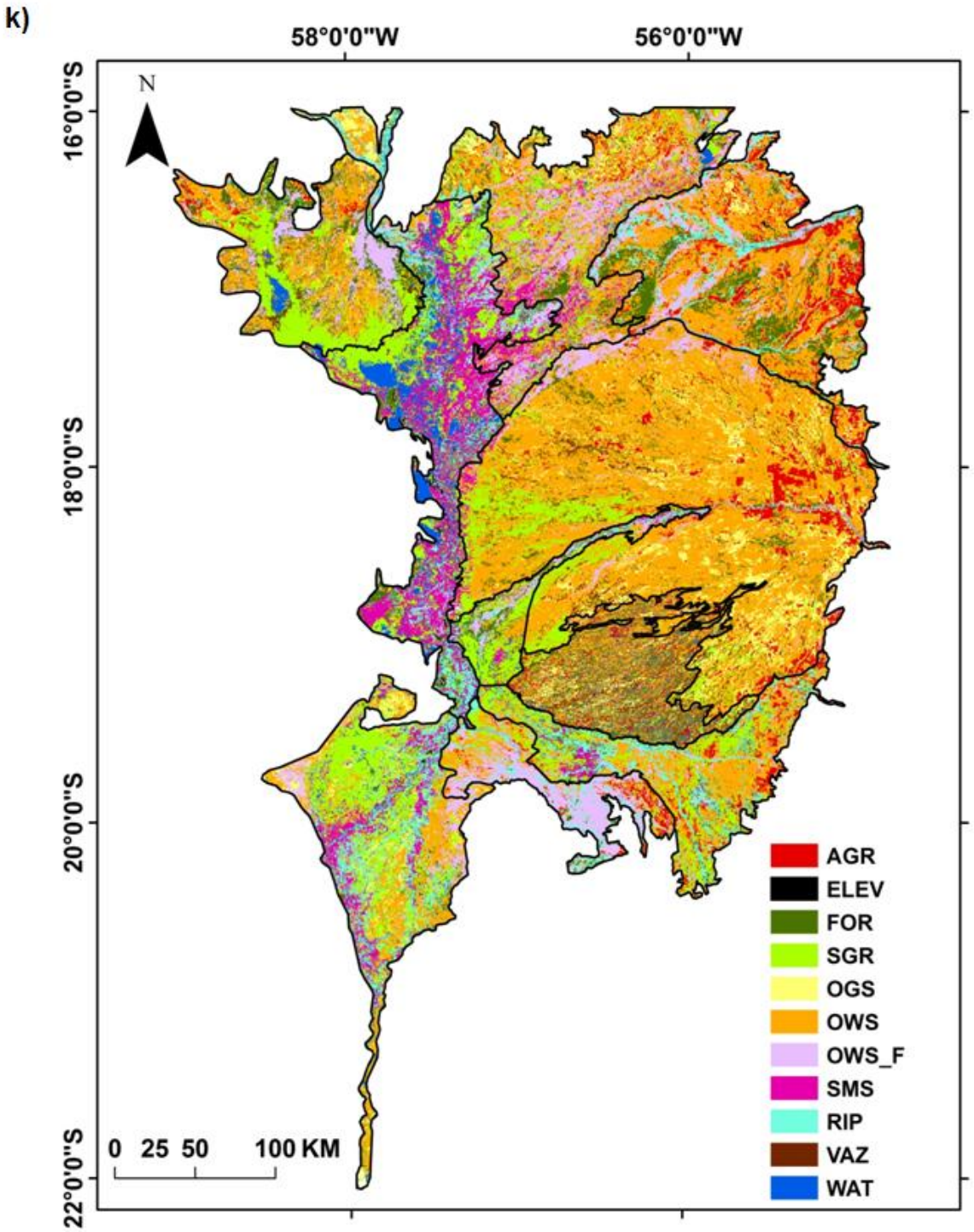

Figure 3.6 (k): Classification output map - whole Pantanal - Agriculture (AGR); Elevation (ELEV – *Morrarias*, manually classified); Forest/Woodland (FOR); Swampy Grassland (SGR); Open Grass Savanna (OGS); Open Wood Savanna (OWS); Open Wood Savanna subject to prolonged flooding (OWS_F); Swampy Mixed Savanna (SMS); Riparian Forest (RIP); *Vazantes* (VAZ); Water (WAT).

The produced classification maps show a landscape dominated by the Open Wood Savanna class (OWS - 39% total coverage) followed by: Swampy Grassland (SGR - 14%); Open Wood Savanna subject to prolonged flooding (OWS_F - 9%); Forest/Woodland (FOR - 7%); Riparian Forest (RIP - 7%); Swampy Mixed Savanna (SMS - 7%); Agriculture (AGR - 6%); Open Grass Savanna (OGS - 6%); Water (WAT - 3%); and *Vazantes* (VAZ - 2%) (Table 3.5). Total area (km^2), and percentage of land coverage for each of the classes for each subregion separately, and combined for the whole Pantanal wetland, is seen in Table 3.5. The dominant land cover class for each subregion is as follows: NHEC (OWS – 40%); TAQF (OWS – 60%); AQUI (OWS – 40%); MIRA (OWS_F – 44%); CUIA (OWS – 37%); PARA (SMS – 31%); PIQU (OWS – 48%); CORI (OWS – 32%); NABI (OWS – 27%); TAQR (SGR – 33%).

.

Table 3.5 Classification results - area in km2 and percent coverage per class/subregion, and collectively for the whole Pantanal

Class	AQUI		CORI		CUIA		MIRA		NABI	
	area (km^2)	% cover	area (km^2)	% cover	area (km^2)	% cover	area (km^2)	% cover	area (km^2)	% cover
FOR	426	5	1,748	16	825	6	112	2	734	5
RIP	1,717	19	88	1	494	3	722	15	2,515	18
OWS	3,683	40	3,513	32	5,397	37	1,141	24	3,738	27
OWS_F	329	4	1,734	16	2,667	18	2,122	44	754	5
OGS	0	0	315	3	726	5	0	0	1,001	7
SGR	1,908	21	2,793	25	2,004	14	341	7	3,451	25
SMS	233	3	0	0	1,468	10	0	0	1,568	11
AGR	721	8	292	3	646	4	392	8	0	0
VAZ	0	0	273	2	0	0	0	0	0	0
WAT	191	2	200	2	382	3	13	0	209	1
ELEV	1	0	0	0	13	0	0	0	4	0
Total	9,209	100	10,956	100	14,622	100	4,843	100	13,974	100

Class	NHEC		PARA		PIQU		TAQF		TAQR		Pantanal	
	area (km^2)	% cover	area (km^2)	% cover	area (km^2)	% cover	area (km^2)	% cover	area (km^2)	% cover	area (km^2)	% cover
FOR	961	12	1,310	8	2,312	14	1,225	3	515	18	10,168	7
RIP	0	0	2,707	16	1,565	10	0	0	224	8	10,032	7
OWS	3,277	40	657	4	7,670	48	24,179	60	535	19	53,790	39
OWS_F	0	0	683	4	1,688	11	1,527	4	455	16	11,959	9
OGS	740	9	502	3	132	1	5,126	13	0	0	8,542	6
SGR	622	8	3,490	20	0	0	3,933	10	951	33	19,493	14
SMS	0	0	5,255	31	0	0	337	1	108	4	8,969	7
AGR	900	11	0	0	2,529	16	2,487	6	0	0	7,967	6
VAZ	574	7	0	0	0	0	1,254	3	0	0	2,101	2
WAT	1,130	14	2,373	14	67	0	40	0	98	3	4,703	3
ELEV	0	0	66	0	13	0	2	0	0	0	99	0
Total	8,204	100	17,043	100	15,976	100	40,110	100	2,886	100	137,823	100

3.5 Discussion

3.5.1 Classification

Overall, the primary sources of error for this classification were due to 1) similarities in vegetation structure and/or inundation regime, and thus similar backscattering characteristics; 2) issues of the scale of the image objects in regards to the heterogeneity of the habitats within the landscape.

The greatest confusion for all classification results was found with adjacent successional classes, often with similar inundation regimes and vegetation structure: for example, Forest/Woodland with Open Wood Savanna; Open Wood Savanna with Open Grass Savanna; Riparian Forest with Open Wood Savanna subject to prolonged flooding; Swampy Grassland with *Vazantes* and Open Grass Savanna. These errors were expected given the similarity of these classes in terms of vegetation structure and flooding regime, and therefore similar backscattering characteristics. In many cases these habitats are found adjacent to one another, and clear cut borders between the different cover types are not readily apparent, especially given the dynamic nature of the landscape in terms of inundation. For instance, *Vazantes* and Swampy Grassland are fundamentally the same type of cover in terms of vegetation structure and inundation patterns, and thus show similar backscattering characteristics; they are differentiated only by the defined drainage channel aspect of the *Vazantes* compared to the more amorphous shape of the Swampy Grassland, and the timing and duration of inundation. However, in the case of Swampy Grassland and *Vazantes*, the ability to consider object shape and compactness, likely aided in separating the two classes compared to the separation possible by using thresholds based on mean backscattering values alone.

There was also a high degree of confusion between the Swampy Mixed Savanna and Open Wood Savanna subject to prolonged flooding classes, resulting in the highest error of omission (56%) for Swampy Mixed Savanna. These classes only occur in areas subject to prolonged, or even permanent flooding, typically in close proximity to major rivers, and combining a mixture of open water, woody and herbaceous vegetation cover. This similar mixture of cover and flooding characteristics, as well as a lack of difference in flooding regime between the two seasonal sets of imagery, hindered separability of these two classes based on backscattering mean thresholds alone. This same issue of similar vegetation/flooding characteristics likely caused some confusion between the Agriculture and Swampy Grassland classes. Although planted pasture (Agriculture) typically occurs in areas not prone to long periods of inundation, this is not always the case, and in such cases Agriculture may have been erroneously classified as Swampy Grassland. The similarity between Open Grass Savanna and Agriculture (both are, in the context of this classification, essentially different forms of grasslands), also contributed to some confusion between the two as both can exhibit a mix of grassland and sparsely distributed woodland/shrub vegetation. As well, Forest/Woodland and Open Wood Savanna are both comprised of differing degrees of woody vegetation with no straightforward border between the two, contributing to the degree of confusion observed between those two classes. As noted in Hoekman et al. (2010) in a land cover classification conducted in Borneo, many classes form continua along a biomass and/or wetness gradient, and when arbitrary ranges are chosen delineating membership to each class, some confusion among adjacent classes is likely.

Within the individual subregions, overall, the highest classification accuracy was found in the PARA (95%) and NABI (93%) subregions. Although these were two subregions for which prior firsthand knowledge of vegetation classes was not sufficient, the high accuracy is largely due to the relative homogeneity of land cover compared to the very high heterogeneity of, for example, the Nhecolândia subregion. Although Nhecolândia was the subregion with the greatest amount of prior firsthand knowledge it had relatively lower overall accuracy (75%); this is in part a result of the high heterogeneity of the landscape at the spatial resolution of the imagery (50 m). Furthermore, the utilization of the lakes mask (created from fine spatial resolution imagery – 12.5 m, Chapter 2) may have contributed to the lower accuracy results for the Nhecolândia region, as these very small image objects may have broken up areas that would have been segmented into larger objects had the mask not been used. This high heterogeneity of land cover would also account for the relatively poor classification accuracy results of the CUIA subregion (50%).

As observed in the backscattering analysis of the various classes, a straightforward classification based on thresholds built from class mean and standard deviation backscattering values alone was of little use for this study area for several reasons: 1) there was a high degree of similarity in vegetation structure and/or flooding characteristics between adjacent classes (i.e. Swampy Mixed Savanna and Open Wood Savanna subject to prolonged flooding); 2) while inundation in any particular subregion may have been receding to low water in the August/September imagery (Table 3.1), even a very shallow depth of water on the ground would result in a backscattering signal characteristic of flooded terrain in SAR imagery; 3) in many cases flooding was

inconsistent and/or only localized within individual subregions resulting in some objects from the same class being flooded and others not flooded during the same time period, further contributing to confusion between classes. Because backscattering mean and standard deviation thresholds combined with a hierarchical classification were not sufficient alone to successfully complete the classification, the feature space optimization (FSO) routine combined with the supervised nearest neighbour algorithm was necessary to achieve the relatively high final accuracy results (overall accuracy of 80%).

3.5.2 Spatial Distribution of Habitat Classes

3.5.2.1 Forest/Woodland

The Forest/Woodland class makes up 7% of total Pantanal land cover, and is mainly comprised of dry forest (*cerrado/cerradão*) vegetation. This habitat is expressed primarily as large stands of dry forest (*cerradão*) in the northern subregions (CORI, PIQU and CUIA), as well in NHEC, PARA, and TAQR subregions. These forested areas largely occur on ancient levees (*cordilheiras*) found at slightly higher elevations than the floodplain, and thus, rarely flood (Pott et al., 2011). These forested levees are also noted adjacent to riparian forest in the PARA and TAQR subregions (Damasceno-Junior et al., 2005).

3.5.2.2 Riparian Forest

The Riparian Forest class makes up 7% of total Pantanal land cover. The largest distribution of this class can be found along the Paraguay River (PARA), and in the southern subregions (NABI, AQUI and MIRA), although is well represented along all of the main rivers of the Pantanal. As such, it is subjected to periodic flooding. Specifically along the Paraguay River, riparian forest vegetation is mainly located in convex parts of meanders, in agreement with observations by Damasceno-Junior et al. (2005). Although

primarily located adjacent to fluvial systems, some riparian species (*Combretum lanceolatum, Licania parvifolia, Vochysia divergens*) may grow several kilometers away from the rivers, as observed in the PARA, NABI and AQUI subregions, often in closed monodominant stands (Pott et al., 2011).

3.5.2.3 Open Wood Savanna

At 39% total land coverage, the Open Wood Savanna class is the dominant land cover of the Pantanal as a whole, and also the dominant land cover in every subregion except MIRA, PARA and TAQR. The subregions with the highest overall percentage of Open Wood Savanna cover (TAQF and PIQU at 60% and 48%, respectively) are both located on the eastern border of the Pantanal, which are subject to a less intense and shorter duration flooding regime than the other subregions: this high distribution on the east-central regions of the floodplain is consistent with the spatial distribution for this class reported in Pott et al. (2011).

3.5.2.4 Open Wood Savanna – Prolonged Flood

Although this class makes up only 9% of total land coverage in the Pantanal, it is the dominant class (44% in the MIRA subregion), and shows considerably high coverage in the CUIA, CORI and TAQR subregions. These subregions (or significant portions of these subregions) are subject to medium-long duration and intensity flooding. Often, homogenous plots of monodominant species (*Pombeiral, Cambarazal*) colonize these areas after certain types of disturbance and/or abnormally high flooding (Alho, 2011b).

3.5.2.5 Open Grass Savanna

The Open Grass Savanna class makes up 6% of total land cover in the Pantanal, primarily in the TAQF and NHEC subregions. Although this class may be subjected to

periodic flooding, its spatial distribution is largely in areas subject to a medium to low intensity and duration inundation regime. This class was not observed in the AQUI, MIRA and TAQR subregions, although this is likely due to a lack of field data regarding this class in those subregions,

3.5.2.6 Swampy Grassland

The Swampy Grassland class makes up 14% of the entire Pantanal. A considerable portion of this total land coverage is found in the Taquari Fan (TAQF, TAQR and PARA subregions), as well as in the heavily flooded areas of the NABI, AQUI and CORI subregions. This class also includes areas of permanently waterlogged swampy herbaceous terrain, coinciding with regions of heavy siltation deposits from the Upper Paraguay River (CORI) and the Taquari River (TAQF, TAQR) (GEF 2004).

3.5.2.7 Swampy Mixed Savanna

The Swampy Mixed Savanna class makes up 7% of the entire Pantanal. This class is found primarily along the Paraguay River in the AQUI, CUIA, NABI, TAQF, TAQR and PARA subregions. At 31%, it is the dominant land cover class of the PARA subregion. Many of the species inhabiting this class are pioneer species (influenced by the Amazon biome to the north) which colonize flooded grasslands and/or recently built-up riverbanks that remain inundated for prolonged periods of time, and are in various successional stages (Damasceno-Junior et al., 2005).

3.5.2.8 Agriculture

The Agriculture class makes up 6% of total land cover in the Pantanal. This class showed the highest distribution along the eastern border of the Pantanal in the Aquidauana, Taquari Fan and Piquiri/ São Lourenço subregions in areas subject to short

duration, low amplitude flooding, adjacent to major agricultural areas found on the eastern plateau bordering the Pantanal wetlands. The high distribution of this class along the eastern border of the Pantanal may also be due to these areas being within the easiest access to regional markets and trade routes through urban centers (Cuiaba, Rondonopolis, Coxim, Campo Grande), as suggested in Seidl et al. (2001).

3.5.2.9 Vazantes

The *Vazantes* class makes up only 2% of total land cover in the Pantanal, and was found only in the CORI, TAQF and NHEC subregions in the present classification. Although this land cover is likely present in other subregions, there was a lack of ground reference data corresponding to this class in other subregions. Furthermore, the similarity in vegetation cover and adjacency to the Swampy Grassland class made it difficult to distinguish as a separate class in subregions subject to a more prolonged and intense flooding regime.

3.5.2.10 Water

The Water class makes up 3% total land cover in the Pantanal. The main source of this class was the large number of lakes in both the PARA and NHEC subregions, as well as the contribution from major rivers in the other subregions. The percentage of total permanent water in the Pantanal is likely higher than observed; however for the present classification, the Water class did not include permanently waterlogged terrain, which was incorporated in the Swampy Grassland and Swampy Mixed Savanna classes.

3.5.2.11 Entire Pantanal

Overall, the greatest distribution of swampy land cover (Swampy Grassland and Swampy Mixed Savanna), and Water was found in regions adjacent to the Paraguay

River, along the western border of the Pantanal, as well as within the Taquari Fan, and in the southern portion of the Corixo Grande subregion; however, the greatest percentage of land cover for a single subregion, for both the *Vazantes* and Water classes, was found in the Nhecolândia subregion. Riparian Forest and Open Wood Savanna subject to prolonged flooding were found adjacent to most major river systems. In general, the land cover associated with short duration or no flooding (Forest/Woodland, Open Wood Savanna, and Open Grass Savanna) was found primarily in the eastern Pantanal in the Taquari Fan and Piquiri/ São Lourenço subregions, although Nhecolândia had a high percentage of these classes as well.

In general, the assessment of the Pantanal wetland as dominated by a savanna landscape observed in the present classification is consistent with several other studies of the region (Por, 1995; Abdon et al., 1998; GEF 2004; Junk et al., 2006; Pott et al., 2011). Yet, despite this dominance, the present classification results show a vast wetland with an extreme heterogeneity and diversity of habitats, and a high variability both within and among the distinct subregions. This environmental heterogeneity of habitats is critical to the high biodiversity of the fauna of the region. These different habitats function as dispersion corridors, feeding sites, breeding sites, refuges for migratory species, and stepping stones between other key habitats.

Specifically, Desbiez et al. (2009) identifies several key landscapes selected by native mammalian species, including: floodplain landscape (Pampas deer, capybara); *cerrado* (Open Wood Savanna) (crab-eating fox); forest (Forest/Woodland) (peccaries, howler monkeys, coati, southern anteater, ocelot, and jaguar); scrub grassland (Open Grass Savanna) (giant anteater); and forest-edge (grey brocket deer, and southern

anteater). Some of these landscape categories, such as Forest/Woodland, are of key importance as night time shelter from prey for species that prefer open grasslands during the day, and also as vital refuges for all terrestrial species during times of extreme flooding, as they occur at slightly higher elevations (Desbiez et al., 2009). Furthermore, the aquatic habitats (Water, Swampy Grassland, Swampy Mixed Savanna, *Vazantes*) play an important role for many bird species, such as the Jabiru Stork and Agami Heron, during drought periods (Donatelli, 2001; Hamilton, 2002b). The Pantanal wetland contains the highest wetland bird species richness in the world. In addition to the large number of permanent avian inhabitants, the Pantanal is also a key migration route for many transitory species (Tubelis & Tomas, 2003). The temporary waterways (*Vazantes*) formed during flood periods provide vital migration corridors for many fish species (Fernandes et al., 2010). The permanently inundated areas (Water, some Swampy Grassland and Swampy Mixed Savanna) are essential refuges for amphibious and aquatic species during the dry season (Hamilton, 2002b). The aquatic macrophytes found in many of these flooded habitats are also an important food source for white-lipped peccaries during periods when fruits are scarce (Donatelli, 2001), as well as for Marsh Deer (Tomas et al., 2000).

As mentioned previously, the greatest threat to these natural habitats are chiefly caused by agricultural pressures occurring both within the floodplain and on the surrounding plateau. Conversion of the natural *cerrado* landscape in favour of intensive agriculture, and conversion to artificial pastures for cattle in the Taquari River catchment area on the eastern plateau has led to severe erosion causing increased siltation in the TAQR and TAQF subregions, clearly visible as the large area of Swampy Grassland

observed in these subregions (Harris, 2005; Junk & Nunes da Cunha, 2005). Although siltation in this area occurs naturally, it has accelerated in the past 30 years, coinciding with the increase in agriculture on the plateau (Godoy, 2002; Assine, 2005). This increased sedimentation has caused an overflow of the Taquari River, permanently flooding areas that previously only flooded seasonally, converting an estimated area of roughly 11000 km^2 into permanent swamp, resulting in relocation of the local human population, and a severe impact on the native fish stocks (Jongman et al, 2005, Harris et al, 2005). Although there is little in the literature on this subject concerning the CORI subregion, it has been listed as an area of critical siltation in GEF (2004). Given the high degree of agriculture occurring on the plateau north of this subregion, along the Paraguay River, a similar cause/effect relationship can be assumed, and is demonstrated by the large area of Swampy Grassland observed in the southern CORI subregion.

In an escalating economic competition with cattle ranchers on the surrounding plateau, ranchers inside the Pantanal floodplain have been pressured to increase the number of animals in their herds and accelerate conversion of natural habitat to artificial pasture (Junk & Nunes da Cunha, 2005; Junk et al., 2006). Because most natural pasture areas in the Pantanal remain under water during flood season, ranchers are introducing exotic grass species on high ground, often resulting in a loss of critical forest and *cerrado* habitat (Seidl et al, 2001; Alho, 2011b). According to Padovani et al. (2004), by the year 2000, the total area where original vegetation had been removed and replaced with exotic grasses for pasture was approximately 12000 km^2. The present classification underestimates this number; however, it is likely that some areas of pasture conversion were erroneously classified as either Swampy Grassland or Open Grass Savanna due to

the similarity in vegetation structure, as Padovani et al., (2004) considered all changes in vegetation cover caused by fire, or due to old grazing, as part of the area of original vegetation replaced by exotic grasses. Furthermore, the Padovani study was conducted on imagery from the year 2000; therefore some of these areas may have reverted back to natural grasslands by the time of the present imagery acquisition (2008).

3.5.3 Comparison with Previous Classifications

Evans et al. (2010) used a combination of C-band HH/HV and L-band HH (50m and 100m spatial resolution, respectively) to map 5 classes for the whole Pantanal wetland using an OBIA approach, and classifying image objects based solely on class backscattering thresholds (mean +/- 1 standard deviation), object standard deviations, and object proximity rules. The present classification methodology defines 10 land cover classes by incorporating all imagery at a finer spatial resolution, additional L-band HV imagery, and the Feature Space Optimization routine.

The finer scale imagery allowed for improved separation among classes because of the small size of some of the habitats within the Pantanal. For example, the Pantanal contains many very small habitats of forest vegetation known as *capões*, which represent dense stands of tall trees with an area of approximately 8000 m^2 (Nunes da Cunha & Junk, 2011). At a spatial resolution of 50 m, the smallest of these habitats would correspond to approximately 3 pixels, however, at the coarser spatial resolution of 100 m, *capões* cannot be distinguished from the surrounding landscape, but would likely be part of a mix of different vegetation structures within one pixel. C*ordilheiras*, another landscape unit of the Pantanal, are characterized by an average width of 100 m, a length of up to several kilometres, and are colonized by tall dense trees (Nunes da Cunha &

Junk, 2011). These habitats would correspond to more than 2 pixels at 50 m resolution imagery, but again, would be lost as an individual landscape unit at 100 m resolution. Given this difference in spatial resolution, image objects that incorporate these landscapes would classify differently between 50 m and 100 m resolution. For example, in the 100 m resolution imagery, an image object representing a landscape of Open Wood Savanna populated with *capões* and *cordilheiras* would likely present a homogenous group of pixels with similar backscattering, as these individual habitats would not be defined in the 100 m pixel size. Conversely, at 50 m resolution, the same image object representing a landscape of Open Wood Savanna would likely distinguish the *capões* and *cordilheiras* as individual pixels with higher backscattering values than the surrounding neighbour pixels. Consequently, the observed standard deviation for the same Open Wood Savanna image objects at 50 m resolution is generally 23% greater than the equivalent standard deviation at 100 m resolution.

The addition of the August L-band HV polarization imagery for the present study contributed to a superior classification result compared to Evans et al. (2010). For example, when looking at the Forest/Woodland, Open Wood Savanna and Open Grass Savanna classes, the difference in backscattering signal was higher at HV compared to HH polarizations (4 dB compared to 2 dB between Forest/Woodland and Open Wood Savanna, and 11 dB compared to 7 dB between Open Wood and Open Grass Savannas). When comparing these pairs of classes using the FSO tool, in both cases the August L-band HV image was selected as one of the optimal features to be included in the classification set (Figure 3.4b). The advantage of dual polarization SAR imagery for wetlands classification has been documented (Henderson & Lewis, 2008; Souza-Filho et

al., 2011; Li et al., 2012).The addition of the FSO tool combined with the supervised nearest neighbour classification methodology improved class separability by utilizing a number of parameters (area, roundness, brightness, compactness, shape index, and length/width) that were not a part of the Evans et al., (2010) classification.

Evans et al. (2010) relied on training and validation data from only a small subset of the Pantanal and thus a complete understanding of the habitats in the other subregions was lacking – this limitation was acknowledged by the authors in the previous paper. Because the present study utilized robust ground reference dataset, spatially distributed across the majority of the Pantanal, the confidence in the present validation assessment is much higher than the previous study.

A comparison of classification accuracy results with similar large-scale land cover classifications showed a range from 74% to 89% overall accuracy considering various numbers of classes, spatial and spectral resolution of imagery, and classification approach (Laba et al., 2002, Simard et al., 2002 , Durieux et al. 2007, Hoekman et al., 2010). For the present study, a higher classification accuracy was likely prevented by the high heterogeneity of the Pantanal landscape compared to other regions. However, the results are within the published ranges of classification accuracies of land cover, and specifically, for wetlands, as outlined above.

3.5 Conclusion

The results of this research provide a detailed classification showing the spatial distribution of aquatic, terrestrial and transitional habitats for the entire Pantanal wetland based on a combination of L-band dual polarization/dual season, and C-band dual polarization/dry season SAR 50 m resolution satellite imagery. The present classification

maps provide an improvement over previous classification maps of the Pantanal, specifically, that produced in Evans et al. (2010), by dividing the Pantanal into hydrological subregions, and utilizing a more robust set of ground reference data, and a higher spatial resolution imagery set. Further, the overall classification accuracy results of 80% are within the overall accuracy ranges reported by similar wetlands studies.

Sources of error in the present classification were largely a result of backscattering similarity between similar classes in areas with comparable inundation characteristics. Although the present study incorporated a dual-season imagery set, it only included one band/polarization (L-band HH) for the wet season, and the dry season imagery (August) was not necessarily the lowest water imagery possible. Additionally, particularly in areas of high heterogeneity, the spatial scale of the imagery may have been too coarse to adequately define smaller habitats. Therefore, the authors conclude that improvements can be made on the present classification by maintaining a separate subregion classification approach, and: 1) acquiring dry season imagery more representative of the lowest possible water for the entire Pantanal (October/November); 2) including a dual-season approach for C-band as well as L-band as greater differences in herbaceous habitats have been observed for wet season C-band imagery (Chapter 2); 3) incorporating finer spatial resolution imagery (12.5m L-band available from ALOS/PALSAR and 25m C-band from RADARSAT-2), and 4) the possible incorporation of dry season optical imagery (cloud free wet season optical imagery would be difficult to obtain for the study area).

The produced habitat spatial distribution maps will provide vital habitat information for determining refuge zones for terrestrial species, connectivity of aquatic

habitats during the dry season, examination of species distribution as a result of a flood-pulse regime, and risks of environmental changes to the animal population. The generated maps will also provide valuable baseline data to aid in monitoring changes in the region, and to help define conservation strategies for habitat in this wetland.

Chapter 4. Summary and Conclusions

4.1 Summary

Chapter 2 examined the usefulness of multi-temporal, fine spatial resolution (12.5 m), L-band ALOS/PALSAR, C-band RADARSAT-2, and ENVISAT/ASAR data to map the various habitats, and create a lake distribution map of the Lower Nhecolândia subregion in the Brazilian Pantanal. A backscattering analysis conducted on individual training objects of each class generally showed backscattering characteristics consistent with those reported for similar classes in relevant literature (Wang et al., 1994; Dobson et al., 1996; Hill et al., 1999; Hess et al., 2003; Costa & Telmer, 2006; Evans et al., 2010). The general classification scheme for the Lower Nhecolândia subregion was divided into three levels: Level 1 separated the lakes from the rest of the terrain ("Lakes", "Not Lakes"); Level 2 classified all land cover ("Not Lakes"), and defined six vegetation habitats (Forest/Woodland, Open Wood Savanna, Open Grass Savanna, Agriculture, Swampy Grassland and *Vazantes*), achieved at an overall accuracy of 83%; Level 3 classified the "Lakes" based on relationship found between lake vegetation and geochemistry, and separated the lakes into, a) Fresh (*baías*) and Brackish (*salinas*) lakes (accuracy results of 98%); and a further classification level separating the fresh lakes, b) Fresh Lakes with floating and emergent vegetation (*baías*), and Fresh Lakes with the presence of *Typha (salobras)* (accuracy results of 81%).

For Chapter 3, dual-season L-band ALOS/PALSAR, and C-band RADARSAT-2 imagery at a medium spatial resolution of 50 m, as well as a comprehensive set of ground reference points, were utilized to map the diverse habitats of the hydrologically variant subregions of the Pantanal by using a hierarchical object based image analysis approach.

In order to exploit the spatial and temporal variation in flooding regime throughout the Pantanal, the region was first divided into subregions based on hydrology and geology, and then each subregion was classified separately. First, mean and standard deviation values of image object training sites were evaluated, and used as the basis for forming preliminary land cover class thresholds for each subregion. Then, a combination of additional refined thresholds, hierarchical rules, and a supervised nearest neighbour algorithm (eCognition feature space optimization) employing several features as primary inputs (mean, standard deviation, seasonal change detection, brightness, maximum difference, shape and compactness) was utilized, resulting in the definition and classification of ten habitat classes: Forest/Woodland, Riparian Forest, Open Wood Savanna, Open Wood Savanna subject to prolonged flooding, Open Grass Savanna, Agriculture, Swampy Grassland, Swampy Mixed Savanna, *Vazantes*, and Water. This classification was achieved with an overall accuracy of 80% for the entire Pantanal.

The Lower Nhecolândia subregion was chosen to compare the classification results between the 12.5 m (Chapter 2) and 50 m (Chapter 3) spatial resolution products as this was the only subregion for which classification was achieved at both resolutions. Section 4.2 examines accuracy results between the two classification products regarding issues of: 1) arbitrarily defined class membership, 2) spatial resolution and scale related to the spatial heterogeneity of the landscape and the size of the individual habitats, and, 3) uncertainty of localized flooding conditions at the time of imagery acquisition. Section 4.3 will provide a comparison and discussion of the present classification results with previous Pantanal classification products, specifically, those produced by GEF (2004), PROBIO (2007) and Evans et al. (2010) for the 50 m spatial resolution product, and

Costa & Telmer (2006) and Novack et al. (2010) for the 12.5 m spatial resolution lakes classification, specifically. Finally, section 4.5 will outline the final conclusions of this research, as well as any recommendations for improvement on the present classification products.

4.2 Comparison of 12.5 m and 50 m spatial resolution classification results (Nhecolândia subregion)

Figures 4.1a and 4.1b show the spatial distribution of land cover units for the Nhecolândia subregion of the Pantanal at 12.5 m (Chapter 2) and 50 m (Chapter 3) spatial resolutions, respectively. Validation results for the classification maps of this subregion are seen in Table 4.1a (Chapter 2) and 4.1b (Chapter 3), respectively. As expected, overall accuracy is higher for the 12.5 m resolution classification product (83%) than the 50 m resolution (72%). In general, the highest degree of confusion when considering both the 12.5 m and 50 m resolution Nhecolândia classifications related to issues of 1) issues related to arbitrary membership assignment of classes, 2) the scale of habitats in relation to spatial resolution of the imagery, and 3) variable flooding patterns.

The medium resolution classification resulted in some confusion between the Forest/Woodland and Open Grass Savanna classes with the Open Wood Savanna class. Although 100% of the Open Wood Savanna validation objects were correctly classified as such, an additional 35% of Forest/Woodland and 20% of Open Grass Savanna were erroneously classified as Open Wood Savanna as well. The first factor causing this confusion related to class membership assignment. Forest/Woodland and Open Wood Savanna are both comprised of differing degrees of woody vegetation with no straightforward border between the two. Similarly, Open Wood Savanna and Open Grass Savanna are comprised of differing degrees of herbaceous grassy stratum. Many classes

form a continuum along a biomass gradient, and when arbitrary ranges are chosen for delineating membership to each class, some confusion among adjacent classes is likely to occur (Hoekman et al., 2010).

The second factor resulting in confusion between the Forest/Woodland, Open Wood Savanna and Open Grass Savanna classes was related to matters of landscape scale when considering the high spatial heterogeneity of the Nhecolândia landscape. Because of this high spatial heterogeneity, the habitats may not have been adequately captured at 50 m spatial resolution. For example, the region contains many very small islands of forest vegetation known as *capãos*, which are habitats representing islands of dense tall trees with an average area of approximately 8000 m^2 (Nunes da Cunha & Junk, 2011), and would correspond to approximately 50 pixels at 12.5 m resolution and 3 pixels at 50 m resolution imagery. C*ordilheiras*, another landscape unit of the Pantanal, are characterized by an average width of 100 m, a length of up to several kilometres, and are colonized by tall dense trees (Nunes da Cunha & Junk, 2011). C*ordilheiras* would correspond to a width of approximately 8 pixels at 12.5 m resolution and 2 pixels at 50 m resolution imagery. The small number of pixels representing these habitats in 50 m spatial resolution imagery would not allow for proper classification; the mix of grassy patches and/or forest islands together in one image object would have been classified as Open Wood Savanna instead of Forest/Woodland. In comparison, for the fine spatial resolution classification, only 10% of Forest/Woodland, and 5% of Open Grass Savanna validation objects were erroneously classified as Open Wood Savanna, a marked improvement from the medium resolution classification.

The difference in classification results between these three classes was apparent when comparing the final area (km^2) between the medium and fine spatial resolution maps. For the fine resolution classification, Nhecolândia had the highest overall contribution from the Open Grass Savanna Class (2230 km^2, 27%), followed by Forest/Woodland (1790 km^2, 22%), and Open Wood Savanna (1270 km^2, 15%). However, the results for the medium resolution classification were dramatically different, with an increase in total land coverage for Open Wood Savanna (3275 km^2, 40%), and a decrease in total land coverage for the Forest/Woodland (961 km^2, 12%) and Open Grass Savanna (740 km^2, 9%) classes. This further supports the conclusion that the fine resolution imagery is key for separating discrete habitats given the high spatial heterogeneity of this landscape.

Additional issues related to landscape scale and spatial resolution were encountered when considering the numerous lakes in Lower Nhecolândia. These lakes are generally smaller than 50 000 m^2 (Costa & Telmer, 2007), which roughly corresponds to 320 pixels and 20 pixels for 12.5 and 50m resolution, respectively. Further, the majority of the saline lakes have an average area of 5 000 m^2 (Medina-Junior & Reitzler, 2005), thus corresponding to 32 and 2 pixels at a 12.5 and 50 m resolution respectively. Again the smaller number of pixels representing each lake, especially the saline lakes, is not adequate for proper lakes classification with imagery at a 50 m spatial resolution (Costa & Telmer, 2007). As such, the classification of a water class (lakes) at 50 m resolution was deliberately avoided; instead the classified lake mask from the 12.5 m resolution product was imported.

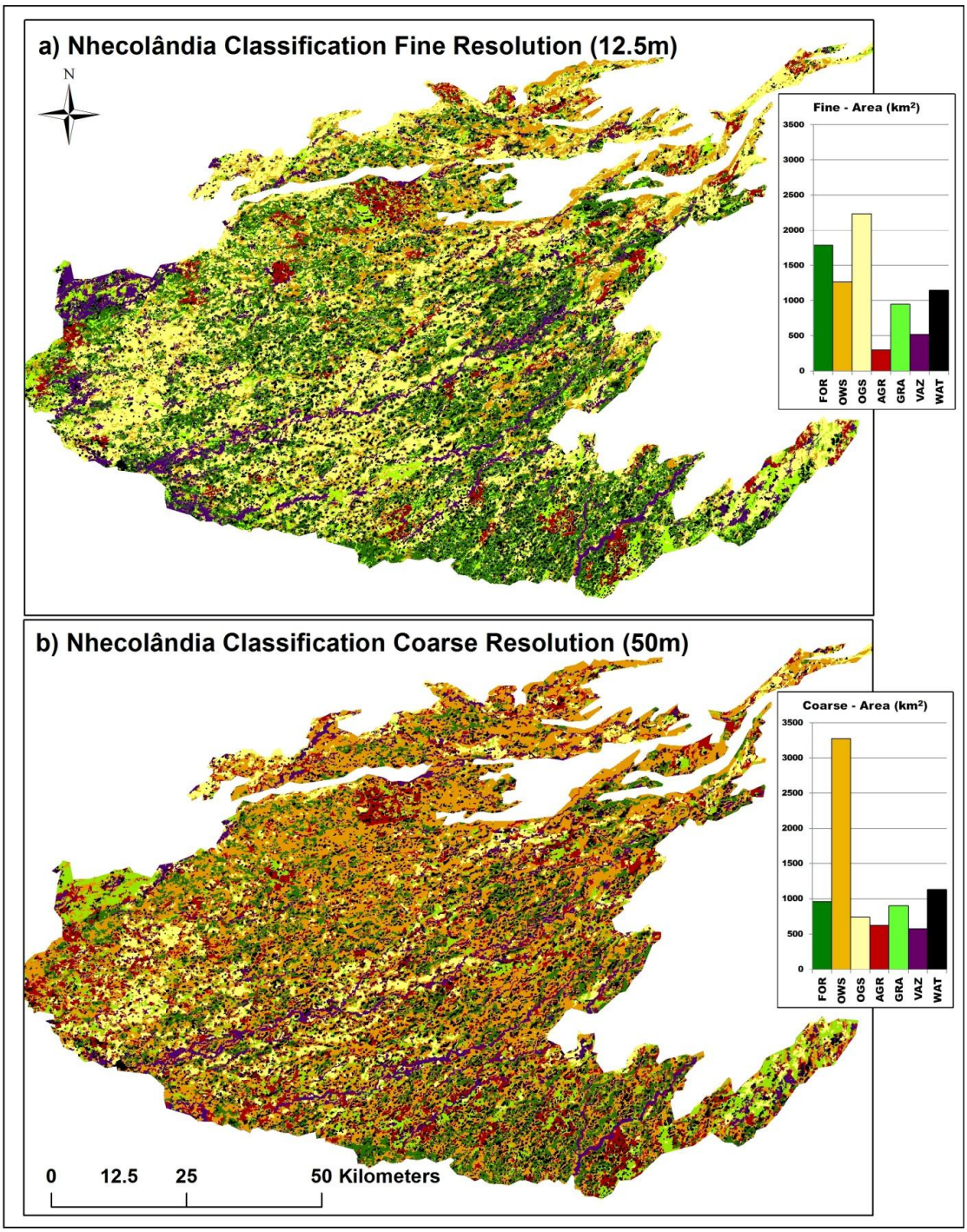

Figure 4.1 Comparison of a) fine (12.5 m) and b) medium (50 m) spatial resolution classification maps of the Nhecolândia subregion

Table 4.1 Accuracy assessment results for a) Lower Nhecolândia, 12.5 m spatial resolution land cover classes, b) Lower Nhecolândia 12.5 m spatial resolution lake classes, c) Entire Pantanal, 50 m spatial resolution, land cover classes.

a) Nhecolândia (12.5m)		CLASSIFIED AS								
		Forest Woodland	Open Wood Savanna	Open Grass Savanna	Agriculture	Swampy Grassland	Vazante	Water	Row Total	Error of Omission (%)
REFERENCE DATA	Forest Woodland	39	5	2	0	0	0	0	46	15
	Open Wood Savanna	2	27	3	1	0	1	0	34	21
	Open Grass Savanna	1	2	38	0	1	2	0	44	14
	Agriculture	0	1	2	21	1	1	0	26	19
	Swampy Grassland	0	0	9	0	23	2	0	34	32
	Vazante	0	0	1	1	4	20	1	27	26
	Water	0	0	4	0	4	0	78	86	9
	Column Total	42	35	59	23	33	26	79	297	
	Error of Commission (%)	7	23	36	9	30	23	1	accuracy (% correct)=	83

b) Nhecolândia (50m)		CLASSIFIED AS								
		Forest Woodland	Open Wood Savanna	Open Grass Savanna	Agriculture	Swampy Grassland	Vazante	Water	Row Total	Error of Omission (%)
REFERENCE DATA	Forest Woodland	11	6	0	0	0	0	0	17	35
	Open Wood Savanna	0	9	0	0	0	0	0	9	0
	Open Grass Savanna	0	2	7	0	1	0	0	10	30
	Agriculture	0	0	1	3	1	0	0	5	40
	Swampy Grassland	0	0	0	1	7	0	0	8	13
	Vazante	0	0	0	3	1	11	0	15	27
	Water	0	0	0	0	0	0	0	0	
	Column Total	11	17	8	7	10	11	0	67	
	Error of Commission (%)	0	47	13	57	30	0		accuracy (% correct)=	72

		CLASSIFIED AS:											
	c) PANTANAL (50m)	Forest Woodland	Riparian Forest	Open Wood Savanna	Open Wood Savanna Flood	Open Grass Savanna	Swampy Grassland	Swampy Mixed Savanna	Agriculture	Vazante	Water	Row Total	Error of Omission (%)
REFERENCE DATA	Forest Woodland	60	4	14	5	0	0	0	0	0	0	83	28
	Riparian Forest	4	23	0	3	0	0	1	0	0	0	31	26
	Open Wood Savanna	1	0	66	0	0	1	0	0	0	0	68	3
	Open Wood Savanna Flood	0	4	5	31	0	0	0	1	0	0	41	24
	Open Grass Savanna	0	0	3	0	17	0	0	3	0	0	23	26
	Swampy Grassland	0	0	1	0	4	51	0	3	2	1	62	18
	Swampy Mixed Savanna	0	1	0	3	0	1	4	0	0	0	9	56
	Agriculture	0	0	0	0	3	2	0	22	0	0	27	19
	Vazante	0	0	0	0	1	6	0	1	23	0	31	26
	Water	0	0	0	0	0	0	0	0	0	14	14	0
	Column Total	65	32	89	42	25	61	5	30	25	15	389	
	Error of Commission (%)	8	28	26	26	32	16	20	27	8	6	accuracy (% correct)=	80

The third major source of confusion for the 50 m classification of Lower Nhecolândia was related to uncertainty in localized flooding conditions at time of imagery acquisition. In this respect, the medium resolution classification showed the greatest degree of confusion with the *Vazante* class, where 7% of image objects were misclassified as Swampy Grassland, and 20% as Agriculture. Further, 20% of Agriculture validation objects were misclassified as Open Grass Savanna, and 20% as Swampy Grassland. In this case, the fine spatial resolution classification did not perform much better: for the Swampy Grassland class, 26% was misclassified as Open Grass Savanna, and for the Vazante class, 14% was misclassified as Swampy Grassland. There are two possible explanations for these errors. 1) although planted pasture (Agriculture) typically occurs in areas not prone to long periods of inundation, given the abundance of fresh water lakes in some of the larger agricultural plots, it is likely that at least some partial/localized flooding does occur in these areas, 2) *Vazantes* and Swampy Grassland are fundamentally the same type of cover in terms of vegetation structure and inundation patterns, and thus show similar backscattering characteristics; they are differentiated only by the geometrically defined drainage channel aspect of the *Vazantes* compared to the more amorphous shape of the Swampy Grassland, and the timing and duration of inundation. Further, the utilization of the water mask (created from the fine spatial resolution imagery) may have contributed additional confusion for the medium resolution classification, as these very small image objects may have broken up areas that would have been segmented into larger objects had the mask not been used. Nonetheless, the use of the mask was necessary to preserve the lakes as individual entities. Regardless of these sources of error, there was no significant change in the overall area (km^2) for any of these

cover types between the fine and medium spatial resolution classification maps with the exception of Agriculture, which increased from 300 km^2 to 600 km^2.

4.3 Comparison of Pantanal classification results with previous work

The achieved classification results for the present study (Chapter 3, entire Pantanal at 50 m spatial resolution) were compared with other large scale classification maps that cover the entire Pantanal wetland. Generally, these are maps produced by GEF (2004), PROBIO (2007), and Evans et al. (2010). Unfortunately, the GEF (2004) and PROBIO (2007) maps, both derived from satellite imagery, do not provide an accuracy assessment. A visual comparison of our classification map to the map supplied by GEF (2004) based on a mosaic of 5 years of Landsat mosaicked imagery, shows that the current produced map offers a more detailed spatial distribution of habitats for the region, as well as a greater number of classes (10, compared to GEF's 5). For example, the GEF map has combined the present Forest/Woodland, Riparian Forest and Open Wood Savanna - Flood classes into one Forest class, and large areas of the present Swampy Grassland and Swampy Mixed Savanna classes are included in the Water class for the GEF classification. While it has been acknowledged that the present Swampy Mixed Savanna and Swampy Grassland classes do include areas that are permanently waterlogged, the GEF classification seems to include all herbaceous areas subjected to prolonged inundation within the same class as permanent water bodies, such as rivers and lakes. Moreover, the GEF map combines the present Open Wood Savanna and Open Grass Savanna into one *Cerrado* class. That being said, the GEF spatial distribution of these combined classes, as well as their Pasture class (the present Agriculture), are in general

agreement with the present corresponding classes; however, no accuracy assessment was provided with the GEF classification.

Comparison of the present results with the PROBIO (2007) derived map, which was based on 2002 Landsat imagery acquired from July to October (dry season), shows a considerable amount of agreement. The spatial distribution of both our Forest/Woodland, and Agriculture classes correspond well with PROBIO's *Cerradão* and Planted Pasture classes, respectively, and much of the region is classified by PROBIO as varying combinations of Forested (*Florestada*), Woody (*Arborizada*) and Grassy (*Gramineo-Lenhosa*) Savannas, thus matching our Forest/Woodland, Open Wood Savanna and Open Grass Savanna classes, respectively. The greatest divergence between PROBIO and the present classification appears to be in the PROBIO Pioneer classes: PROBIO uses the Pioneer term for large areas of the present Swampy Grassland, Swampy Mixed Savanna and Open Wood Savanna-Flood classified areas. However, we acknowledge that the present corresponding classes often have a high component of pioneer species; therefore, any disagreement with PROBIO is largely a result of the methods for categorizing land cover. For instance, PROBIO has chosen to group their land cover classes according to vegetation species, whereas the present classification was based largely on vegetation structure and inundation regime. In addition, we classify the PROBIO's Chaco biome in the southwest Pantanal as dominated by Open Wood Savanna, Open Wood Savanna-Flood and Swampy Grassland classes, which match PROBIO's description of woody and grassy Chaco savanna for this region (again, the present class descriptions acknowledge the presence of Chaco vegetation for Open Wood Savanna classes in the NABI and MIRA subregions). The chief differences between the present classification and PROBIO

are related to 1) differences in nomenclature; 2) differences in class organization, and 3) a lack of a flooding dynamic component in the PROBIO classification. Regardless of these differences, the spatial distribution of the land cover units in the present classification still agrees well with corresponding land cover units in the PROBIO map; however, as with GEF (2004), the accuracy assessment of the classification map from PROBIO was not included.

Evans et al. (2010) used a combination of C and L-band (50m and 100m spatial resolution, respectively) to map 5 classes for the whole Pantanal wetland using an OBIA approach, and classifying image object based solely on class backscattering thresholds (mean +/- 1 standard deviation), object standard deviations, and object proximity rules. Evans et al. (2010) combined the present Forest/Woodland, Riparian Forest and Open Wood Savanna-Flood into one Forest class, and permanently waterlogged areas of the present Swampy Grassland class were previously categorized as Aquatic Vegetation. The previous classification also combined areas of Swampy Grassland, Agriculture and Open Grass Savanna into one Grasslands/Agriculture class. Taking these combined classes into account, there is general agreement between the present classification and the Evans et al. map, although the present Open Wood Savanna class covers a greater area of the Pantanal than previously reported. The previous classification relied on training and validation data from only a small subset of the Pantanal (primarily NHEC with some sites in AQUI, MIRA and TAQF) and thus a complete understanding of the habitats in the other subregions was lacking – this limitation was acknowledged by the authors in the previous paper. Because the present study utilized a far more robust ground reference dataset covering the majority of the Pantanal, the confidence in the present validation

assessment is much higher than the previous study. In addition, the present classification methodology incorporated the use of the Feature Space Optimization routine to define the optimal set of features for class separability, and utilized a number of feature parameters (area, roundness, brightness, compactness, shape index, and length/width) that were not included in the previous classification. Further, the present classification utilized additional L-band HV polarization image data not available for the previous classification, allowing increased separability between classes. Finally, the present classification map defines 10 land cover classes (compared to the previous 5) and with a finer spatial resolution allows for a more detailed product than was possible with Evans et al., (2010).

A comparison of the present 12.5 m spatial resolution lakes classification of the Nhecolândia subregion (Chapter 2) Level 3a results (Fresh Water Lake vs. Brackish Lake) with Novack et al. (2010) Lower Nhecolândia Lakes classification performed using a similar OBIA classification methods, but using ASTER imagery (optical bands, 15m-30m spatial resolution), revealed a much higher overall accuracy of the present classification results (fresh water/brackish water classes - 98%) compared to Novack et al. (80% non-*salina*/*salina* classes). Moreover, Novack et al.'s study was comprised of only a small subset of the Lower Nhecolândia subregion, and did not include a separation of fresh water aquatic vegetation. A more suitable comparison is found with Costa & Telmer (2006)'s lake classification of a larger subset of Lower Nhecolândia using L and C-band HH dry season SAR imagery (JERS-1 and RADARSAT-2, respectively). A visual comparison of the present Level 3a-b classifications with the 2006 Level 1-2 classifications (same classes for both levels) shows general agreement in the spatial

distribution of the lakes, however, Costa & Telmer's brackish water is overrepresented compared to the present results. The imagery dataset used for this study included both HH and HV polarization, dual season imagery, which may have resulted in detection of aquatic vegetation not possible with HH polarization only, or the detection of vegetation present only during the wet season. Regardless, the present overall accuracy results are comparable to the above authors (98% and 81% compared to 91% and 83% for levels 3a/1 and 3b/2 respectively). However, the current study presents a classification of the entire Lower Nhecolândia subregion, and offers an updated spatial distribution map using more recent and comprehensive field data. As with the present 50 m classification of the whole Pantanal, the 12.5 m resolution classification of Nhecolândia incorporated the use of the Feature Space Optimization routine to define the optimal set of features for class separability, further aiding in class separation.

4.4 Conclusions

The Pantanal wetland is home to a great biodiversity of flora and fauna species, many of them threatened; yet, it is one of the least protected ecosystems with respect to the International Union for Conservation of Nature, with less than 5% of the ecosystem in reserve (Rylands & Brandon, 2005). Despite its importance, the Pantanal wetland is under threat from a number of anthropogenic causes. An increase in high intensity agricultural activity on the north and eastern plateau has resulted in a critical sedimentation problem, particularly observed in the Taquari Fan and Corixo Grande subregions, as well as in contamination of the floodplain waters with agrochemicals and other pollutants (da Silva & Girard, 2004; Assine, 2005). Within the floodplain, the removal of native vegetation in favour of exotic grasses optimal for cattle grazing, as well

as the burning of grasslands to renew pasture and control weeds, have resulted in increased natural habitat loss (Harris et al., 2005; Desbiez et al., 2009). The ecological structure and spatial distribution of habitats in the Pantanal are closely tied to the seasonal hydrological regime. The considerable spatial variability in the timing and extent of the seasonal inundation cycle in the Pantanal explains many of the ecological differences in habitat among the different subregions. As such, there is a vital need for 1) a detailed account of present habitat spatial distribution; and 2) methods that allow the quantification and monitoring of the occurring changes and impacts in the region so that sustainable management practices and effective conservation units can be established.

The results of this research provide a detailed classification showing the spatial distribution of aquatic, terrestrial and transitional habitats for the entire Pantanal wetland based on a combination of L-band dual polarization/dual season, and C-band dual polarization/dry season SAR satellite imagery at 12.5 m and 50 m spatial resolution, for the Lower Nhecolândia subregion, and the entire Pantanal wetland, respectively.

The results of the research in Chapter 2 provide the first fine spatial resolution (12.5 m) land cover classification showing the spatial distribution of aquatic, terrestrial and transitional habitats, and included a spatial distribution map of the three geochemically variant lake types. Overall accuracy was achieved at 83% for the Level 2 land cover classification, and 98% and 81% for the Levels 3a and 3b lakes classification, respectively. In addition, the results of the research in Chapter 3 provide a detailed classification showing the spatial distribution of aquatic, terrestrial and transitional habitats for the entire Pantanal wetland based on a combination of L-band dual polarization/dual season and C-band dual polarization/dry season SAR satellite imagery

with overall accuracy of 80%. The backscattering analysis conducted at both levels showed that a single image did not allow for proper separation among the classes of interest, and that even class thresholds built from object mean and standard deviation values on multiple images concurrently were not sufficient to adequately separate the various classes. The combination of dual-season, C and L-band, high spatial resolution imagery, coupled with a combination of mean thresholds, hierarchical rules, and the utilization of the Feature Space Optimization tool using additional parameters, such as object shape and compactness, were essential for providing the relatively high overall accuracy results. The present classification maps provide a considerable improvement over previous classification maps of the Pantanal, specifically, that produced in Evans et al. (2010), by dividing the Pantanal into hydrological subregions, utilizing a far more robust set of ground reference data and a higher spatial resolution imagery set, and employing a more complex classification scheme. Furthermore, utilizing SAR imagery allowed the advantage of image acquisition year-round regardless of cloud cover, thus allowing classification of dynamic land cover affected by seasonal inundation, while the PROBIO map was compiled using only optical imagery from July to October, generally during the dry period, due to the lower degree of cloud cover present in this season (PROBIO, 2007). The produced map provides spatial information on hydrology and vegetation that is unprecedented in its detail for the entire Pantanal region.

A comparison of fine (12.5 m) and coarse (50 m) spatial resolution classification maps of the Nhecolândia subregion, produced using the same methods, shows that a considerable improvement in classification accuracy was achieved with the fine spatial resolution imagery (83% vs. 72% for fine and coarse resolution, respectively). Given this

result, the conclusion is that significant improvements could also be achieved in other subregions of the Pantanal, particularly those with a high heterogeneity of landscape, as well as a lower than desired accuracy result for the present coarse resolution classification, for example the Cuiaba subregion (overall accuracy of only 50%). In addition, further improvements in accuracy could be gained by the addition of both L and C-band data acquired at several temporal points throughout the entire hydrological cycle rather than just a single wet and single dry date.

The detailed classification methods presented in this thesis are highly site specific. However, the main classification steps using eCognition (definition of class thresholds, FSO routine, additional refinement of rules) is transferrable to other global wetland classifications studies. Additionally, the suggestions for improvements to the present research also hold true for other large scale tropical wetland studies.

The produced fine and medium spatial resolution maps will provide vital habitat information for determining refuge zones for terrestrial species, connectivity of aquatic habitats during the dry season, examination of species distribution as a result of a flood-pulse regime, and risks of environmental changes to the animal population. The generated maps will also provide valuable baseline data to aid in monitoring changes in the region, and to help define conservation strategies for habitat in this wetland.

Chapter 5. Bibliography

Abdon, M., da Silva, J., Pott, V. J., Pott, A., & Da Silva, M. P. (1998). Utilization of analogic data of Landsat_TM on screening vegetation of part of the Nhecolandia subregion of the Brazilian Pantanal. Brazilian Journal of Agricultural Research, 33, 1799-1813.

Ah, B., Kwon, G. J., & Kim, J. G. (2007). The Optimal Environmental Ranges for Wetland Plants : II. Scirpus tabernaemontani and Typha latifolia. Journal of Ecology and Field Biology, 30(2), 151-159.

Alho, C. J. R. (2008). Biodiversity of the Pantanal: response to seasonal flooding regime and to environmental degradation. Brazilian journal of biology, 68(4 Suppl), 957–966.

Alho, C. J. R., Camargo, G., & Fischer, E. (2011a). Terrestrial and aquatic mammals of the Pantanal. Brazilian Journal of Biology, 71(1 Suppl 1), 297–310.

Alho, C. J. R., Mamede, S., Bitencourt, K., & Benites, M. (2011b). Introduced species in the Pantanal: implications for conservation. Brazilian Journal of Biology, 71(1 Suppl. 1), 321-325.

Almeida, T. I. R., Sígolo, J. B., Fernandes, E., Queiroz Neto, J. P., Barbiero, L., & Sakamoto, A. Y. (2003). Proposta de classificação e gênese das lagoas da baixa Nhecolândia-MS combase em sensoriamento remote e dados de campo, Revista Brasileira de Geociências, 33(2 (supplemental), 83-90.

Almeida, T. I. R., Calijuri, M. D. C., Falco, P. B., Casali, S. P., Kupriyanova, E., Filho, A. C. P., Sigolo, J. B., & Bertolo, R. A. (2011). Biogeochemical processes and the diversity of Nhecolândia lakes, Brazil. Annals of the Brazilian Academy of Sciences, 83(2), 391-407.

Anderson, B. J. R., Hardy, E. E., Roach, J. T., & Witmer, R. E. (1976). A Land Use and Land Cover Classification System for Use with Remote Sensor Data. Geological Survey Professional Paper 964. United States Government Printing Office, Washington.

Arieira, J., Karssenberg, D., de Jong, S. M., Addink, E. A., Couto, E. G., Nunes da Cunha, C., & Skøien, J. O. (2011). Integrating field sampling, geostatistics and remote sensing to map wetland vegetation in the Pantanal, Brazil. Biogeosciences, 8(3), 667–686.

Assine, M. (2005). River avulsions on the Taquari megafan, Pantanal wetland, Brazil. Geomorphology, 70(3-4), 357–371.

Baghdadi, M., Bernier, R., Gauthier, N., & Neeson, I. (2001). Evaluation of C-band SAR data for wetlands mapping. International Journal of Remote Sensing, 22(1), 71-88.

Barbiéro, L., de Queiroz Neto, J. P., Ciornei, G., Sakamoto, A. Y., Capellari, B., Fernandes, E., & Valles, V. (2002). Geochemistry of Water and Ground Water in the Nhecolândia, Pantanal of Mato Grosso, Brazil: Variability and Associated Processes. Wetlands, 22(3), 528-540.

Batzer, D. P. & Sharitz, R. (2006). Ecology of freshwater and estuarine wetlands. Los Angeles: University of California Press. p. 568.

Beall, A. D. & Lewis, A. J. (1998). Detecting and mapping flotant using synthetic aperture radar data. IGARSS 1998: Sensing and Managing the Environment: 1998 IEEE International Geoscience and Remote Sensing Symposium proceedings : Seattle, 6-10 July, 1998, Sheraton Seattle, Seattle, WA, USA

Benson, B. J., Mackenzie, M. D., Street, N. P., & Street, D. (1995). Effects of sensor spatial resolution on landscape structure parameters. Landscape Ecology, 10(2), 113–120.

Benz, U., Baatz, M., Schreier, G. (2001). OSCAR-object oriented segmentation and classification of advanced radar allow automated information extraction. Proceedings of IGARSS, Sydney session: Visualization, GIS and Data Fusion, 1913-1915.

Blaschke, T., & Hay, G. J. (2001). Object-oriented image analysis and scale-space: theory and methods for modeling and evaluating multiscale landscape structure. International Archives of Photogrammetry and Remote Sensing, 34(Part 4/W5), 22-29.

Brown, R., Brisco, B., D'Iorio, M., Prevost, C., Ryerson, R. And Singhroy, V. (1996). RADARSAT applications: review of GlobeSAR Program. Canadian Journal of Remote Sensing, 22, 404-419.

Campos Filho, L.V. S. (2002). Tradição e ruptura: cultura e ambiente pantaneiros. Cuiabá: Entrelinhas, 180 p.

Carpenter, L., Stone, J. & Griffin, C.R. (2011) Accuracy of Aerial Photography for Locating Seasonal (Vernal) Pools in Massachusetts. Wetlands, 31, 573–581.

Cavalcanti, S. M. C., & Gese, E. M. (2009). Spatial ecology and social interaction of jaguars (*Panthera onca*) in the southern Pantanal, Brazil. Journal of Mammalogy, 90(4), 935-945.

Chopra, R., Verma, V. K., & Sharma, P. K. (2001). Mapping, monitoring and conservation of Harike wetland ecosystem, Punjab, India, through remote sensing. International Journal of Remote Sensing, 22(1), 89-98.

Comber, A., Medcalf, K., Lucas, R., Bunting, P., Brown, A., Clewley, D., Breyer, J., & Keyworth, S. (2010). Managing uncertainty when aggregating from pixels to objects: habitats, context-sensitive mapping and possibility theory. International Journal of Remote Sensing, 31(4), 1061-1068.

Congalton, R. (1991). A review of assessing the accuracy of classifications of remotely sensed data. Remote Sensing of Environment, 37(1), 35-46.

Costa, M. P. F., Niemann, O. Novo, E., Ahern, F., & Mantovani, J. (2002). Biophysical properties and mapping of aquatic vegetation during the hydrological cycle of the Amazon floodplain using JERS-1 and Radarsat. International Journal of Remote Sensing, 23 (7), 1401-1426.

Costa, M. P. F. (2004). Use of SAR satellites for mapping zonation of vegetation communities in the Amazon floodplain. International Journal of Remote Sensing, (25), 1817-1835.

Costa, M. P. F., & Telmer, K. H. (2006). Utilizing SAR imagery and aquatic vegetation to map fresh and brackish lakes in the Brazilian Pantanal wetland. Remote Sensing of Environment, 105, 204 - 213.

Costa, M. P. F. & Telmer, K. H. (2007). Mapping and monitoring lakes in the Brazilian Pantanal wetland using synthetic aperture radar imagery. Aquatic Conservation: Marine and Freshwater Ecosystems, 17, 277-288.

Cserhalmi, D., Nagy, J. Kristof, D., Neidert, D. (2011). Changes in Wetland Ecosystem: A Vegetation Reconstruction Study Based on Historical Panchromatic Aerial Photographs and Succession Patterns. Folia Geobotanica, 46, (4), 351-371.

da Silva, C. J., & Girard, P. (2004). New challenges in the management of the Brazilian Pantanal and catchment area. Wetlands Ecology and Management, 12, 553-561.

Damasceno-Junior, G. A., Semir, J., Antonio Maës Dos Santos, F., & de Freitas Leitão-Filho, H. (2005). Structure, distribution of species and inundation in a riparian forest of Rio Paraguai, Pantanal, Brazil. Flora - Morphology, Distribution, Functional Ecology of Plants, 200(2), 119–135.

Davidson, N. C., & Finlayson, C. M. (2007). Earth Observation for wetland inventory , assessment and monitoring, 228, 219–228.

De Souza, O.C., M.R. Aruajo, L.A.K. Mertes and J.M. Melack. Form and process along the Taquari River alluvial fan, Pantanal, Brazil. Zeitschrift fur Geomorphologie, 129, 73-107.

Desbiez, A. L. J., Bodmer, R. E., & Santos, S. A. (2009). Wildlife habitat selection and sustainable resources management in a Neotropical wetland. International Journal of Biodiversity and Conservation, 1(1), 011-020.

Dobson, M. C., Pierce, L. E., & Ulaby, F. T. (1996). Knowledge-Based Land-Cover Classification Using ERS- l/JERS- 1 SAR Composites. IEEE Transactions on Geoscience and Remote Sensing, 34(1), 83-99.

Donatelli, R. J. (2001). Monitoring bird richness and diversity: birds and dynamic habitat mosaics in the Pantanal, southwestern Brazil. Report in: Brazil Conservation Research Initiative – Annual update 2001. Earthwatch Institute.

Dunnett, C. W. (1980). Pairwise Multiple Comparisons in the Unequal Variance Case. Journal of the American Statistical Association, 75(372), 796- 800.

Durieux, L., Kropácek, J., de Grandi, G. D., & Achard, F. (2007). Object-oriented and textural image classification of the Siberia GBFM radar mosaic combined with MERIS imagery for continental scale land cover mapping. International Journal of Remote Sensing, 28(18), 4175-4182.

Eaton, D. P. (2001). Conservation of fresh water invertebrates, fishes, and habitats in the Pantanal wetlands. Report in: Brazil Conservation Research Initiative – Annual update 2001. Earthwatch Institute.

Esch, T., Thiel, M., Bock, M., Roth, A., & Dech, S., (2008). Improvement of Image Segmentation Accuracy Based on Multiscale Optimization Procedure. IEEE Geoscience and Remote Sensing Letters, 5(3), 463-467.

Evans, T. L., Costa, M., Telmer, K., & Silva, T. S. F. (2010). Using ALOS/PALSAR and RADARSAT-2 to Map Land Cover and Seasonal Inundation in the Brazilian Pantanal. IEEE Journal of Selected Topics in Applied Earth Observations and Remote Sensing, 3(4), 560-575.

Fernandes, I. M., Machado, F. A., & Penha, J. (2010). Spatial pattern of a fish assemblage in a seasonal tropical wetland : effects of habitat, herbaceous plant biomass, water depth, and distance from species sources. Neotropical Ichthyology, 8(2), 289-298.

Galvão, L. S., Filho, W. P., Abdon, M. M., Novo, E. M. M. L., Silva, J. S. V., & Ponzoni, F. J. (2003). Spectral reflectance characterization of shallow lakes from the Brazilian Pantanal wetlands with field and airborne hyperspectral data. International Journal of Remote Sensing, 24(21), 4093-4112.

GEF (Global Environment Facility) Pantanal/Upper Paraguay Project, Implementation of Integrated River Basin Management Practices in the Pantanal and Upper Paraguay River Basin. Strategic Action Program for the Integrated Management of the Pantanal and Upper Paraguay River Basin. Brasilia: TDA Desenho and Arte Ltda, ANA/GEF/UNEP/OAS, 2004.

Girard, P. (2011). Hydrology of surface and ground waters in the Pantanal floodplains. In Wolfgang Johannes Junk, C. J. da Silva, C. Nunes da Cunha, and K. M. Wantzen (Eds.), The Pantanal: Ecology, biodiversity and sustainable management of a large neotropical seasonal wetland Sofia-Moscow: Pensoft Publishers, 103-126.

Godoy, J. M., Padovani, C. R., Guimarães, J. R. D., Pereira, J. C. A., Vieira, L. M., Carvalho, Z. L., & Galdino, S. (2002). Evaluation of the Siltation of River Taquari, Pantanal, Brazil, through 210Pb Geochronology of Floodplain Lake Sediments. Journal of the Brazilian Chemical Society, 13(1), 71–77.

Grenier, M., Labrecque, S., Garneau, M., & Tremblay, A. (2008). Object-based classification of a SPOT-4 image for mapping wetlands in the context of greenhouse gases emissions: the case of the Eastmain region, Québec , Canada. Canadian Journal of Remote Sensing, 34(2-Supplemental), 398-413.

Hamilton, S. K., Sippel, S. J., & Melack, J. M. (1996). Inundation patterns in the Pantanal wetlands of South America determined from passive microwave remote sensing. Archiv für Hydrobiologie, 137(1), 1-23.

Hamilton, S. K. (2002a). Comparison of inundation patterns among major South American floodplains. Journal of Geophysical Research, 107(0), 1–14.

Hamilton, S. K. (2002b). Hydrological controls of ecological structure and function in the Pantanal Wetland (Brazil). The Ecohydrology of South American Rivers and Wetlands (IAHS Special), 133–158.

Harris, M. B., Tomas, W., Mourao, G., da Silva, C. J., GuiMaraes, E., Sonoda, F., & Fachim, E. (2005). Safeguarding the Pantanal Wetlands: Threats and Conservation Initiatives. Conservation Biology, 19(3), 714-720.

Harvey, K. R., & Hill, G. J. E. (2001). Vegetation mapping of a tropical freshwater swamp in the Northern Territory, Australia: a comparison of aerial photography, Landsat TM and SPOT satellite imagery. International Journal of Remote Sensing, 22(15), 2911-2925.

Heckman, C. W. (1998). The Pantanal of Poconé: Biota and ecology in the northern section of the world's largest pristine wetland. Kluwer Academic Publishers, The Netherlands.

Henderson, F., & Lewis, A. (2008). Radar detection of wetland ecosystems: a review. International Journal of Remote Sensing, 29(20), 5809-5835.

Hess, L. L., Melack, J. M., & Filoso, S. (1995). Delineation of inundated area and vegetation along the Amazon floodplain with the SIR-C synthetic aperture radar. IEEE Transactions on Geoscience and Remote Sensing, 33(4), 896-904.

Hess, L. L., Melack, J. M., Barbosa, C. C. F., & Gastil, M. (2003). Dual-season mapping of wetland inundation and vegetation for the central Amazon basin. Remote Sensing of Environment, 87, 404 - 428.

Hewes, L. (1951). The Northern wet prairie of the United States - nature, sources of information, and extent. Annals of the Association of American Geographers, 41(4), 307-323.

Hill, M. J., Donald, G. E., & Vickery, P. J. (1999). Relating radar backscatter to biophysical properties of temperate perennial grassland. Remote Sensing of Environment, 67, 15-31.

Hoekman, D. H., Vissers, M. A. M., & Wielaard, N. (2010). PALSAR wide-area mapping of Borneo: methodology and map validation. IEEE Journal of Selected Topics in Applied Earth Observations and Remote Sensing, 3(4), 605-617.

Howland, W. (1980) Multispectral aerial photography for wetland vegetation mapping. Photogrammetrical Engineering and Remote Sensing, 46, 7–99.

Jongman, R. H. G. (ed.) (2005). Pantanal-Taquari Tools for decision making in Integrated Water Management. Holanda: Alterra, Wageningen UR, 40.

Junk, W. J., Bayley, P. B., & Sparks, R. E. (1989). The flood pulse concept in river-floodplain systems. Canadian Special Publication of Fisheries and Aquatic Sciences, 106, 110-127.

Junk, W., & Cunha, C. (2005). Pantanal: a large South American wetland at a crossroads. Ecological Engineering, 24(4), 391–401.

Junk, W. J., Cunha, C. N., Wantzen, K. M., Petermann, P., Strüssmann, C., Marques, M. I., & Adis, J. (2006). Biodiversity and its conservation in the Pantanal of Mato Grosso, Brazil. Aquatic Sciences, 68(3), 278-309.

Junk, W. J., Nunes da Cunha, C., da Silva, C. J., & Wantzen, K. M. (2011). The Pantanal: A large South American wetland and its position in limnological theory. In Wolfgang Johannes Junk, C. J. da Silva, C. Nunes da Cunha, & K. M. Wantzen (Eds.), The Pantanal: Ecology, biodiversity and sustainable management of a large neotropical seasonal wetland Sofia-Moscow: Pensoft Publishers, 23-44.

Kasischke, E. S., Melack, J. M., & Dobson, M. C. (1997). The Use of Imaging Radars for Ecological Applications A Review. Remote Sensing of Environment, 59, 141-156.

Keddy, P. a., Fraser, L. H., Solomeshch, A. I., Junk, W. J., Campbell, D. R., Arroyo, M. T. K., & Alho, C. J. R. (2009). Wet and Wonderful: The World's Largest Wetlands Are Conservation Priorities. BioScience, 59(1), 39–51.

Kerr, J. T., & Ostrovsky, M. (2003). From space to species: ecological applications for remote sensing. Evolution, 18(6), 299-305.

Laba, M., Gregory, S., Braden, J., Ogurcak, D., Hill, E., Fegraus, E., Fiore, J., & DeGloria, S.D. (2002). Conventional and fuzzy accuracy assessment of the New York Gap Analysis Project land cover map. Remote Sensing of Environment, 81(2-3), 443-455.

Laur, H., Bally, P., Meadows, J., Sanchez, J., Schaettler, B., & Lopinto, E. (1997). Derivation of the backscatter coefficient sigma in ESA ERS SAR PRI products. ESA Document no. ES-TN-RS-PM-HL09, 1997.

Lee, K.H., & Lunetta, R.S. (1996) Wetland detection methods. In: Lyon JG, McCarthy J (eds) Wetland and Environmental Application of GIS. Lewis Publishers, New York, 249–284.

Lehner, B., & Döll, P. (2004). Development and validation of a global database of lakes, reservoirs and wetlands. Journal of Hydrology, 296(1-4), 1–22.

Li, J., & Chen, W. (2005). A rule-based method for mapping Canada's wetlands using optical, radar and DEM data. International Journal of Remote Sensing, 26(22), 5051-5069.

Li, L., Ustin, S. L., & Lay, M. (2005). International Journal of Remote Application of multiple endmember spectral mixture analysis (MESMA) to AVIRIS imagery for coastal salt marsh mapping: a case study in China Camp , CA , USA. International Journal of Remote Sensing, 26(23), 5193-5207.

Lowry, J., Ramsey, R. D., Thomas, K., Schrupp, D., Sajwaj, T., Kirby, J., Waller, E., Schrader, S., Falzarano, S., Langs, L., Manis, G., Wallace, C., Schulz, K., Comer, P., Pohs, K., Rieth, W., Velaquez, C., Wolk, B., Kepner, W., Boykin, K., O'Brien, L., Bradford, D. Thompson, B., & Prior-Magee, J. (2007). Mapping moderate-scale land-cover over very large geographic areas within a collaborative framework: A case study of the Southwest Regional Gap Analysis Project (SWReGAP). Remote Sensing of Environment, 108, 59 - 73.

Lucas, R. M., Mitchell, A. L., & Rosenqvist, A. K. E. (2007). The potential of L-band SAR for quantifying mangrove characteristics and change: case studies from the tropics. Aquatic Conservation: Marine and Freshwater Ecosystems, 17, 245-264.

Lucas, R., Armston, J., Fairfax, R., Fensham, R., Accad, A., Carreiras, J., Kelley, J., Bunting, P., Clewley, D., Bray, S., Metcalfe, D., Dwyer, J., Bowen, M., Eyre, T., Laidlaw, M., & Shimada, M. (2010). An Evaluation of the ALOS PALSAR L-Band Backscatter — Above Ground Biomass Relationship Queensland, Australia: Impacts of Surface Moisture Condition and Vegetation Structure. IEEE Journal of Selected Topics in Applied Earth Observations and Remote Sensing, 3(4), 576-593.

Luscombe, A. (2009). Image quality and calibration of RADARSAT-2. IEEE International Geoscience and Remote Sensing Symposium, II-757-II-760.

MDA (MacDonald, Dettwiler and Associates Ltd.), (2008). RADARSAT-2 Product Format Definition. RN-RP-51-2713. Issue 1/7.

Mamede, S. B., & Alho, C. J. R. (2006). Response of wild mammals to seasonal shrinking-and-expansion of habitats due to flooding regime of the Pantanal, Brazil. Brazilian Journal of Biology, 66(4), 991–8.

Mariot, M., Dudal, Y., Furian, S., Sakamoto, A., Vallès, V., Fort, M., & Barbiero, L. (2007). Dissolved organic matter fluorescence as a water-flow tracer in the tropical wetland of Pantanal of Nhecolândia, Brazil. The Science of the Total Environment, 388(1-3), 184–93.

Martinez, J. M., & le Toan, T. (2007). Mapping of flood dynamics and spatial distribution of vegetation in the Amazon floodplain using multitemporal SAR data. Remote Sensing of Environment, 108, 209 - 223.

Medina-Junior, P. B., & Rietzler, A. C. (2005). Limnological study of a Pantanal saline lake. Brazilian Journal of Biology, 65, 651-659.

Medri, Í. M., & Mourão, G. (2005). Home range of giant anteaters (*Myrmecophaga tridactyla*) in the Pantanal wetland, Brazil. Journal of Zoology, 266(4), 365-375.

Mitchell, S. C. (2005). How useful is the concept of habitat? Oikos, 3, 634-638.

Mitsch, W. J. & Gosselink, J. G. (2007). Wetlands. 4th. edition. John Wiley & Sons, Hoboken, USA, p. 600.

Muasya, A. M., Hover, V. C., Ashley, G. M., Owen, R. B., Michelle, F., & Kimeli, M. (2004). Diversity and Distribution of Macrophytes in a Freshwater Wetland, Loboi Swamp (Rift Valley) Kenya. Journal of East African Natural History, 93(1), 39-47.

Mufarrege, M. M., Di Luca, G. a, Hadad, H. R., & Maine, M. a. (2011). Adaptability of *Typha domingensis* to high pH and salinity. Ecotoxicology, 20(2), 457-65.

Newton, A. C., Hill, R. A., Echeverria, C., Golicher, D., Rey Benayas, J. M., Cayuela, L., & Hinsley, S. A. (2009). Remote sensing and the future of landscape ecology. Progress in Physical Geography, 33(4), 528–546.

Nogueira, F., Silveira, R. M. L., da Silva, C. J., Abdon, M., Girard, P., & Wantzen, K. M. (2011). Hydrochemistry of lakes, rivers and groundwater. In Wolfgang Johannes Junk, C. J. da Silva, C. Nunes da Cunha, and K. M. Wantzen (Eds.), The Pantanal: Ecology, biodiversity and sustainable management of a large neotropical seasonal wetland, Sofia-Moscow: Pensoft Publishers, 167-198.

Novack, T., Hayakawa, E. H., Bertani, T. D. C., & Zani, H. (2010). Classification of Lakes in the Pantanal of Nhecolândia (Brazil) Using Object-Based Image Analysis. Revista Geográfica Acadêmica, 4(1), 32-46.

Nunes da Cunha, C., Junk, W. J., & Leitao-Filho, H. F. (2007). Woody vegetation in the Pantanal of Mato Grosso, Brazil - a preliminary typology. Amazonia, XIX((3/4)), 159-184.

Nunes da Cunha, C., & Junk, W. J. (2011). A preliminary classification of habitats of the Pantanal of Mato Grosso and Mato Grosso do Sul , and its relation to national and international wetland. In Wolfgang Johannes Junk, C. J. da Silva, C. Nunes da Cunha, & K. M. Wantzen (Eds.), The Pantanal: Ecology, biodiversity and sustainable management of a large neotropical seasonal wetland (pp. 127-141). Sofia-Moscow: Pensoft Publishers.

Oliver, C. & Quegan, S., (2004), Understanding Synthetic Aperture Radar Images. Raleigh, NC: SciTech Publishing, p. 475.

Olson,D., E. Dinerstein, P. Canevari, I.Davidson,G. Castro,V. Moriset, R. Abell, & E. Toledo. (1998). Freshwater biodiversity of Latin America and the Caribbean: a conservation assessment. Biodiversity Support Program,WorldWildlife Fund,Washington, D.C.

Ozesmi, S. L., & Bauer, M. E. (2002). Satellite remote sensing of wetlands. Wetlands Ecology and Management, 10, 381-402.

Padovani, C. R., Cruz, M. L. L., & Padovani, S. L. A. G. (2004). Desmatamento do Pantanal brasileiro para o ano 2000. Simpósio sobre recursos naturais e sócio-econômicos do Pantanal, Embrapa Pantanal. Empresa Brasileira de Pesquisa Agropecuária (Embrapa)-Pantanal, Corumbá, Brasil, 1-7.

Polis, D.F., Salter, M. & Lind, H. (1974) Hydrographic Verification of Wetland Delineation by Remote Sensing. Photogrammetric Engineering & Remote Sensing, 75–78.

Pope, K. O., Rejmankova, E., Paris, J. F., & Woodruff, R. (1997). Detecting Seasonal Flooding Cycles in Marshes of the Yucatan Peninsula with S IR-C Polarimetric Radar Imagery. Remote Sensing of Environment, 59, 157-166.

Por, F. D., (1995). The Pantanal of Mato Grosso (Brazil): World's largest wetlands. Monographiae Biologicae, H. J. Dumont and M. J. A. Werger, Eds. Dordrecht, Netherlands: Kluwer, vol. 73.

Pott, V. J. & Pott, A., (2000) Plantas Aquaticas do Pantanal. EMBRAPA, Brazil.

Pott, A., Oliveira, A. K. M., Damasceno-Junior, G. A., & Silva, J. S. V. (2011). Plant diversity of the Pantanal wetland. Revista brasleira de biologia, 71(1 Suppl 1), 265-273.

Pott, V. J. & Pott, A., (2011a). Species diversity, distribution and biomass of aquatic macrophytes of the Pantanal. In Wolfgang Johannes Junk, C. J. da Silva, C. Nunes da Cunha, & K. M. Wantzen (Eds.), The Pantanal: Ecology, biodiversity and sustainable management of a large neotropical seasonal wetland (pp. 257-280). Sofia-Moscow: Pensoft Publishers.

Pott, V. J. & Pott, A., (2011b). Species diversity of terrestrial plants and human impact on the vegetation of the Pantanal. In Wolfgang Johannes Junk, C. J. da Silva, C. Nunes da Cunha, & K. M. Wantzen (Eds.), The Pantanal: Ecology, biodiversity and sustainable management of a large neotropical seasonal wetland. Sofia-Moscow: Pensoft Publishers. 281-300.

PROBIO, (2007) Levantamento e mapeamento dos remanescentes da cobertura vegetal do bioma Pantanal, period de 2002 na escala de 1:250000. Embrapa Informática Agropecuária, 45 p.

Ramsey, E. W. I., & Laine, S. C. (1997). Coastal Comparison of Landsat Thematic Mapper and High Complex Coastal Wetlands. Journal of Coastal Research, 13(2), 281-292.

Rebelo, L. M., Finlayson, C.M., Nagabhatla, N. (2009). Remote sensing and GIS for wetland inventory, mapping and change analysis. Journal of Environmental Management. 90, 2144-2153

Rebelo, L. M. (2010). Eco-Hydrological Characterization of Inland Wetlands in Africa Using L-Band SAR. IEEE Journal of Selected Topics in Applied Earth Observations and Remote Sensing, 3(4), 554-559.

Rosenqvist, A. K. E., Finlayson, C. M. A. X., Lowry, J., & Taylor, D. (2007). The potential of long-wavelength satellite-borne radar to support implementation of the Ramsar Wetlands Convention, Aquatic Conservation: Marine and Freshwater Ecosystems, 244, 229-244.

Rosich B., & Meadows P., (2004). Absolute calibration of ASAR Level 1 products. ESA, Issue 1 revision 5, 07 October 2004, 26 p.

Rundquist, D. C., Narumalani, S., & Narayanan, R. M. (2001). A review of wetlands remote sensing and defining new considerations. Remote Sensing Reviews, 20, 207-226.

Rylands, A. B., & Brandon, K. (2005). Brazilian Protected Areas. Conservation Biology, 19(3), 612-618.

Schmullius, C. and Evans, D. (1997). Synthetic aperture radar (SAR) frequency and polarization requirements for applications in ecology, geology, hydrology, and oceanography: a tabular status quo after SIR-C/X-SAR. International Journal of Remote Sensing, 18, 2713-2722.

Seevers, P.M., Lewis, D. T., & Drew, J. V. (1976). The use of Landsat-1 imagery in mapping and managing soil and range resources in the Sand Hills Region of Nebraska. PAPER-A14, NASA. Goddard Space Flight Center 3d ERTS-1 Symp., Vol 1, Sect A, 225-232.

Seidl, A. (2000). Global valuation of ecosystem services: application to the Pantanal da Nhecolândia, Brazil. Ecological Economics, 33(1), 1-6.

Seidl, A. F., Silva, J. D. S. V. D., & Moraes, A. S. (2001). Cattle ranching and deforestation in the Brazilian Pantanal. Ecological Economics, 36(3), 413–425.

Shimada, M., Isoguchi, O., Tadono, T., & Isono, K. (2009). PALSAR Radiometric and Geometric Calibration. IEEE Transactions on Geoscience and Remote Sensing, 47(12), 3915-3932.

Shimada, M., Member, S., & Ohtaki, T. (2010). Generating Large-Scale High-Quality SAR Mosaic Datasets : Application to PALSAR Data for Global Monitoring, IEEE Journal of Selected Topics in Applied Earth Observations and Remote Sensing, 3(4), 637–656.

Silva, T. S. F., Costa, M. P. F., Melack, J. M., & Novo, E. M. L. M. (2008). Remote sensing of aquatic vegetation: theory and applications. Environmental Monitoring and Assessment, 140(1-3), 131-45.

Silva, T. S. F., Costa, M. P. F., & Melack, J. M. (2010). Spatial and temporal variability of macrophyte cover and productivity in the eastern Amazon floodplain: A remote sensing approach. Remote Sensing of Environment, 114(9), 1998-2010.

Simard, M., De Grandi, G., Saatchi, S., & Mayaux, P. (2002). Mapping tropical coastal vegetation using JERS-1 and ERS-1 radar data with a decision tree classifier. International Journal of Remote Sensing, 23(7), 1461-1474.

Siqueira, P. (2003). The coregistration, calibration, and interpretation of multiseason JERS-1 SAR data over South America. Remote Sensing of Environment, 87(4), 389-403.

Souza-Filho, P. W. M., Paradella, W. R., Rodrigues, S. W. P., Costa, F. R., Mura, J. C., & Gonçalves, F. D. (2011). Discrimination of coastal wetland environments in the Amazon region based on multi-polarized L-band airborne Synthetic Aperture Radar imagery. Estuarine, Coastal and Shelf Science, 95(1), 88-98. Elsevier Ltd.

Stehman, S. (1996). Use of auxiliary data to improve the precision of estimators of thematic map accuracy. Remote Sensing of Environment, 58(2), 169-176.

Stoline, M. R. (1981). The Status of Multiple Comparisons: Simultaneous Estimation of All Pairwise Comparisons in One-Way ANOVA Designs. The American Statistician, 35(3), 134.

Suarez, Y. R., Petrere, M., & Catella, & A. C. (2004). Factors regulating diversity and abundance of fish communities in Pantanal lagoons, Brazil. Fisheries Management and Ecology, 11(1), 45-50.

Tews, J., Brose, U., Grimm, V., Tielbörger, K., Wichmann, M. C., Schwager, M., & Jeltsch, F. (2004). Animal species diversity driven by habitat heterogeneity/diversity: the importance of keystone structures. Journal of Biogeography, 31(1), 79–92.

Tomas, W. M., & Salis, S. M. (2000). Diet of the marsh deer (Blastocerus dichotomus) in the Pantanal wetland, Brazil. Studies on Neotropical Fauna and Environment, 35(3), 165–172.

Tomas, W. M., Souza, L. L., & Tubelis, D. P.(2004). Espécies de aves ameaçadas que ocurrem no Pantanal. Pp 1-10 in IV Simpósio sobre recursos naturais e sócio-econômicos do Pantanal. Brasileira de Pesquisa Agropecuária (Embrapa) Pantanal. Corumbá. Brasil

Tubelis, D. P. & W. M. Tomas. (2003). Bird species of the wetland, Brazil. Ararajuba 11(5)–37.

Ulaby, F. T., Moore, R. K. and Fung, A. K. (1981). Microwave remote sensing: microwave remote sensing fundamentals and radiometry. Artech House. US. Vol. 1, 456p.

Walker, W. S., Member, A., Stickler, C. M., Kellndorfer, J. M., Member, S., Kirsch, K. M., & Nepstad, D. C. (2010). Large-Area Classification and Mapping of Forest and Land Cover in the Brazilian Amazon : A Comparative Analysis of ALOS / PALSAR and Landsat Data Sources. IEEE Transactions on Geoscience and Remote Sensing, 3(4), 594-604.

Wang, Y., Hess, L. L., Solange, F., & Melack, J. M. (1994). Canopy penetration studies: modeled radar backscatter from Amazon floodplain forests at C-, L- and P-band. Geoscience and Remote Sensing Symposium. IGARSS. Surface and Atmospheric

Remote Sensing: Technologies, Data Analysis and Interpretation, 2 (8-12), 1060-1062.

Wang, K., Franklin, S. E., Guo, X., He, Y., & McDermid, G. J. (2009). Problems in remote sensing of landscapes and habitats. Progress in Physical Geography, 33(6), 747-768.

Wilen, B. O., Carter, V., Jones, R. J., (1999) National Water Suary on Wetlnd Resources. United States Geological Survey Water Supply Paper 2425. Accessed online: Aug. 27, 2012, http://water.usgs.gov/nwsum/WSP2425/mapping.html